Title

First Contact: 7-Phenyl-2-Aminoquinolines, Potent and Selective Neuronal Nitric Oxide Synthase Inhibitors That Target an Isoform-Specific Aspartate

Journal

Journal of Medicinal Chemistry, 63(9)

ISSN

0022-2623

Authors

Cinelli, Maris A
Reidl, Cory T
Li, Huiying
et al.

Publication Date

2020-05-14

DOI

10.1021/acs.jmedchem.9b01573

HHS Public Access

Author manuscript

J Med Chem. Author manuscript; available in PMC 2021 May 14.

Published in final edited form as:

J Med Chem. 2020 May 14; 63(9): 4528–4554. doi:10.1021/acs.jmedchem.9b01573.

First Contact: 7-Phenyl-2-Aminoquinolines, Potent and Selective Neuronal Nitric Oxide Synthase Inhibitors That Target an Isoform-Specific Aspartate

Maris A. Cinelli[1,†], **Cory T. Reidl**[1,†], **Huiying Li**[2], **Georges Chreifi**[2], **Thomas L. Poulos**[2], **Richard B. Silverman**[1,*]

[1]Department of Chemistry, Department of Molecular Biosciences, Chemistry of Life Processes Institute, Center for Molecular Innovation and Drug Discovery, Northwestern University, 2145 Sheridan Road, Evanston, Illinois 60208-3113, United States

[2]Departments of Molecular Biology and Biochemistry, Pharmaceutical Sciences, and Chemistry, University of California, Irvine, Irvine, California 92697-3900, United States

Abstract

Inhibition of neuronal nitric oxide synthase (nNOS), an enzyme implicated in neurodegenerative disorders, is an attractive strategy for treating or preventing these diseases. We previously developed several classes of 2-aminoquinoline-based nNOS inhibitors, but these compounds had drawbacks including off-target promiscuity, low activity against human nNOS, and only modest selectivity for nNOS over related enzymes. In this study, we synthesized new nNOS inhibitors based on 7-phenyl-2-aminoquinoline, and assayed them against rat and human nNOS, human eNOS, and murine and (in some cases) human iNOS. Compounds with a *meta*-relationship between the aminoquinoline and a positively charged tail moiety were potent and had up to nearly 900-fold selectivity for human nNOS over human eNOS. X-ray crystallography indicates that the amino groups of some compounds occupy a water-filled pocket surrounding an nNOS-specific aspartate residue (absent in eNOS). This interaction was confirmed by mutagenesis studies, making 7-phenyl-2-aminoquinolines the first aminoquinolines to interact with this residue.

Graphical Abstract

*To whom correspondence should be addressed. Tel.:+1 847 491 5653; Fax: +1 847 491 7713 (R.B.S.); Tel.:+1 949 824 7020. (T.L.P.). Agman@chem.northwestern.edu (R.B.S), poulos@uci.edu (T.L.P).

†These authors contributed equally to this work.

Supporting Information. Crystallographic data collection and refinement statistics for rat and human nNOS and human eNOS structures. Results and Discussion pertaining to constrained amine analogues (**16–18**) and small 4-alkyloxy-3-aminomethyl analogues **25–28**, and binding behavior of **31**, **36**, and **37**. Relevant X-ray structures for **25**, **26**, **28**, **31**, **36**, **37** and protein secondary structure displacement (Figures S1–S6), molecular docking protocol, synthesis and analytical data for relevant precursor compounds **46–49**, **67**, **73**, **77–80**, **85**, **87–88**, **90**, **92–95**, **98**, **100–116**, and full PDSP secondary binding assay results. A Molecular Formula Strings table (.csv) is also available.

PDB ID Codes. PDB codes for X-ray crystal structures described in this study have been deposited in the Protein Data Bank under the following accession codes (See Table S1 in SI for details): 6PMV, 6PMW, 6PMX, 6PMY, 6PMZ, 6PN0, 6PN1, 6PN2, 6PN3, 6PN4, 6PN5, 6PN6, 6PN7, 6PN8, 6PN9, 6PNA, 6PNB, 6PNC, 6PND, 6PNE, 6PNF, 6PNG, 6PNH, 6PO5, 6PO7, 6PO8, 6PO9, 6POA, 6POB, 6POC, 6POT, 6POU, 6POV, 6POW, 6POX, 6POY, 6POZ, 6PP0, 6PP1, 6PP2, 6PP3, 6PP4.

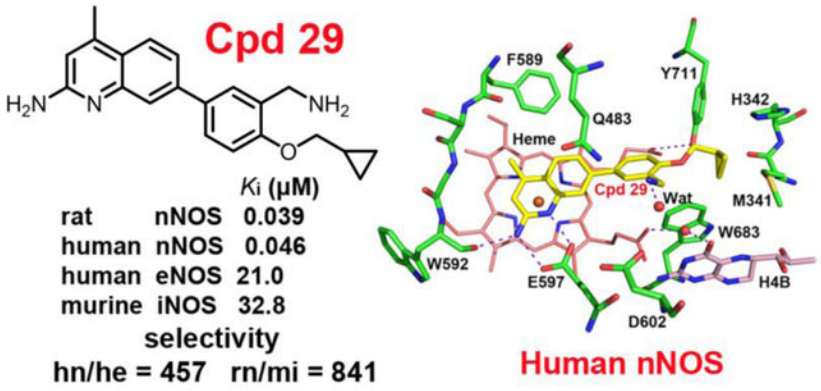

Introduction

Neurodegenerative diseases such as Alzheimer's, Huntington's, Parkinson's, and amyotrophic lateral sclerosis (ALS), are characterized by the gradual loss of neuronal integrity and are responsible for a wide range of neurological deficiencies. Neuronal damage or death associated with stroke, ischemic events, and cerebral palsy (as well as acute or chronic brain injuries) has also been linked to similarly debilitating motor, cognitive, and psychological impairments. The overproduction of the vital secondary messenger nitric oxide (NO), produced by neuronal nitric oxide synthase (nNOS) in tissues of the central (CNS) and peripheral nervous system (PNS), is directly implicated in these disorders.[1,2] Because NO plays a key role in these diseases, rational control of NO levels in neuronal tissues *via* nNOS-specific inhibition is therapeutically desirable.

Nitric oxide synthases (NOS) are a family of homodimeric enzymes that are responsible for the biosynthesis of NO. Functional regulation of NO is differentiated by subcellular localization, tissue distribution, and regulatory gene expression of three isoforms of NOS: endothelial NOS (eNOS), inducible NOS (iNOS), and neuronal NOS (nNOS), which are responsible for regulating blood pressure and vascular tone, immune activation, and normal neuronal communication, respectively.[3] Functional NOS is a homodimer. Each NOS monomer contains a reductase domain and an oxygenase domain, separated by a flexible region where calmodulin binds when activated by calcium ions. The reductase domain contains binding sites for flavin adenine dinucleotide (FAD), flavin mononucleotide (FMN), and reduced nicotinamide adenine dinucleotide phosphate (NADPH), whereas the oxygenase domain contains binding sites for (6*R*)-5,6,7,8-tetrahydrobiopterin (H_4B), the metallocofactor heme, and the substrate L-arginine. Electron flow proceeds from one monomer's reductase domain, sequentially through NADPH, FAD, and FMN, to the opposite monomer's oxygenase domain, where the electron is transferred between FMN and heme, by which L-arginine is oxidized to L-citrulline and NO.[4]

Most compounds initially investigated for nNOS inhibition were designed as competitive mimics of L-arginine. These inhibitors have high basicity and polarity, a large total polar surface area (tPSA), and an overabundance of hydrogen bond donors, and as a result, suffer

from poor bioavailability and blood-brain barrier (BBB) penetrability. Furthermore, many promising L-arginine-mimetic inhibitors are not nNOS-selective, owing to the high sequence similarity and nearly identical active-site architecture between the three NOS isoforms. High nNOS selectivity is crucial; non-selective inhibitors have the potential for dangerous side effects. For example, iNOS inhibition could impair immune system activation, while eNOS inhibition can lead to severe hypertension or other cardiovascular complications.[5]

We have been investigating 2-aminoquinoline-based scaffolds as isoform-selective arginine bioisosteres with more favorable pharmacokinetic properties. Since 2014, we have reported several generations of aminoquinolines that are modestly potent and selective towards nNOS (Figure 1). The first generation of aminoquinolines (such as **1**[6]), were found to be potent and selective nNOS inhibitors with improved pharmacokinetics. Unfortunately, **1** was found to have high rat nNOS (rnNOS) over human nNOS (hnNOS) selectivity, low hnNOS over human eNOS (heNOS) selectivity and caused toxic side effects, possibly because of its off-target promiscuity.[4] The second generation of NOS inhibitors, (e. g., phenyl ether **2**[7]) reduced off-target binding while preserving potency and selectivity against rnNOS. However, these compounds suffered from decreased Caco-2 permeability, low hnNOS activity, and similarly low hn/heNOS selectivity. Newer generation inhibitors, such as **3** and **4**, improved upon their respective parent series by incorporating elements such as the quinoline 4-methyl group and cyano-containing tail moieties.[8,9] These compounds have greatly enhanced hnNOS potency, hn/heNOS selectivity, and improved cellular permeability and off-target profiles.

Because of some of the drawbacks associated with previous inhibitor generations, we have been investigating alternative aminoquinoline-containing scaffolds. Interestingly, the 7-phenylquinoline compound **5** appears in the literature as part of a Glaxo-SmithKline screening library and was recently employed in several high-throughput screening studies.[10,11] However, there are no articles, patents, or other reports of what research program this compound may have belonged to originally, but it appears to now be part of an “open source” drug discovery program.

Because of its distinctively nNOS inhibitor-like structure but with fewer rotatable bonds than earlier series, a docking study with **5** in a nNOS crystal structure was conducted. Consequently, **5** was predicted to bind in an nNOS inhibitor-like mode, in which the aminoquinoline forms a salt-bridge with Glu592/Glu597 (rnNOS/hnNOS) and the phenethylamine tail portion faces out toward the regions of the active site. To this end, lead compound **5** and related compounds **6–9** (modified at the amine portion (Figure 2) were designed, synthesized, and assayed against purified NOS isoforms to test the hypothesis that **5** and analogues could act as nNOS inhibitors. Satisfyingly, these compounds possessed encouraging nNOS inhibitory activity and good isoform selectivity, and we chose to undertake a more thorough structure-activity relationship (SAR) study. First, we investigated whether *meta*- or *ortho*-substitution of the central phenyl ring (compounds **10–13**) might be more effective than the *para*-substitution of the parent compound. This early optimization revealed that *meta*-substituted analogue **12** displayed good inhibitory potency against rat and human nNOS, excellent hn/heNOS selectivity and n/i selectivity, as well as good solubility and desirable properties (few rotatable bonds and low tPSA).

Encouraged by both the inhibitory constants and the agreement between X-ray crystallography and our docking results, **12** was used as a launching point for further optimization. Efforts were made to develop a set of compounds with modifications made at the 5-position of the central phenyl ring (e.g., nitrile **14** and pyridine **15**) to investigate whether additional interactions could be made with the heme propionate or another active site residue.

Because of **12**'s high n/eNOS selectivity, we hypothesized that the flexible tail amino group might be contacting (directly or otherwise) a specific aspartate residue (Asp597/Asp602 in rnNOS/hnNOS, respectively). This residue is missing in eNOS isoforms, replaced by asparagine. Consequently, contact (H-bonding or electrostatic) between an inhibitor and this residue can impart very high n/eNOS selectivity (1000-fold or more). We hypothesized that a second set of compounds could be designed to solidify any existing contacts with Asp597/Asp602 by incorporating the tail amino group functionality into a rigid ring system, thereby reducing its overall flexibility and locking the interaction in place. As the amino group of **5** is quite flexible, both *meta*-/*para*- and *ortho*-/*meta*-constrained derivatives (isoindoline **16** and the two isomeric racemic indanylamines **17** and **18**) were prepared.

Additional docking studies indicated that a variety of groups might be accommodated at the 4-position of the central phenyl ring of **12**, which could form van der Waals interactions with Met336/Met341 (rnNOS/hnNOS), a residue that was previously implicated in high n/eNOS selectivity for 2-aminoquinoline-based inhibitors[7] as it is absent in eNOS isoforms (replaced by a smaller valine).[12] To this end, 3,4-substituted compounds **19–37** (Figure 3), possessing a variety of steric, electronic, and H-bonding substituents at the 4-position were investigated to determine if this substitution pattern could make extra contacts with the isoform-specific residues Met336/Met341 and/or the hnNOS-specific residue His342.

All synthesized compounds were assayed against rnNOS, and selected compounds were also assayed against hnNOS. Murine iNOS and human eNOS were used to determine selectivity, and selected compounds were also assayed against human iNOS.

Results and Discussion

Chemistry.

To prepare compound **5**, we envisioned that the quinoline-aryl bond could be constructed *via* Suzuki coupling. To this end, we sought to install the boron-containing moiety on the quinoline, taking advantage of a large and diverse set of available aryl halides (which are less expensive and easier to synthesize than an analogous series of boronates or boronic esters). Using versatile 7-bromoquinoline **38**,[8] a 7-BPin moiety was first installed *via* Miyaura borylation (Scheme 1). This intermediate was not isolated but rather converted to trifluoroborate **39**, which was readily purified because of its insolubility in most organic solvents.

To prepare the halide precursor, commercially available 4-bromophenethylamine **40** was Boc-protected to yield **41.** Many Suzuki conditions were screened for the coupling of **39** and **41**, but the strong protic bases usually required for reductive elimination and activation of **39**

often led to deacetylation of the quinoline and decomposition. The use of $NaHCO_3$ as the base[13] in a mixed aqueous solvent was more successful, and microwave irradiation of this mixture yielded phenylquinoline **42** within 25 minutes at 120 ˚C without substantial deacetylation. The intermediate protected phenylquinolines were not extensively characterized but were isolated and immediately deprotected. Deprotection was accomplished stepwise, first with K_2CO_3 in refluxing methanol to cleave the acetyl group, followed by treatment of the free aminoquinoline with methanolic HCl to remove the Boc group and provide **5** as its water-soluble dihydrochloride salt.[6]

To prepare the initial set of derivatives with different *para*-aminoalkyl tail portions (**6–9**), the halides were first prepared. Compound **41** was methylated to yield **43** (Scheme 2A). Commercially available iodobenzylamine **44** was Boc-protected to yield **45**, which was also methylated to yield **46** (Scheme 2B). For the (*S*)-alpha-methyl-phenethylamine group of **9**, the Ellman auxiliary method[14] was used (Scheme 2C). Ketone **47** was condensed with (*S*)-*tert*-butylsulfinamide, and the intermediate sulfinyl imine was reduced at low temperature to afford (*S,S*)-**48** in a good d.r. of ~7:1.

Desulfinylation under acidic conditions and Boc-protection subsequently afforded derivative **49**. For *ortho*- and *meta*-substituted derivatives **10**/**11** and **12**/**13**, respectively, the commercially available benzylamines (**50**, **54**) and phenethylamines (**51**, **55**) were Boc-protected to yield *o*-substituted (**52**, **53**) and *m*-substituted (**56**, **57**) bromides, respectively (Schemes 2D and 2E). Suzuki coupling between **39** and these halides under the conditions described above (Scheme 3) was facile and displayed a high substrate tolerance, affording protected phenylquinolines **5–65** in good yields. Generally, the only impurity isolated was a small amount (<10%) of proto-deborylated acetamidoquinoline. Deprotection of **58–66** (Scheme 3) afforded analogues **6–13**.

To synthesize 5-cyano derivative **14**, bromobenzene **66** was prepared as previously described. Treatment of **66** with the anion derived from Boc_2NH (Scheme 4A) yielded, surprisingly, mono-Boc protected amine **67**, indicating that one Boc group was cleaved during the reaction or workup. Suzuki coupling with **39** yielded **68**, which was then deprotected to provide amine **14**. In contrast, heating Boc_2NH and pyridine **69** under basic conditions (Scheme 4B) afforded the *N,N*-di-Boc compound (**70**).[15] Likewise, the major product (**71**) isolated upon coupling of **70** and **39** contained both Boc groups intact. During deacetylation, a longer period of heating (4.5 h) was employed to remove both the acetyl group and one Boc group, and the second Boc group was then removed with HCl to yield **15**.

Synthesis of isoindoline derivative **16** (Scheme 5A) commenced with commercially available 4-bromoisoindoline salt **72**, which was converted to the free base and Boc-protected to yield **73**. Coupling with **39** afforded **74,** which then yielded **16** upon deprotection. Indanylamine derivatives **17** and **18** (Scheme 5B) were prepared from the 5- and 6-bromoindanones (**75** and **76)**, respectively. The Ellman method (as in Scheme 2C)[14] was used to install the amino group as its racemate. However, yields of sulfinamides **77** and **78** were fairly low, and large amounts of insoluble ketone condensation by-products were obtained. Nonetheless, **77** and **78** were desulfinylated and Boc-protected, and carbamates **79**

and **80** were readily amenable to Suzuki coupling with **39**, affording **81** and **82**, which were deprotected to yield, respectively, **17** and **18**.

We envisioned that 4-substituted derivatives **19**-**24** could be accessed from commercially available benzaldehydes or toluene derivatives via conversion to the benzyl halides. To this end, fluorotoluene **83** and chlorotoluene **84** (for **19** and **20**) were converted to benzyl bromides **85** and **86**. A Delépine reaction, involving treatment with hexamethylenetetramine and acidic hydrolysis of the resulting hexaminium adduct, and subsequent Boc-protection of the amine yielded **87** and **88** (Scheme 6A). For the trifluoromethyl derivative *en route* to **21**, commercially available nitrile **90** was reduced with BH_3-DMS,[16] and the isolated amine was protected to yield **91** (Scheme 6B). 2-Ethybenzaldehyde (**91**, for **22**) was complexed with $AlCl_3$[17] and brominated to yield the major regioisomer (**92b**) as an inseparable 3:1 mixture with **92a**. Following borohydride reduction, the isomers were separated, and the major isomer (**93**) was chlorinated to yield **94**. Delépine reaction and Boc protection provided bromobenzene derivative **95** (Scheme 6C).

Methoxybenzyl alcohol **96** (for **23**) was prepared as previously described (Scheme 6D) and elaborated *via* **97** as described above to yield **98**. Finally, ethoxylated toluene **99** was brominated to yield **100** (Scheme 6E). Delépine reaction and Boc protection afforded carbamate **101**.

As the multiple steps of this route would make the preparation of many similar analogues time consuming, and the Boc_2NH method of Scheme 4 was unpredictable, a slightly different strategy was used to prepare 4-ether halide derivatives **25–37** (Scheme 7). In this route, protected amine **103** was first prepared *via* reduction of **102**, and then the ether functionality was installed by deprotonation of the phenol and treatment with alkyl or benzyl halides.

By this method, the *n*-propyl (**104**), isopropyl (**105**), isobutyl (**106**), methylcyclobutyl **(107**), methylcyclopropyl (**108**), 3-fluorobenzyl (**109**), 4-cyanobenzyl (**110**), (5-methylisoxazol-3-methyl (**113**), 4- and 5-methyl thiazoles **(114**/**116)**, and oxazol-4-methyl (**115**) ethers were prepared. As the thiazol-5-methyl chloride and pyridylmethyl bromides are only commercially available as the HCl and HBr salts, respectively, these salts were converted to their free base immediately prior to the formation of the 2-pyridylmethyl (**111**), 3-pyridylmethyl (**112**), and thiazol-5-methyl **(116)** ethers. All of these ether-containing halides were subjected to Suzuki coupling with **39** to yield protected phenylquinolines **117–135** in moderate to excellent yields, and stepwise deprotection as described above yielded final analogues **19–37**.

nNOS Inhibitory Assay and Crystallography.

The hemoglobin capture assay (see Experimental Section) was used to determine the inhibition constants (K_i) of synthesized compounds **5–37**.[18,19] All compounds were assayed against purified rnNOS as a prescreen, and eighteen of the most potent compounds against rnNOS were further assayed against purified human nNOS (hnNOS), murine iNOS (miNOS), and human eNOS (heNOS) to determine isoform selectivity. Table 1 summarizes the apparent K_i values and isoform selectivities for **5–37**. Values for compounds **1–4** are

included for comparison. The rnNOS and miNOS isoforms were used to approximate n/i isoform selectivity, because they are the easiest to express and purify, and those are the species used for crystallography. Furthermore, for preclinical purposes, it is essential to prove efficacy and selectivity in lower animals prior to advancement to clinical trials. Recent advances have made it possible to obtain and crystallize both hnNOS and heNOS, which were used to support our human isoform SAR development. Because high-resolution structures of murine and human iNOS were not available until more recently, the majority of the structural discussion will focus on nNOS and eNOS; discussion of a comparison between murine and human iNOS inhibition follows that.

Initial Inhibitory and Structural Analysis of Modified Amine Tail Analogues.

The initial lead 7-phenyl-2-aminoquinoline (**5**) has good rat and human nNOS inhibitory activity (105 nM and 122 nM, respectively) with moderately high n/iNOS and n/eNOS selectivity of 207-fold and 191-fold, respectively. The X-ray crystal structure of **5** bound to rnNOS, hnNOS, and heNOS (Figure 4A–C) revealed the structural basis for inhibitory potency. The quinoline portion of **5** mimics arginine and forms a bifurcated hydrogen bond system with the main chain carbonyl of Trp587/Trp592 (rnNOS/hnNOS) and the side chain carboxylate of Glu592/Glu602 (rnNOS/hnNOS). This is identical to the structural details observed for other nNOS inhibitors containing a 2-aminoquinoline.[6,7,8,9] All three crystal structures clearly reveal that the central phenyl ring resides between heme propionates A and D. In the hnNOS-**5** structure, the tail phenethylamine moiety makes a direct H-bond interaction with the H_4B and propionate A, displacing the water there, while the rnNOS-**5** structure only makes H-bonding contacts with the carbonyl of the H_4B and is unable to displace the water molecule bridging propionate A and H_4B.

In heNOS there are two molecules of **5** bound. Ligand A binds in the active site in a manner very similar to the nNOS structures, while Ligand B displaces H_4B, with the aminoquinoline positioned in the pterin binding pocket. As a result, the tail ethylamine of **5** bound to heNOS is oriented in the opposite direction to what we observed in the nNOS structures, and instead interacts with propionate D. Ligand B is stabilized by aromatic stacking interactions with both Trp447 as well as Trp74 and Phe460 from the opposite chain at the dimer interface. Two-site binding is not unique to **5** and has been observed in several NOS-inhibitor structures.[20,21] In all four molecules of the asymmetric unit of heNOS, the aminoquinoline and phenyl rings of **5** are clearly defined. The electron density is weaker for the tail ethylamines, with slightly more density observed near propionate D, indicating a potential interaction with the heme propionate. Interestingly, the ability of **5** and other compounds to bind in both sites has little correlation with inhibitory potency, indicating that active site binding (and not H_4B displacement) determines potency.

With the goal of improving hnNOS activity and isoform selectivity, we made efforts to optimize the conformational positioning of the tail amine of **5**. To this end, homologation, chain shortening, and isomerization of lead molecule **5** resulted in compounds **6–13**. Methylation of the tail nitrogen atom of **5** (compound **6**) resulted in over a 2-fold loss in rnNOS activity, while shortening the ethylene linker between the central ring and the terminal nitrogen atom by one carbon (compound **7**) resulted in a 2.3-fold increase in rnNOS

activity. Moreover **7** showed increased hnNOS inhibitory activity, as well as improvements in both rn/miNOS and hn/heNOS selectivity ratios, relative to parent molecule **5**. The X-ray crystal structures of **7** bound to rnNOS and hnNOS (Figure 5) reveal well-defined density at the aminoquinoline and central ring regions that closely overlaps with lead **5**. However, the orientation of the tail aminomethyl group in both structures could not be determined because of poor density, even at a low contour levels, suggesting free rotation of the aminomethyl occurs toward either propionate A and the H_4B site water, as modeled in Figure 5A and B, or toward propionate D and Tyr706/Tyr711 (rnNOS/hnNOS). In both nNOS structures, the position of the central phenyl ring of **7** forces heme propionate D into a downward conformation. As observed for **5** and **6**, methylation of the tail nitrogen atom of **7** to yield **8** resulted in a loss of potency against both rat and human nNOS, suggesting that a primary amino group at this position is important for achieving maximal inhibitory activity against nNOS isoforms.

It appears that some parts of the phenylaminoquinoline SAR overlap with that of the previously reported phenyl ether compounds.[7] For example, phenyl ether compounds with one methylene between the amino group and the aryl ring (benzyl) are more potent and selective than those with two (phenethyl) or more methylenes, and the same trend is observed here (cf. **7** and **8** vs. **5** and **6**); compound **9** (K_i (rnNOS) = 140 nM) also has slightly less potency than **5**. Nonetheless, other parts of the SAR are distinct from the previous aminoquinoline SARs. For instance, *N*-methylated compounds (**6**, **8**) are less potent than the desmethyl analogues (**5**, **7**), which is the reverse of what was generally observed for benzyl and phenethyl ether compounds.

The *o*-substituted isomers (**11** and **10**) possess less inhibitory potency (**11**, K_i (rnNOS) = 935 nM; **10**, K_i (rnNOS) = 119 nM) than their corresponding *para*-substituted derivatives **5** and **7**, respectively. Furthermore, **10** displays a similar loss in hnNOS potency and a sharp decrease in rn/miNOS selectivity. However, poor binding affinity to heNOS (**10**, K_i (heNOS) = 41,900 nM) results in a gain in hnNOS selectivity over heNOS compared to **7**. In contrast to *o*-substitution, *m*-substituted isomers **13** and **12** exhibited comparable potencies to **5** and **7**, respectively [**13**, K_i (rnNOS) = 107 nM; **12**, K_i (rnNOS) = 55 nM]. Moreover, **12** also has very good nNOS selectivity over iNOS (rn/miNOS = 440) and outstanding selectivity over eNOS (hn/heNOS = 877). The assay data for **12** suggest that placing the aminoalkyl tail portion *meta*- to the quinoline favors binding to the human nNOS isoform, which prompted examination of the crystal structures of both rnNOS-**12** and hnNOS-**12**. As shown in Figures 6A and 6B, the tail amino group in the *meta*-position of the benzene ring may participate in maximal binding interactions with a water-filled polar pocket composed of the carboxylate of propionate A, the side chains of Gln478/Gln483 and Arg481/Arg486, and, most notably, Asp597/Asp602 (rnNOS/hnNOS, respectively), resulting in reduced flexibility in the tail aminomethyl group.

In sharp contrast, the tail aminomethyl group in the heNOS-**12** structure (Fig. 6C) shows a different orientation, making H-bonds with heme propionate A. It is important to note that there is a major difference in the active site of human eNOS, namely, Asn366 replaces Asp597/Asp602 (rnNOS/hnNOS) in the polar pocket noted for nNOS. In earlier studies we found that this Asp/Asn difference makes substantial contributions to isoform selectivity.[22]

This is the likely the basis for the high selectivity observed for **12,** because the aminomethyl group is oriented toward Asp597/Asp602 in the rnNOS/hnNOS structures.

We proposed that homologated analogue **13** could have improved activity because the longer chain might allow it to potentially displace one of the structural waters near the nNOS-specific Asp residue. However, the nNOS inhibitory activity of **13** is weaker, comparable to *para*-substituted derivative **5** (and about two-fold lower than **12**), indicating that either a) this water molecule is not displaced, or b) any energy gained from water displacement does not offset entropic costs of chain elongation, internal torsion, or other negative interactions between the enzyme and inhibitor. The crystal structures of rnNOS-**13** and hnNOS-**13** (Figure 7) support the former hypothesis; the tail amino group does not occupy this polar pocket, but rather only displaces the water molecule bridging propionate A and the H_4B. Consequently, the aminoethyl group can only reach the closer heme propionate A for an electrostatic interaction rather than the farther Asp597/Asp602 site (rnNOS/hnNOS).

Previously, installation of a nitrile at the 5-position of phenyl ether-linked aminoquinolines greatly improved potency, as the nitrile fit into a small, previously undiscovered auxiliary pocket, where it formed a H-bond with a deep structural water and stabilized binding;[8] likewise, 1,3,5-trisubstituted nitrile-containing aminopyridine derivatives[23] exert augmented potency and selectivity via differential interactions with the Asp site (vs. the Asn site in eNOS). For the phenylquinoline scaffold, however, the nitrile is a very deleterious modification [**14**, K_I (rnNOS) = 10,300 nM]. Examination of the crystal structure of **12** (Figure 6A) indicates that the 5-position nitrile of the more compact and rigid phenylquinoline (compared to the more flexible phenyl ether molecule) cannot reach this auxiliary pocket. Instead, the position of the phenyl ring of **14** (just like **12**) would force heme propionate D into a downward conformation; thus, the 5-position nitrile would cause serious clashes with nearby residues. This is another area where the SARs of phenyl ether-linked aminoquinolines and phenylquinolines drastically diverge.

On the basis of the **12**-bound NOS crystal structures (Figure 6), pyridine **15** was expected to be a potent inhibitor. In addition to having an identical binding mode to **12**, the pyridine nitrogen atom forms a hydrogen bond with heme propionate D in all three NOS structures (Figure 8). The aminomethyl group of **15** approaches Gln478 in rnNOS, and is disordered but may point to Asp602 in hnNOS, and heads to the water molecule near heme propionate A in heNOS, where a second molecule of **15** is bound in the pterin site. Nonetheless, the pyridine analogue is approximately 5-fold less potent than **12** in rnNOS, contradicting both the crystallographic observations and previous results for pyridine-containing 2-aminopyridine and 2-aminoquinoline compounds.[7] The unpredicted effect may be electronic, or the pyridine may influence interactions of the aminomethyl group with nearby water molecules.

Constrained Amine Analogues 16–18.

See Supporting Information for details.

4-Alkoxy-3-aminomethyl Analogues 19–29.

Docking studies with **12** also indicated that a variety of groups might be accommodated at position 4 of the phenyl ring (Supporting Information Figure S1). Substituents at this position could form favorable van der Waals interactions with Met336/Met341 or Leu337/His342 (rnNOS/hnNOS), residues that have previously been implicated in high n/eNOS selectivity for 2-aminoquinoline-based inhibitors,[7] and which are replaced by Val104 and Phe105 in heNOS, respectively.[12] To this end, **19–29**, which have a variety of steric, electronic, and H-bonding properties that could provide crucial SAR information, were prepared and assayed for NOS inhibitory potency. In general, small substituent modifications at the 4-position of lead **12**, such as fluorine (**19**), chlorine (**20**), ethyl (**22**), and methoxyl (**23**) do not add additional good contacts in the rat nNOS active site, resulting in a loss of potency. Compound **21** is also a less potent inhibitor given that the trifluoromethyl group of **21** is likely too bulky to fit. However, changing the 4-position methoxyl group (**23**) to an ethoxyl group (**24**) restored the potency in rnNOS. The crystal structure of **24** bound to rnNOS (Figure 9A) shows strong density for the aminoquinoline and central phenyl ring as seen in parent compound **12**. While the aminomethyl moiety occupies the water site between H_4B and propionate A, the ethoxyl group is large enough to establish some contacts with Met336. It seems that as a minimum a 3-atom, nonpolar moiety at the 4-position fits better into rnNOS.

In the hnNOS-**24** structure, the central phenyl ring of **24** flips 180° relative to the orientation seen in rnNOS. The aminomethyl moiety interacts with Asn574 (Figure 9B) and the ethoxyl group still can reach Met341 for contact. It might be that the polar nature of His342 pushes the ethoxyl group away and causes the central phenyl ring to flip. The binding mode of **24** in heNOS (Figure 9C) is almost identical to that observed in rnNOS (Figure 9A). The better nonbonded contacts between the ethoxyl moiety of **24** and the bulky Phe105 side chain makes the inhibitor more ordered in structure and leads to rather low n/e selectivity (164).

Discussion of the small-4-alkoxy-3-aminomethyl and 4-cycloalkoxy analogues (**25–28**) is in the Supporting Information.

A further improvement for rnNOS inhibition was observed by the addition of a small cycloalkyl group (**28** and **29**). The addition of a cyclobutyl tail moiety allows **28** to form van der Waals interactions in the Met336-Leu337-Tyr706 pocket, resulting in good potency with rnNOS (K_i(rnNOS) = 49 nM). The slightly less bulky cyclopropane analogue **29** was found to have even greater rnNOS potency [K_i(rnNOS) = 39 nM], making it the most potent rnNOS inhibitor in the entire series. The X-ray crystal structure of **29** bound to rnNOS (Figure 10A) reveals that the tail cyclopropane ring fits nicely into the hydrophobic pocket surrounded by Met336, Leu337, and Tyr706, with the side chain of Tyr706 occupying two alternate conformations. Propionate D is pushed by **29** into the downward conformation. However, the orientation of the aminomethyl group shows two alternate directions that form H-bonds to either the H_4B site water (as shown in Figure 10A) or with the side chain of Arg481 via water bridging. Compound **29** has a nearly 2-fold increase in rn/miNOS selectivity compared to **12** (**29**, rn/miNOS = 841; **12**, rn/miNOS = 441).

Not only does **29** have high inhibition potency against rnNOS, but it also maintains equally high potency against hnNOS, making it a potent dual rnNOS and hnNOS inhibitor. Similar to the binding mode found in the rnNOS-**29** structure, the central phenyl ring of **29** bound to hnNOS presses into heme propionate D. The polar nature of His342 forces the tail cyclopropyl group to move away from the imidazole side chain, making contacts with Met341 instead. The binding conformation of the tail cyclopropyl group closely overlaps with the tail cyclobutyl group of **28** in the hnNOS-**28** structure, suggesting the placement of the aminomethyl substituent gives rise to the difference in hnNOS activity between **28** and **29**. In hnNOS-**29**, the density for the aminomethyl group is weak. However, there is no sign that the tail amino group interacts with the H_4B site water as is the case in the hnNOS-**28** structure. Rather, there is electron density to support H-bonding with water near Gln483, which is very similar to the binding conformation of the aminomethyl moiety of **12** bound to hnNOS. The positive ammonium group of **29** faces a water-filled pocket noted above for **12** that is influenced by the negative charge of Asp602. In heNOS, again the bulky Phe105 pushes the cyclopropyl group toward heme propionate A, allowing the aminomethyl moiety to make H-bonds with both the propionate and H_4B. The aminomethyl group would not point to the water-filled pocket because there is no negatively charged residue lining the pocket in heNOS. Rather, Asn366 is part of this pocket and is very likely the origin of the 457-fold hn/heNOS selectivity.

4-Phenyloxymethylaryl Analogues 30–37.

Thus far, it appears that considerably larger alkoxyl substituents can be accommodated at the 4-position. Aryl substituents are also tolerated; for example, compound **30**, with its bulky 3-fluorobenzyl group at position 4, is only slightly less potent than **24**, although it is considerably less potent than an aminopyridine-pyrrolidine compound (18 nM) after which it is modeled.[24] This trend is also observed with the benzonitrile ring of **31**; previously, 4-cyanoaryl compounds had good hnNOS activity, but lower hn/heNOS selectivity (generally ~30-fold),[9] but in this phenylquinoline scaffold, the hn/heNOS selectivity is higher with the 4-cyanoaryl group present. However, the hn/heNOS selectivity of **31** remains inferior to leads **5**, **12**, and **24** because of increased binding to heNOS (8300 nM). The unusual crystallographic binding behavior of **31** is discussed in the Supporting Information.

Given the lower hn/heNOS selectivity for **31**, as well as the disfavored binding to the human nNOS active site, we decided to reduce the overall length of the inhibitors to better fit into the hnNOS active site, while maintaining H-bond accepting capability in the tail ring. The 2- and 3-pyridinylmethyl ether groups of **32** and **33**, respectively, were introduced to provide contact with either Leu337 in rnNOS or His342 in hnNOS. Relative to **12**, both pyridinyl modifications provided slight improvements in rnNOS potency (**32**, K_i = 52 nM; **33**, K_i = 44 nM). The crystal structure of rnNOS-**32** with compound **33** overlaid (Figure 11A) shows nearly identical binding positions for the aminoquinoline and tail pyridine, with the pyridinyl nitrogen facing away from Leu337 in both cases (to allow hydrophobic interactions). The difference lies in the orientation of the central phenyl ring. As a result, the central-ring aminomethyl group of **33** displaces the H_4B site water, whereas this moiety points away from the existing water in **32**.

In the hnNOS-**32** structure (Figure 11B), the overall binding remains largely the same, although the orientation of the middle phenyl ring is different in the two nNOS cases. Here, the ring does not press sufficiently against heme propionate D, and the latter is not distorted as seen in the rnNOS-**32** structure. The differences might be the result of the Leu337 (rat) and His342 (human) variation, where the bulkier His342 side chain in human nNOS pushes the tail pyridine of **32** away so that the central phenyl ring does not make such close contacts with heme propionate D. Because of the 2-position of the pyridine nitrogen, a H-bond with the His342 side chain is not possible. Additionally, the position of the aminomethyl group on the phenyl ring has some uncertainty, although some weak electron density supports a likely interaction with Asn574. These deleterious interactions lead to a decreased binding affinity of **32** to hnNOS (K_i = 76 nM). However, by virtue of substantially diminished binding potency towards miNOS and heNOS, the rn/miNOS and hn/heNOS selectivities of **32** remain quite high (rn/miNOS = 879, hn/heNOS = 312).

Compound **32** is unique in that previously reported aminoquinolines substituted with pyridines[3] generally had only 10–20-fold n/eNOS selectivity. However, **32** exhibits fairly good hn/heNOS selectivity (312-fold). The main difference is that in the heNOS-**32** crystal structure (Figure 11C) the orientation of the central phenyl ring is perpendicular to the aminoquinoline ring rather than parallel as in hnNOS-**32**. As a result, the amino group of **32** in heNOS is about 2 Å farther from heme propionate D than it is in hnNOS-**32**. In addition, the amino group in hnNOS-**32** H-bonds with Asn574. These interactions are possible reasons for the good hn/heNOS selectivity.

The 3-pyridylmethyl ether of **33** moderately increases hnNOS potency (K_i = 45 nM for **33** vs. 60 nM for **12**). This is not the first instance that the 3-pyridyl moiety has improved binding to hnNOS,[9,25] although it is the first example where such a compound has equal potency for both the rat and human enzymes. The hnNOS-**33** X-ray structure (Figure 12B) shows good density for the aminoquinoline and central phenyl rings. The tail pyridine portion shows signs of disorder, but a potential H-bond between the pyridine and His342 is more feasible for **33** than for **32**. In the rnNOS-**33** structure, however, the hydrophobic portions of the pyridine about the nonpolar residues Leu337 and Met336 (Figure 12A), suggesting that the pyridine can be either a hydrophobic or a H-bonding moiety depending on the nNOS isoform it is bound to. The aminomethyl moiety of **33** still interacts with Asn574 of hnNOS (Figure 12B), while in rnNOS-**33** it makes an electrostatic interaction with heme propionate A (Figure 12A). Both interactions are favorable, and the results taken together may suggest a reason for equal potency against rat and human enzymes.

In heNOS-**33**, the aminomethyl moiety H-bonds heme propionate A (Figure 12C), rather than pointing out toward Gln247 as in the case of **32** (Figure 11C). How could the pyridinyl nitrogen atom position make such a large difference? The pyridine ring nitrogen atom of **33** can make an extra H-bond with a water molecule next to the H_4B, which pulls the inhibitor closer to heme propionate A and results in better interactions. This may explain the 3-fold improvement in binding affinity of **33** (7700 nM) versus **32** (23,700 nM) toward heNOS, which leads to the poorer n/eNOS selectivity observed for **33** (172-fold).

The incorporation of heterocyclic H-bond acceptors leads to favorable increases in both potency and selectivity. Utilizing heterocycles with the dual ability to form hydrophobic interactions in rnNOS while also forming H-bonding interactions with isoform-specific His342 in hnNOS may be advantageous for *in vivo* studies (where activity in rats is necessary). Considering the importance of the heterocycle, we also sought to exchange the bulky pyridine for smaller heterocycles (as in analogues **34–37**). These compounds all demonstrated high potencies against rnNOS, with K_i values all below 60 nM.

The use of isoxazole (as in **34**) resulted in lost activity against hnNOS. However, 4-(methyloxy)-1,3-thiazole (**35**) resulted in a K_i of 31 nM against hnNOS, making **35** the most potent hnNOS inhibitor in this series. Comparing the X-ray crystal structures of rnNOS-**35** (Figure 13A) and hnNOS-**35** (Figure 13B) reveals a common binding orientation of the aminoquinoline ring, but with differences in the central phenyl ring resulting from different interactions between the thiazole ring and the enzyme. In the rnNOS structure, the thiazole is positioned near Leu337 with its carbon atom making the closest contact. In hnNOS-**35**, the thiazole is near His342, with its S atom facing toward His342 and its N atom H-bonding with a water molecule. The bulkier His342 in hnNOS pushes **35** slightly farther away from the heme than its position in rnNOS. Therefore, the aminomethyl group on the central phenyl ring in hnNOS H-bonds with Asn574, whereas the same moiety points toward Gln478 in rnNOS, and the phenyl ring flips almost 180°. Unfortunately, single digit micromolar inhibitory activity of **35** against miNOS and heNOS results in low rn/mi and hn/heNOS selectivities relative to **32**.

The use of oxazole (**36**) results in a slight loss in hnNOS potency (K_i = 63 nM). However, reduced inhibitory activity against miNOS and heNOS led to excellent selectivities (rn/miNOS = 382, hn/heNOS = 433). Crystallographic details of **36** and **37** are discussed in the Supporting Information.

Human iNOS Inhibition Study.

Recently, we successfully expressed and purified human iNOS protein[21] that showed robust activity. Human iNOS (hiNOS) assay data were collected for eight compounds, including the three simple aminomethyl compounds, **7**, **10**, and **12**, as well as a sampling of the more potent compounds from the latter series (**29**, **32**, **36**, and **37**) to determine the SAR for the human system. K_i values obtained from rat and human nNOS, as well as murine and human iNOS, were used to approximate the cross-species selectivity between lower (rn/mi) and higher order species (hn/hi) (*vide infra*). The major difference between murine and human iNOS that might affect inhibitor binding is that Asn115 in miNOS is Thr121 in hiNOS. The tail part of many inhibitors might reach the site based on observations in the available nNOS and eNOS structures. Without an iNOS-inhibitor structure, we can only speculate on potential interactions by superimposing the iNOS structures onto the known nNOS-inhibitor structures.

The general inhibition trends in Table 2 are more or less consistent (<2-fold) between murine and human iNOS, with only **7** and **33** as the principal exceptions. Compound **7** is a compact inhibitor that makes weaker contacts with the Asn115/Thr121 (miNOS/hiNOS)

site. The two-fold difference in binding affinity might result from the variation in a water-mediated H-bonding network or another unknown reason. Contrarily, overlaying the structure of miNOS or hiNOS on hnNOS-**33** (Figure 14) reveals that the pyridine nitrogen atom of **33** is capable of making a direct H-bond with either Asn115 or Thr121. The three-fold weaker binding affinity to hiNOS might indicate a weaker interaction with Thr121 in hiNOS (than with Asn115 in miNOS). In the same overlay, another variation site, Ser256/Ala262 (miNOS/hiNOS) is more than 5.0 Å from the potential position of the aminomethyl moiety of **33**, likely too far away to influence inhibitor binding.

Directed Mutagenesis Supports Water-mediated Interaction of Inhibitors with Asp597.

Previous studies indicated that Asp597 in rnNOS electrostatically stabilizes cationic inhibitors and can account for much of the e/nNOS selectivity (as this residue is Asn in heNOS). A second difference, Met336 in rnNOS (Val in heNOS), can provide better nonpolar contacts with inhibitors and impart selectivity. To test the importance of these differences further, we determined the K_i values for certain compounds against various rnNOS mutants (Table 3).

All tested compounds exhibited decreased potency against the single mutant enzyme (D597N) (perhaps, as expected), but against the double mutant, all compounds had potency comparable to the single mutant (except for **12,** where it was greatly reduced). Compound **36**, actually displayed 5-fold increased potency against the double mutant (versus the single mutant). The rnNOS-**36** structure shows that the tail end of the inhibitor contacts Met336 and Leu337. These two residues are Val104 and Phe105 in heNOS, and contacts made with the tail end of the inhibitor may involve more than the Met/Val difference. It is possible that the local environment near the Val336 and Leu337 residues in the M336V/D597N double mutant enables better contacts with the tail end of the inhibitor than the same area in the D597N single mutant does, thus improving the potency against the double mutant versus the single mutant. This trend is reflected in the behaviors of **29**, **32**, and **36**, which all have a long tail moiety that fits in this region of the enzyme. On the other hand, more compact inhibitors might be less sensitive to the Met/Val mutation site.

We conclude by focusing on **12**, since this inhibitor exhibits the best hn/heNOS selectivity (877-fold). The D597N mutant decreases potency 8-fold, which further drops to 29-fold against the M336V/D597N mutant – even though this inhibitor does not appear to make contact with the Met/Val site. It is perhaps more instructive to consider the change in ΔG_{bind} obtained from the K_i values, where $\Delta G_{bind} = -RT\ln K_i$. ΔG_{bind} for WT hnNOS, WT heNOS, and the hnNOS D597N mutant are −9.9, −4.5, and −7.3 kcal/mol, respectively. Thus the Asp/Asn difference accounts for about half of $\Delta\Delta G_{bind}$ between heNOS and hnNOS, leaving about −2.6 kcal/mol of binding affinity unexplained. This underscores the limitation of quantitatively explaining selectivity (against isoforms or mutants) by a few simple amino acid differences and a comparison of static X-ray structures. There are clear examples of differences in active site dynamics and the ability of even conserved side chains to adjust to inhibitor binding that could also contribute to selectivity (anchored plasticity) in cases like this.[26]

Off-Target Profiling.

Four structurally diverse compounds from this series (**12**, **29**, **32**, and **33**) were screened by the National Institute of Mental Health's Psychoactive Drug Screening Program (PDSP, Table 4). In this assay,[27] compounds were screened against a panel of 45 pharmacologically relevant CNS targets and receptors using a radioligand displacement assay. Initially, the assay used a primary high dose (10 μM) and then a secondary K_i determination was performed for compounds showing >50% binding in the primary assay. We classify off-target binding using the following rubric: concerning (K_i < 100 nM, or <~2 × nNOS K_i value), moderate (100–300 nM, or ~2–5 × nNOS K_i value), weak (>300 nM, or > ~5 × nNOS K_i value, typically ~1 μM), and insignificant (<50% at 10 μM). The off-target profiles of previous aminoquinolines **1** and **4** have been included for comparison. Although not as effective as **4**, a slight decrease in the fraction of concerning or moderate hits for **32** is observed (11/45 for **32** compared to 15/45 for **1**), while this fraction decreases further to 8/45 for **33**. Unfortunately, most of the flagged targets for **32** and **33** are serotonin receptors, suggesting that the heteroaryl-alkyl tails may resemble a GPCR-ligand-like pharmacophore.[28] Conversely, the off-target profiles for **12** and **29** reveal the cleanest CNS counterscreening observed for 2-aminoquinolines to date, flagging only the H2 and H3 receptors as concerning for **12** and **29**, respectively, which is unsurprising as these receptors are known to bind cationic amidine groups (e.g., ranitidine), while **29** only flagged an additional 4/45 targets for moderate binding.[29] For **12**, 21/45 targets were classified as weak (27/45 for **29**), while 23/45 (**12**) and 13/45 (**29**) were classified as insignificant. These results indicate that reducing the tail group's size (as in **29**) or eliminating it completely (as in **12**) are both effective strategies to reduce off-target CNS binding, which may translate to improved safety *in vivo.*

Membrane Permeability and Microsome Stability.

As our ultimate goal is to utilize these compounds as CNS drugs, membrane permeability for compounds **7**, **12**, **29**, **33** and **37** was determined using the parallel artificial membrane permeability for the blood–brain barrier (PAMPA-BBB) assay. In this assay, an artificial membrane containing BBB phospholipids is used to assess permeability. A compound is predicted to have good BBB penetration and is classified as a "CNS (+)" molecule if its effective permeability (P_e) in this assay is larger than 4.0×10^{-6} cm s^{-1}.[30,31,32,33] Additionally, the web tool SwissADME was used to make *in-silico* passive-BBB penetrability predictions based on their validated BOILED-Egg (Brain Or IntestinaL EstimateD permeation) predictive model.[34,35] Table 5 contains P_e values of three commercial drug standards and selected nNOS inhibitors **7**, **12**, **29**, **33** and **37**. All of the selected nNOS inhibitors are predicted "CNS (+)" with P_e values up to 15.5 × 10–6 cm/s. Compounds **33** and **37** display the lowest permeability among the selected compounds (P_e = $8.09 \pm 0.67 \times 10^{-6}$ cm s^{-1} and $7.04 \pm 2.43 \times 10^{-6}$ cm s^{-1}, respectively), indicating that the presence of the heterocyclic tail portion may reduce the permeability of these compounds. However, while the P_e values for **33** and **37** were high enough to score as "CNS (+)", the BOILED-Egg permeant model predicted they would not have BBB penetration because of their higher tPSA values of 87.05 $Å^2$ and 115.29 $Å^2$, respectively, although these two compounds, along with all the tested compounds, have predicted LogD and LogP values that

are favorable for BBB penetration. Cyclopropyl compound **29**, which lacks **33** and **37**'s polar heterocycles, has a lower tPSA (74.16 $Å^2$), a two-fold higher P_e, and is predicted to be BBB (+). Eliminating the substitution at the 4-position gave mixed results. Although not as high as **29**, compound **7** maintained a high P_e value ($11.3 \pm 1.64 \times 10^{-6}$ cm s^{-1}) relative to **33** and **37**, although compound **12** was found to have the highest P_e out of all compounds assayed. Additional cellular pharmacokinetic assays are in progress.

Additionally, stability in the presence of human liver microsomes (HLM) was determined for **12** and positive control terfenadine. The results of this study (Table 6) show that **12** displays high stability relative to the positive control, as indicated by a half-life ($t_{1/2}$) >60 minutes. However, **12** did show a sign of degradation in buffer control samples (Supporting Information, Table S3).

Conclusions

In summary, we prepared a series of novel 7-phenyl-2-aminoquinolines possessing tail amines designed to target nNOS-specific aspartate residues Asp597/Asp602 (rnNOS/hnNOS), and thereby result in higher n/eNOS selectivity. Initially, screening compounds **5–13** revealed a preference for *meta*-substituted benzylamines, such as **12**, which shows excellent potency and outstanding selectivity for nNOS over the other isozymes. A number of modifications to **12** were made, which included reducing or constraining amino group flexibility, substituting the 4-position of the phenyl ring, and using a 1,3,5-tri-substituted phenyl core. While the amine cannot be constrained effectively, and 1,3,5-tri-substitutions clash deleteriously with heme propionates in the enzyme, some 4-position additions enhance potency and maintain high isoform selectivity *via* favorable interactions with isoform-specific residues on the far end of the substrate access channel, namely, Leu337/His342 (rnNOS/hnNOS). Crystal structures indicate that these compounds act as competitive arginine mimics, where the aminoquinoline forms hydrogen bonds with the active-site glutamate residue, but also that substitutions at the 4-position can reduce phenyl ring rotation to favor interactions with the Asp (Asp597/Asp602)/H_4B/propionate A site over the propionate D site. Mutagenesis studies confirmed the influence of the Asp site on inhibitor potency, making this class of aminoquinolines the first with the ability to target this site in nNOS, although preference for this site varies from compound to compound. Finally, with these inhibitors, the hn/heNOS selectivity derives more from a weakening of affinity to heNOS rather than an increase in affinity for hnNOS; inhibitors more complex than **12** tend to be less selective because of an increased affinity for heNOS. Apparently, more complex substituents provide additional contacts that improve binding to heNOS relative to hnNOS. On the basis of both their good potency and selectivity, clean CNS counterscreening (PDSP) profiles, and excellent permeability in our PAMPA-BBB assay, the most promising compounds, **12** and **29**, are being advanced into preclinical studies.

Experimental Section

General Procedures.

Anhydrous solvents (THF, CH_2Cl_2, MeOH, Et_3N, and DMF) were distilled prior to use. All other solvents, reactants, and reagents were purchased from commercial vendors and were

used without further purification. Methanolic HCl (3 M, for ammonium hydrochloride salt formation and Boc-deprotection) was prepared fresh by the reaction of acetyl chloride and anhydrous MeOH at 0 ˚C. Melting points were determined in capillary tubes using a Buchi melting point B-540 apparatus and are uncorrected. ^{1}H-NMR spectra were recorded at 500 MHz, using a Bruker Avance III 500 (direct cryoprobe), and ^{13}C-NMR spectra were obtained at 126 MHz using the same instrument. High-resolution mass spectral data were obtained at the Integrated Molecular Structure Education and Research Center (IMSERC, Northwestern University) on an Agilent 6210A TOF mass spectrometer in positive ion mode coupled to an Agilent 1200 series HPLC system. Data were processed using MassHunter software version B.04.00. Flash column chromatography was performed using an Agilent 971-FP automated flash purification system with a Varian column station and SiliCycle cartridges (12–80 g, both normal and High Performance). Analytical HPLC was performed using an Agilent Infinity 1260 HPLC system with injection volumes of 5–10 μL. A Phenomenex Luna 5 μm C-8(2) 100 Å column, 50 × 4.60 mm, was used for all HPLC experiments, using a 10-min gradient of 95% H_2O/5% acetonitrile + 0.05% TFA to 95% acetonitrile/5% H_2O + 0.05% TFA, at 1.5 mL/min. *The purity of all final target compounds was found to be ≥95% by HPLC.* Analytical thin-layer chromatography was performed on Silicycle extra-hard 250 μm TLC plates. Compounds were visualized with short-wavelength UV light, and with ninhydrin and CAM stains, where appropriate. The preparation of quinoline precursors and assembly of final compounds is described below, while the preparation of other precursors is discussed in the Supporting Information. Compounds **38**[8], **41**[36], **43**[37], **45**[38], **52**[39], **53**[40], **56**[41], **57**[8], **66**[42], **69**[43], **70**[15], **86**[44], **89**[45], **90**[40], and **96**[46] were prepared by literature procedures or are known, and their spectral or analytical data are identical to those reported.

General Procedure 1: Suzuki Coupling between 39 and Aryl Halides.

Compound **39** (1 eq.), the requisite aryl halide (1–1.2 eq.), Pd(dppf)Cl_2 (5 mol%) and $NaHCO_3$ (3.5–4 eq.) were combined in dimethoxyethane/H_2O (3:1, 4 mL solvent per 0.25 mmol **39** is sufficient) in a 20 mL sealable microwave vial. The mixture was briefly sparged with argon, sealed, and heated to 120 ˚C under microwave irradiation with stirring (720 rpm) for 20–25 minutes. After cooling, the mixture was partitioned between EtOAc and H_2O (10 mL each), the layers were separated, and the aqueous layer was extracted with EtOAc (3 × 30 mL), and the organic layer was washed with 5% aq. NaCl (2 × 50 mL) and sat. aq. NaCl (50 mL), dried over anhydrous sodium sulfate and concentrated. The crude residue was purified as listed below under subheadings for individual compounds.

General Procedure 2: Deprotection of Aminoquinolines.

The protected intermediate was immediately diluted with MeOH (9–10 mL/0.2 mmol of protected quinoline), and K_2CO_3 (2 eq.) was added. The mixture was heated at reflux for 2–2.5 h, cooled, and concentrated, and the residue was partitioned between EtOAc (10 mL) and H_2O/sat. aq. NaCl (1:1, 10 mL). The layers were separated, the aqueous phase was extracted with EtOAc (3 × 20 mL), and the organic layers were combined, washed with sat. aq. NaCl (20 mL), dried over anhydrous sodium sulfate and concentrated. Purification, if necessary, is described below under subheadings for individual compounds. The resulting free 2-aminoquinoline was dissolved in MeOH or ether/MeOH (10–15 mL), filtered to

remove particulate matter, and treated with methanolic HCl (~3 M, ~1.5–2 mL). The mixture was stirred overnight at r.t. and workup (as described below) afforded the deprotected compounds as hydrochloride salts.

7-(4-(2-Aminoethyl)phenyl)-4-methylquinolin-2-amine Dihydrochloride (5).

Compounds **39** (0.050 g, 0.163 mmol) and **41** (0.050 g, 0.167 mmol) were coupled using General Procedure 1. Purification by flash column chromatography, eluting with a gradient of 5% EtOAc in CH_2Cl_2 to 30% EtOAc in CH_2Cl_2, afforded protected phenylquinoline **42** as a white solid (0.052 g, 76%). This compound was immediately deprotected using General Procedure 2. After workup, the free aminoquinoline was diluted in ether/MeOH (1:1, 20 mL), heated gently to affect solution, filtered, and cooled. After treatment with methanolic HCl, **5** was obtained as a cream-colored solid (0.037 g, 86% from **42**) after triturating with ether and drying in vacuo: ^{1}H-NMR (500 MHz; DMSO-d_6): δ 14.09 (s, 1 H), 8.07–7.94 (m, 5 H), 7.81 (dd, J = 8.5, 1.6 Hz, 1 H), 7.75 (d, J = 8.2 Hz, 2 H), 7.46 (d, J = 8.2 Hz, 2 H), 6.93 (s, 1 H), 3.12–3.08 (m, 2 H), 2.96 (t, J = 7.8 Hz, 2 H), 2.65 (s, 3 H); the aminoquinoline –NH protons are mostly broadened into the baseline at 8.1 and 8.9 ppm; ^{13}C-NMR (126 MHz; DMSO-d_6): δ 154.3, 152.6, 143.8, 138.6, 137.4, 136.9, 130.2 (2 C), 127.8 (2 C), 126.7, 123.9, 120.9, 115.4, 112.9, 33.1, 19.4; one of the aliphatic carbon signals is obscured by the solvent peak; HRMS calcd for $C_{18}H_{20}N_3^+$: 278.1652; found, 278.1661.

4-Methyl-7-(4-(2-(methylamino)ethyl)phenyl)quinolin-2-amine Dihydrochloride (6).

Compounds **39** (0.075 g, 0.245 mmol) and **43** (0.079 g, 0.251 mmol) were coupled using General Procedure 1. Purification by flash column chromatography, eluting with a gradient of 5% EtOAc in CH_2Cl_2 to 30% EtOAc in CH_2Cl_2, afforded protected phenylquinoline **58** as a yellow foam (0.070 g, 70%). This compound was immediately deprotected using General Procedure 2. After workup, the free aminoquinoline was passed through a short SiO_2 plug, eluting with 1% MeOH in EtOAc. The filtrate was concentrated, washed with hexanes, and diluted in ether/MeOH (8:1, 20 mL). After treatment with methanolic HCl, **6** was obtained as a flocculent cream-colored solid (0.057 g, 76% from **58**) after filtering, precipitating from MeOH (1 mL) with ether (5 mL) triturating with ether, and drying in vacuo: mp 307–308.3 ˚C (dec). ^{1}H-NMR (500 MHz; DMSO-d_6): δ 14.09 (s, 1 H), 8.86–8.85 (m, 2 H), 8.06 (d, J = 8.5 Hz, 1 H), 7.94 (d, J = 1.7 Hz, 1 H), 7.82 (dd, J = 8.5, 1.7 Hz, 1 H), 7.77–7.75 (m, 2 H), 7.46 (d, J = 8.3 Hz, 2 H), 6.93 (d, J = 1.0 Hz, 1 H), 3.22–3.16 (m, 2 H), 3.02 (t, J = 8.0 Hz, 2 H), 2.66 (d, J = 0.9 Hz, 3 H), 2.59 (t, J = 5.1 Hz, 3 H); the aminoquinoline –NH protons are mostly broadened into the baseline at 8.1 and 8.9 ppm; ^{13}C-NMR (126 MHz; DMSO-d_6): δ 154.33, 152.50, 143.75, 138.36, 137.40, 136.98, 130.14 (2 C), 127.79 (2 C), 126.66, 123.84, 120.89, 115.42, 112.93, 49.36, 32.93, 31.57, 19.41; HRMS calcd for $C_{19}H_{22}N_3^+$: 292.1808; found, 292.1822.

7-(4-(Aminomethyl)phenyl)-4-methylquinolin-2-amine Dihydrochloride (7).

Compounds **39** (0.075 g, 0.245 mmol) and **45** (0.082 g, 0.245 mmol) were coupled using General Procedure 1. Purification by flash column chromatography, eluting with a gradient of 5% EtOAc in CH_2Cl_2 to 40% EtOAc in CH_2Cl_2, afforded protected phenylquinoline **59** as a yellow solid (0.062 g, 63%). This compound was immediately deprotected using

General Procedure 2. After workup, the free aminoquinoline was precipitated from EtOAc (1 mL) with hexanes (9 mL), triturated with hexanes, and diluted in ether/MeOH (5:1). After treatment with methanolic HCl, **7** was obtained as a cream-colored solid (0.043 g, 84% from **59**) after filtering, precipitating twice from hot MeOH (2 mL) with ether (10 mL), washing with ether, and drying in vacuo: mp >300 ˚C (darkens slowly), >360 ˚C (melts or decomposes). ^{1}H-NMR (500 MHz; DMSO-d_6): δ 14.10 (s, 1 H), 9.06 (br s, 1 H), 8.43 (s, 3 H), 8.30 (br s, 1 H), 8.09 (d, J = 8.5 Hz, 1 H), 7.98 (d, J = 1.7 Hz, 1 H), 7.86–7.84 (m, 3 H), 7.67 (d, J = 8.4 Hz, 2 H), 6.95 (d, J = 1.0 Hz, 1 H), 4.13–4.10 (m, 2 H), 2.67 (d, J = 0.9 Hz, 3 H); ^{13}C-NMR (126 MHz; DMSO-d_6): δ 154.3, 152.6, 143.5, 138.9, 136.7, 135.1, 130.3 (2 C), 127.7 (2 C), 126.7, 124.0, 121.0, 115.5, 113.1, 42.3, 19.4; HRMS calcd for $C_{17}H_{18}N_3^+$: 264.1495; found, 264.1503.

4-Methyl-7-(4-((methylamino)methyl)phenyl)quinolin-2-amine Dihydrochloride (8).

Compounds **39** (0.075 g, 0.245 mmol) and **46** (0.085 g, 0.245 mmol) were coupled using General Procedure 1. Purification by flash column chromatography, eluting with a gradient of 5% EtOAc in CH_2Cl_2 to 40% EtOAc in CH_2Cl_2, afforded protected phenylquinoline **60** as a yellow solid (0.072 g, 70%). This compound was immediately deprotected using General Procedure 2. After workup, the free aminoquinoline was precipitated from EtOAc (1 mL) with hexanes (9 mL). The solid was collected and diluted in ether/MeOH (3:1). After treatment with methanolic HCl, ether (10 mL) was added, and **8** was obtained as a cream-colored solid (0.047 g, 78% from **60**) after filtering, precipitating from hot MeOH (2 mL) with ether (10 mL), washing with ether, and drying in vacuo. ^{1}H-NMR (500 MHz; DMSO-d_6): δ 14.06 (s, 1 H), 9.20 (s, 2 H), 9.00 (br s, 1 H), 8.20 (br s, 1 H), 8.08 (d, J = 8.5 Hz, 1 H), 7.97 (d, J = 1.7 Hz, 1 H), 7.86–7.82 (m, 2.0 Hz, 3 H), 7.70 (d, J = 8.3 Hz, 2 H), 6.94 (d, J = 1.0 Hz, 1 H), 4.21–4.19 (m 2 H), 2.66 (d, J = 0.9 Hz, 3 H), 2.58–2.56 (m, 3 H); ^{13}C-NMR (126 MHz; DMSO-d_6): δ 154.3, 152.6, 143.3, 139.4, 136.8, 133.1, 131.3 (2 C), 127.8 (2 C), 126.7, 124.0, 121.1, 115.6, 113.1, 51.2, 32.6, 19.4; HRMS calcd for $C_{18}H_{20}N_3^+$: 278.1652; found, 278.1664.

(*S*)-7-(4-(2-Aminopropyl)phenyl)-4-methylquinolin-2-amine Dihydrochloride (9).

Compounds **39** (0.075 g, 0.245 mmol) and **49** (0.077 g, 0.245 mmol) were coupled using General Procedure 1. Purification by flash column chromatography, eluting with a gradient of 5% EtOAc in CH_2Cl_2 to 35% EtOAc in CH_2Cl_2, afforded protected phenylquinoline **61** as a pale-yellow foam (0.092 g, 87%). This compound was immediately deprotected using General Procedure 2. After workup, the free aminoquinoline was washed with 10:1 hexanes/CH_2Cl_2 (10 mL). The solid was collected and diluted in ether/MeOH (3:1). After treatment with methanolic HCl, the mixture was concentrated, and the residue was azeotroped with toluene twice. After precipitation of the residue from MeOH (1 mL) with ether (10 mL), **9** was obtained as a tan hygroscopic powder (0.058, 75% from **61**) after washing with ether and drying in vacuo: mp >260 ˚C (darkens slowly), 281–282 ˚C (dec). ^{1}H-NMR (500 MHz; DMSO-d_6): δ 14.27 (s, 1 H), 9.00 (br s, 1 H), 8.20 (br s, 1 H), 8.14–8.13 (m, 3 H), 8.06 (d, J = 8.5 Hz, 1 H), 7.96 (d, J = 1.5 Hz, 1 H), 7.82 (dd, J = 8.5, 1.5 Hz, 1 H), 7.76 (d, J = 8.2 Hz, 2 H), 7.45 (d, J = 8.2 Hz, 2 H), 6.94 (s, 1 H), 3.50–3.45 (m, 1 H), 3.10 (dd, J = 13.4, 5.3 Hz, 1 H), 2.78 (dd, J = 13.4, 8.8 Hz, 1 H), 2.66 (s, 3 H), 1.17 (d, J = 6.5 Hz, 3 H). ^{13}C-NMR (126 MHz; DMSO-d_6): δ 154.3, 152.5, 143.8, 138.1, 137.3, 136.8,

130.7 (2 C), 127.7 (2 C), 126.7, 123.9, 120.8, 115.3, 112.9, 48.4, 19.4, 18.2; one of the aliphatic carbons is obscured by the solvent peak; HRMS calcd for $C_{19}H_{22}N_3^+$: 292.1808; found, 292.1818.

7-(2-(Aminomethyl)phenyl)-4-methylquinolin-2-amine Dihydrochloride (10).

Compounds **39** (0.075 g, 0.245 mmol) and **52** (0.070 g, 0.245 mmol) were coupled using General Procedure 1. Purification by flash column chromatography, eluting with a gradient of 5% EtOAc in CH_2Cl_2 to 35% EtOAc in CH_2Cl_2, afforded protected phenylquinoline **62** as pale-yellow crystals (0.098 g, 99%). This compound was immediately deprotected using General Procedure 2. After workup, the free aminoquinoline was diluted in ether/MeOH (5:1). After treatment with methanolic HCl, the mixture was concentrated, and **10** was obtained as a white solid (0.070 g, 86% from **62**) after precipitating twice from hot MeOH (1 mL) with ether (10 mL), washing with ether, and drying in vacuo: mp 290–291.5 ˚C. ^{1}H-NMR (500 MHz; DMSO-d_6): δ 14.21 (s, 1 H), 9.00 (br s, 1 H), 8.42 (s, 3H), 8.30 (br s, 1 H), 8.07 (d, J = 8.4 Hz, 1 H), 7.74 (d, J = 7.6 Hz, 1 H), 7.67 (s, 1 H), 7.59–7.51 (m, 3 H), 7.39–7.38 (m, 1 H), 6.97 (s, 1 H), 3.97 (br d, J = 4.0 Hz, 2 H), 2.67 (s, 3 H); ^{13}C-NMR (126 MHz; DMSO-d_6): δ 154.4, 143.7, 140.4, 132.0, 130.5, 129.29, 129.18, 129.09, 126.4, 126.0, 120.9, 118.7, 113.3, 19.5; two of the quinoline carbons are not visible due to baseline broadening; one of the aliphatic carbon signals is obscured by the solvent peak; HRMS calcd for $C_{17}H_{18}N_3^+$: 264.1495; found, 264.1503.

7-(2-(2-Aminoethyl)phenyl)-4-methylquinolin-2-amine Dihydrochloride (11).

Compounds **39** (0.075 g, 0.245 mmol) and **53** (0.077 g, 0.257 mmol) were coupled using General Procedure 1. Purification by flash column chromatography, eluting with a gradient of 5% EtOAc in CH_2Cl_2 to 35% EtOAc in CH_2Cl_2, afforded protected phenylquinoline **63** as pale-yellow crystals (0.093 g, 90%). This compound was immediately deprotected using General Procedure 2. After workup, the free aminoquinoline was sonicated with hexanes, and the solid was collected and diluted in ether/MeOH (2:1). After treatment with methanolic HCl, the mixture was concentrated, and **11** was obtained as an off-white powder (0.064 g, 83% from **63**) after precipitating twice from hot MeOH (2 mL) with ether (10 mL), washing with ether, and drying in vacuo: mp >300 ˚C (darkens slowly), 323–325 ˚C (dec). ^{1}H-NMR (500 MHz; DMSO-d_6): δ 14.37 (s, 1 H), 8.10 (br s, 1 H), 8.10 (br s, 1 H), 8.07 (d, J = 8.4 Hz, 1 H), 7.92 (s, 3 H), 7.68 (d, J = 1.0 Hz, 1 H), 7.49–7.39 (m, 4 H), 7.30 (d, J = 7.4 Hz, 1 H), 6.98 (s, 1 H), 2.89–2.86 (m, 4 H), 2.67 (s, 3 H); ^{13}C-NMR (126 MHz; DMSO-d_6): δ 154.2, 152.6, 144.9, 140.5, 136.1, 135.1, 130.40, 130.22, 129.1, 127.6, 126.4, 126.1, 120.7, 118.1, 113.1, 30.7, 19.5; one of the aliphatic carbon signals is obscured by the solvent peak; HRMS calcd for $C_{18}H_{20}N_3^+$: 278.1652; found, 278.1664.

7-(3-(2-Aminoethyl)phenyl)-4-methylquinolin-2-amine Dihydrochloride (12).

Compounds **39** (0.075 g, 0.245 mmol) and **56** (0.070 g, 0.245 mmol) were coupled using General Procedure 1. Purification by flash column chromatography, eluting with a gradient of 5% EtOAc in CH_2Cl_2 to 40% EtOAc in CH_2Cl_2, afforded protected phenylquinoline **64** as a yellow foam (0.089 g, 90%). This compound was immediately deprotected using General Procedure 2. After workup, the free aminoquinoline was precipitated from EtOAc

(2 mL) with hexanes (20 mL), and diluted in ether/MeOH (5:1). After treatment with methanolic HCl, **12** was obtained as a cream-colored flocculent solid (0.053 g, 72% from **64**) after filtering, precipitating twice from hot MeOH (2 mL) with ether (10 mL), washing with ether, and drying in vacuo: mp 305.5–306.5 ˚C. ^{1}H-NMR (500 MHz; DMSO-d_6): δ 14.01 (s, 1H), 9.00 (br s, 1 H), 8.41 (s, 3H), 8.25 (br s, 1 H), 8.11 (d, J = 8.5 Hz, 1 H), 7.95–7.93 (m, 2 H), 7.84 (dd, J = 8.4, 1.2 Hz, 1 H), 7.78 (d, J = 7.6 Hz, 1 H), 7.62–7.59 (m, 2 H), 6.94 (s, 1 H), 4.15 (q, J = 5.3 Hz, 2 H), 2.67 (s, 3 H); ^{13}C-NMR (126 MHz; DMSO-d_6): δ 154.4, 143.7, 139.2, 135.6, 130.1, 129.7, 128.3, 127.6, 126.8, 124.0, 121.1, 115.5, 113.2, 42.7, 19.4; two of the quinoline carbons are not visible due to baseline broadening; HRMS calcd for $C_{17}H_{18}N_3^+$: 264.1495; found, 264.1504.

7-(3-(2-Aminoethyl)phenyl)-4-methylquinolin-2-amine Dihydrochloride (13).

Compounds **39** (0.075 g, 0.245 mmol) and **57** (0.077 g, 0.257 mmol) were coupled using General Procedure 1. Purification by flash column chromatography, eluting with a gradient of 5% EtOAc in CH_2Cl_2 to 45% EtOAc in CH_2Cl_2, afforded protected phenylquinoline **65** as a yellow syrup (0.090 g, 88%). This compound was immediately deprotected using General Procedure 2. After workup, the free aminoquinoline was diluted in ether/MeOH (5:1), and after treatment with methanolic HCl, ether (5 mL) was added and **13** was obtained as a tan hygroscopic semisolid (0.053 g, 71% from **65**) after filtering, precipitating twice from hot MeOH (2 mL) with ether (10 mL), washing with ether, and drying in vacuo: ^{1}H-NMR (500 MHz; DMSO-d_6): δ 14.17 (s, 1 H), 9.00 (br s, 1 H), 8.08–8.06 (m, 5 H), 7.95 (d, J = 1.4 Hz, 1 H), 7.84 (dd, J = 8.5, 1.5 Hz, 1 H), 7.66–7.64 (m, 2 H), 7.53 (t, J = 7.8 Hz, 1 H), 7.39 (d, J = 7.6 Hz, 1 H), 6.94 (s, 1 H), 3.17–3.09 (m, 2 H), 3.01 (t, J = 7.8 Hz, 2 H), 2.66 (s, 3 H); ^{13}C-NMR (126 MHz; DMSO-d_6): δ 154.3, 152.6, 144.1, 139.2, 139.0, 136.7, 130.1, 129.6, 128.0, 126.6, 126.1, 124.1, 120.9, 115.5, 113.0, 33.5, 19.4; HRMS calcd for $C_{18}H_{20}N_3^+$: 278.1652; found, 278.1662.

3-(2-Amino-4-methylquinolin-7-yl)-5-(aminomethyl)benzonitrile Dihydrochloride (14).

Compounds **39** (0.075 g, 0.245 mmol) and **67** (0.083 g, 0.269 mmol) were coupled using General Procedure 1. Purification by flash column chromatography, eluting with a gradient of 5% EtOAc in CH_2Cl_2 to 35% EtOAc in CH_2Cl_2, afforded protected phenylquinoline **68** as a yellow foam (0.082 g, 78%). This compound was immediately deprotected using General Procedure 2. After workup, the free aminoquinoline was purified by flash column chromatography, eluting with a gradient of EtOAc to 5% MeOH in EtOAc to yield a white semisolid that was diluted in ether/MeOH (10:1). After treatment with methanolic HCl, ether (5 mL) was added, and **14** was obtained as a cream-colored solid (0.069 g, 68% from **68**) after filtering, precipitating from hot MeOH (2 mL) with ether (10 mL), washing with ether, and drying in vacuo: mp >320 ˚C (darkens) >360 ˚C (melts or decomposes). ^{1}H-NMR (500 MHz; DMSO-d_6): δ 14.15 (s, 1 H), 9.10 (br s, 1 H), 8.63 (s, 3 H), 8.40 (br s, 1 H), 8.34 (s, 1 H), 8.29 (s, 1 H), 8.14 (d, J = 8.5 Hz, 1 H), 8.08 (s, 1 H), 7.99 (d, J = 1.1 Hz, 1 H), 7.91 (dd, J = 8.5, 1.2 Hz, 1 H), 6.99 (s, 1 H), 4.21 (s, 2 H), 2.67 (s, 3 H). ^{13}C-NMR (126 MHz; DMSO-d_6): δ 154.6, 152.5, 141.6, 140.2, 137.2, 136.6, 133.36, 133.19, 131.1, 127.0, 124.1, 121.6, 118.8, 115.9, 113.6, 112.8, 41.9, 19.5; HRMS calcd for $C_{18}H_{17}N_4^+$: 289.1448; found, 289.1459.

7-(5-(Aminomethyl)pyridin-3-yl)-4-methylquinolin-2-amine Trihydrochloride (15).

Compounds **39** (0.075 g, 0.245 mmol) and **70** (0.114 g, 0.294 mmol) were coupled using General Procedure 1. Purification by flash column chromatography, eluting with a gradient of 5% EtOAc in CH_2Cl_2 to 70% EtOAc in CH_2Cl_2, afforded protected phenylquinoline **71** as a white solid (0.080 g, 65%). ^{1}H-NMR confirmed the presence of two Boc groups. This compound was immediately deprotected using General Procedure 2, and after 3 h, an additional equivalent of K_2CO_3 was added to remove one of the Boc groups. The mixture was heated a total of 4.5 h, and after workup, the free aminoquinoline was precipitated from EtOAc (0.5 mL) with hexanes (5 mL), and diluted in ether/MeOH (1:1). After treatment with methanolic HCl, ether (20 mL) was added and **15** was obtained as a tan solid (0.053 g, 90% from **71**) after filtering, precipitating from hot MeOH (5 mL) with ether (10 mL), washing with ether, and drying in vacuo: mp 290–292 ˚C. ^{1}H-NMR (500 MHz; DMSO-d_6): δ 14.18 (s, 1 H), 9.03 (d, J = 2.0 Hz, 1 H), 8.81 (d, J = 1.6 Hz, 1 H), 8.62 (s, 3 H), 8.52 (s, 1 H), 8.17 (d, J = 8.5 Hz, 1 H), 8.01 (d, J = 1.5 Hz, 1 H), 7.91 (dd, J = 8.5, 1.7 Hz, 1 H), 6.99 (s, 1 H), 4.22 (q, J = 5.7 Hz, 2 H), 2.68 (s, 3 H); the pyridinium –NH proton is broadened into residual water around 4 ppm; ^{13}C-NMR (126 MHz; DMSO-d_6): δ 154.5, 152.7, 149.8, 147.5, 140.4, 137.0, 136.5, 134.4, 131.1, 127.2, 124.1, 121.5, 115.7, 113.6, 19.5; one of the aliphatic carbon signals is obscured by the solvent peak; HRMS calcd for $C_{16}H_{17}N_4^+$: 265.1459; found, 265.1464.

7-(Isoindolin-4-yl)-4-methylquinolin-2-amine Dihydrochloride (16).

Compounds **39** (0.075 g, 0.245 mmol) and **73** (0.077 g, 0.257 mmol) were coupled using General Procedure 1. Purification by flash column chromatography, eluting with a gradient of 5% EtOAc in CH_2Cl_2 to 35% EtOAc in CH_2Cl_2, afforded protected phenylquinoline **74** as a yellow gum (0.093 g, 91%). This compound was immediately deprotected using General Procedure 2. After workup, the free aminoquinoline was purified by flash column chromatography, eluting with EtOAc to yield a pale yellow solid. The solid was diluted in ether/MeOH (2:1). After treatment with methanolic HCl, the mixture was concentrated, and the residue was diluted in MeOH (3 mL) and filtered through a small pad of Celite. Reconcentration afforded a residue that was then precipitated three times from hot MeOH (3 mL) with ether (10 mL) to yield **16** as a pale tan solid (0.040 g, 52% from **74**) after washing with ether and drying in vacuo: mp 220–224 ˚C (softens), 233–235 ˚C (dec). ^{1}H-NMR (500 MHz; DMSO-d_6): δ 13.98 (s, 1 H), 9.87 (s, 2 H), 9.00 (br s, 1 H), 8.20 (br s, 1 H), 8.09 (d, J = 8.5 Hz, 1 H), 7.78 (s, 1 H), 7.63 (d, J = 8.3 Hz, 1 H), 7.59–7.53 (m, 3 H), 6.95 (s, 1 H), 4.64 (s, 2 H), 4.61 (s, 2 H), 2.66 (s, 3 H); ^{13}C-NMR (126 MHz; DMSO-d_6): δ 154.4, 152.3, 142.5, 137.1, 136.8, 135.5, 133.5, 129.9, 128.9, 126.6, 124.9, 123.7, 121.1, 117.2, 113.4, 50.5, 50.2, 19.4; HRMS calcd for $C_{18}H_{18}N_3^+$: 276.1495; found, 276.1508.

7-(1-Amino-2,3-dihydro-1*H*-inden-5-yl)-4-methylquinolin-2-amine Dihydrochloride (17).

Compounds **39** (0.075 g, 0.245 mmol) and **79** (0.076 g, 0.245 mmol) were coupled using General Procedure 1. Purification by flash column chromatography, eluting with a gradient of 5% EtOAc in CH_2Cl_2 to 35% EtOAc in CH_2Cl_2, afforded protected phenylquinoline **81** as a yellow foam (0.091 g, 86%). This compound was immediately deprotected using General Procedure 2. After deprotection, the free aminoquinoline was precipitated from

EtOAc (1 mL) with hexanes (20 mL), and the gel-like solid was filtered and diluted in ether/MeOH (2:1). After treatment with methanolic HCl, ether (8 mL) was added, and **17** was obtained as a white solid (0.059 g, 78% from **81**) after precipitating from hot MeOH (5 mL) with ether (10 mL), washing with ether, and drying in vacuo: mp: >300 ˚C (darkens slowly), >340 ˚C (chars). ^{1}H-NMR (500 MHz; DMSO-d_6): δ 13.98 (s, 1 H), 9.00 (br s, 1 H), 8.49 (s, 3 H), 8.10 (br s, 1 H), 8.07 (d, J = 8.5 Hz, 1 H), 7.94 (s, 1 H), 7.82 (dd, J = 8.5, 1.3 Hz, 1 H), 7.76–7.69 (m, 3 H), 3.20–3.14 (m, 1 H), 3.02–2.95 (m, 1 H), 2.57–2.54 (m, 1 H), 2.10–2.03 (m, 1 H); ^{13}C-NMR (126 MHz; DMSO-d_6): δ 154.3, 145.8, 143.9, 140.5, 139.9, 126.7, 126.32, 126.18, 124.10, 124.01, 121.0, 115.8, 113.1, 54.9, 31.0, 30.4, 19.4; two of the quinoline carbons are not visible due to baseline broadening; HRMS calcd for $C_{19}H_{20}N_3^+$: 290.1652; found, 290.1663.

7-(3-Amino-2,3-dihydro-1*H*-inden-5-yl)-4-methylquinolin-2-amine Dihydrochloride (18).

Compounds **39** (0.075 g, 0.245 mmol) and **80** (0.076 g, 0.245 mmol) were coupled using General Procedure 1. Purification by flash column chromatography, eluting with a gradient of 2% EtOAc in CH_2Cl_2 to 35% EtOAc in CH_2Cl_2, afforded protected phenylquinoline **82** as a yellow semisolid (0.093 g, 88%). This compound was immediately deprotected using General Procedure 2. After deprotection, the free aminoquinoline was purified by flash column chromatography, eluting with EtOAc. Concentration afforded a residue that was diluted in MeOH. After treatment with methanolic HCl, the mixture was concentrated, azeotroped with toluene twice, and **18** was obtained as a white solid (0.064 g, 82% from **82)** after precipitating twice from hot MeOH (2 mL) with ether (10 mL), washing with ether, and drying in vacuo: mp 250–256 ˚C (darkens, then chars). ^{1}H-NMR (500 MHz; DMSO-d_6): δ 14.15 (s, 1 H), 9.00 (br s, 1 H), 8.61 (s, 3 H), 8.20 (br s, 1 H), 8.11 (t, J = 4.2 Hz, 2 H), 7.90 (d, J = 1.5 Hz, 1 H), 7.79 (dd, J = 8.5, 1.6 Hz, 1 H), 7.74 (dd, J = 7.9, 1.5 Hz, 1 H), 7.51 (d, J = 7.9 Hz, 1 H), 6.94 (s, 1 H), 4.83–4.80 (m, 1 H), 3.14 (ddd, J = 19.1, 7.1, 4.3 Hz, 1 H), 2.98–2.92 (m, 1 H), 2.58–2.52 (m, 1 H), 2.10–2.03 (m, 1 H); ^{13}C-NMR (126 MHz; DMSO-d_6): δ 154.5, 145.3, 144.1, 141.1, 137.6, 136.8, 128.4, 126.9, 126.2, 124.3, 123.9, 120.9, 115.2, 113.0, 55.1, 31.0, 30.2, 19.4; HRMS calcd for $C_{19}H_{20}N_3^+$: 290.1652; found, 290.1664.

7-(3-(Aminomethyl)-4-fluorophenyl)-4-methylquinolin-2-amine Dihydrochloride (19).

Compounds **39** (0.075 g, 0.245 mmol) and **87** (0.099 g, 0.282 mmol) were coupled using General Procedure 1. Purification by flash column chromatography, eluting with a gradient of 5% EtOAc in CH_2Cl_2 to 35% EtOAc in CH_2Cl_2, afforded protected phenylquinoline **117** as a dark yellow foam (0.088 g, 85%). This compound was immediately deprotected using General Procedure 2. After workup, the free aminoquinoline was diluted in ether/MeOH (5:1). After treatment with methanolic HCl, **19** was obtained as a cream-colored flocculent solid (0.060 g, 81% from **117**) after precipitating from hot MeOH (1 mL) with ether (10 mL), washing with ether, and drying in vacuo: mp 300–302 ˚C (dec). ^{1}H-NMR (500 MHz; DMSO-d_6): δ 14.08 (s, 1 H), 9.05 (br s, 1 H), 8.52 (s, 3 H), 8.25 (br s, 1 H), 8.12–8.08 (m, 2 H), 7.92 (d, J = 1.4 Hz, 1 H), 7.86–7.82 (m, 2 H), 7.49 (t, J = 9.2 Hz, 1 H), 6.95 (s, 1 H), 4.18 (br d, J = 3.2 Hz, 2 H), 2.67 (s, 3 H); ^{13}C-NMR (126 MHz; DMSO-d_6): δ (162.1 + 160.1, 1 C), 154.5, 152.6, 142.8, 136.6, (135.34 + 135.31, 1 C), (130.90 + 130.87), 1 C), (129.99 + 129.92, 1 C), 126.9, 124.0, (122.47 + 122.35, 1 C), (117.05 + 116.87, 1 C), 115.3,

113.2, (36.17 + 36.14, 1 C), 19.5; HRMS calcd for $C_{17}H_{17}FN_3^+$: 282.1401; found, 282.1408.

7-(3-(Aminomethyl)-4-chlorophenyl)-4-methylquinolin-2-amine Dihydrochloride (20).

Compounds **39** (0.075 g, 0.245 mmol) and **88** (0.105 g, 0.282 mmol) were coupled using General Procedure 1. Purification by flash column chromatography, eluting with a gradient of 5% EtOAc in CH_2Cl_2 to 40% EtOAc in CH_2Cl_2, afforded protected phenylquinoline **118** as a yellow foam (0.095 g, 88%). This compound was immediately deprotected using General Procedure 2. After workup, the free aminoquinoline was diluted in ether/MeOH (5:1). After treatment with methanolic HCl, **20** was obtained as a cream-colored powder (0.057 g, 71% from **118**) after precipitating four times from hot MeOH (2 mL) with ether (15 mL), washing with ether, and drying in vacuo: mp 249–250 ˚C (softens slightly), 255–257 ˚C (melts). ^{1}H-NMR (500 MHz; DMSO-d_6): δ 14.13 (s, 1 H), 8.65 (s, 3 H), 8.13–8.11 (m, 2 H), 7.95 (d, J = 1.5 Hz, 1 H), 7.87 (dd, J = 8.5, 1.1 Hz, 1 H), 7.81 (dd, J = 8.4, 2.2 Hz, 1 H), 7.72 (d, J = 8.4 Hz, 1 H), 6.95 (s, 1 H), 4.24 (s, 2 H), 3.39–3.30 (m, 3 H), 2.66 (s, 3 H); the aminoquinoline –NH protons are not visible as discrete peaks, but are broadened into the baseline around 8.4 ppm; ^{13}C-NMR (126 MHz; DMSO-d_6): δ 154.7, 152.5, 142.3, 138.1, 133.8, 132.9, 130.8, 130.0, 129.1, 126.9, 123.8, 121.4, 115.8, 113.3, 19.4; one of the quinoline carbons is not visible due to baseline broadening; one of the aliphatic carbon signals is obscured by the solvent peak; HRMS calcd for $C_{17}H_{17}ClN_3^+$: 298.1106; found, 298.1114.

7-(3-(Aminomethyl)-4-trifluoromethylphenyl)-4-methylquinolin-2-amine Dihydrochloride (21).

Compounds **39** (0.075 g, 0.245 mmol) and **90** (0.100 g, 0.282 mmol) were coupled using General Procedure 1. Purification by flash column chromatography, eluting with a gradient of 5% EtOAc in CH_2Cl_2 to 35% EtOAc in CH_2Cl_2, afforded protected phenylquinoline **119** as a yellow solid (0.102 g, 88%). This compound was immediately deprotected using General Procedure 2. After workup, the free aminoquinoline was purified by flash column chromatography, eluting with EtOAc to yield a pale yellow gum that was diluted in ether/MeOH (10:1). After treatment with methanolic HCl, ether (5 mL) was added, and **21** was obtained as a cream-colored powder (0.054 g, 62% from **119**) after precipitating from hot MeOH (2 mL) with ether (10 mL), washing with ether, and drying in vacuo: mp 327–329 ˚C. ^{1}H-NMR (500 MHz; DMSO-d_6): δ 14.09 (s, 1H), 9.00 (br s, 1 H), 8.30 (br s, 1 H), 8.76 (s, 3 H), 8.31 (s, 1 H), 8.17 (d, J = 8.5 Hz, 1 H), 8.03 (d, J = 1.5 Hz, 1 H), 7.99–7.95 (m, 3 H), 6.98 (s, 1 H), 4.29 (s, 2 H), 2.68 (s, 3 H); ^{13}C-NMR (126 MHz; DMSO-d_6): δ 154.6, 152.4, 143.0, 141.9, 136.8, 133.6, 130.2, 127.82, (127.77 + 127.73 + 127.68 + 127.64 + 127.59, 1 C), (127.49 + 127.3, 1 C), (125.6 + 123.4, 1 C), 127.0, 124.2, 121.7, 116.1, 113.7, 39.14, 39.13, 19.5; the splitting of the signals for the trifluoromethyl group and nearby carbons is partially obscured by other signals; HRMS calcd for $C_{18}H_{17}F_3N_3^+$: 332.1369; found, 332.1383.

7-(3-(Aminomethyl)-4-ethylphenyl)-4-methylquinolin-2-amine Dihydrochloride (22).

Compounds **39** (0.060 g, 0.196 mmol) and **95** (0.065 g, 0.206 mmol) were coupled using General Procedure 1. Purification by flash column chromatography, eluting with a gradient of 5% EtOAc in CH_2Cl_2 to 35% EtOAc in CH_2Cl_2, afforded protected phenylquinoline **120** as a cream-colored solid (0.074 g, 87%). This compound was immediately deprotected using General Procedure 2. After workup, the free aminoquinoline was triturated with 5% EtOAc in hexanes and the solid was collected, washed with hexanes, diluted in EtOAc, filtered, and concentrated. The residue was diluted in ether/MeOH (6:1). After treatment with methanolic HCl, the mixture was concentrated, and **22** was obtained as a an off-white solid (0.035 g, 56% from **120**) after precipitating three times from hot MeOH (1.5 mL) with ether (10 mL), washing with ether, and drying in vacuo: mp 307–309 ˚C. ^{1}H-NMR (500 MHz; DMSO-d_6): δ 14.06 (s, 1 H), 9.05 (br s, 1 H), 8.48 (s, 3 H), 8.25 (br s, 1 H), 8.10 (d, J = 8.5 Hz, 1 H), 7.94 (t, J = 2.2 Hz, 2 H), 7.88 (dd, J = 8.5, 1.6 Hz, 1 H), 7.73 (dd, J = 8.0, 1.8 Hz, 1 H), 7.46 (d, J = 8.1 Hz, 1 H), 6.94 (d, J = 0.6 Hz, 1 H), 4.16–4.13 (m, 2 H), 2.76 (q, J = 7.5 Hz, 2 H), 2.65 (s, 3 H), 1.22 (t, J = 7.5 Hz, 3 H); ^{13}C-NMR (126 MHz; DMSO-d_6): δ 154.4, 152.7, 143.71, 143.55, 136.65, 136.54, 133.1, 130.0, 128.6, 127.6, 126.7, 124.0, 120.9, 115.0, 113.0, 39.5, 25.1, 19.5, 15.4; HRMS calcd for $C_{19}H_{22}N_3^+$: 292.1808; found, 292.1815.

7-(3-(Aminomethyl)-4-methoxyphenyl)-4-methylquinolin-2-amine Dihydrochloride (23).

Compounds **39** (0.075 g, 0.245 mmol) and **98** (0.085 g, 0.269 mmol) were coupled using General Procedure 1. Purification by flash column chromatography, eluting with a gradient of 5% EtOAc in CH_2Cl_2 to 40% EtOAc in CH_2Cl_2, afforded protected phenylquinoline **121** as a yellow foam (0.077 g, 72%). This compound was immediately deprotected using General Procedure 2. After workup, the free aminoquinoline was triturated with hexanes. The solid was collected and diluted in ether/MeOH (8:1). After treatment with methanolic HCl, **23** was obtained as a yellow amorphous solid (0.057 g, 88% from **121**) after precipitating from hot MeOH (5 mL) with ether (10 mL), washing with ether, and drying in vacuo: mp 232–234 ˚C. ^{1}H-NMR (500 MHz; DMSO-d_6): δ 14.16 (s, 1 H), 9.00 (br s, 1 H), 8.34–8.30 (2 br s, 4 H), 8.07 (d, J = 8.6 Hz, 1 H), 7.91 (d, J = 2.2 Hz, 1H), 7.90 (d, J = 1.4 Hz, 1 H), 7.82 (ddd, J = 8.5, 4.7, 2.0 Hz, 2 H), 7.26 (d, J = 8.7 Hz, 1 H), 6.93 (s, 1 H), 4.08 (q, J = 5.3 Hz, 2 H), 3.92 (s, 3 H), 2.65 (s, 3 H); ^{13}C-NMR (126 MHz; DMSO-d_6): δ 158.3, 154.4, 152.7, 143.5, 136.7, 130.8, 129.7, 129.3, 126.7, 123.7, 123.1, 120.5, 114.5, 112.7, 112.4, 56.4, 38.1, 19.4; HRMS calcd for $C_{18}H_{20}N_3O^+$: 294.1601; found, 294.1611.

7-(3-(Aminomethyl)-4-ethoxyphenyl)-4-methylquinolin-2-amine Dihydrochloride (24).

Compounds **39** (0.075 g, 0.245 mmol) and **101** (0.089 g, 0.269 mmol) were coupled using General Procedure 1. Purification by flash column chromatography, eluting with a gradient of 5% EtOAc in CH_2Cl_2 to 40% EtOAc in CH_2Cl_2, afforded protected phenylquinoline **122** as a cream-colored solid (0.072 g, 65%). This compound was immediately deprotected using General Procedure 2. After workup, the free aminoquinoline was triturated with hexanes. The solid was collected and diluted in ether/MeOH (2:1). After treatment with methanolic HCl, **24** was obtained as a yellow glassy solid (0.060 g, 99% from **122**) after washing with 2% MeOH in ether, diluting in MeOH and reconcentrating, washing with ether, and drying in vacuo: mp 250 ˚C softens), 265–267 ˚C (bubbles, melts). ^{1}H-NMR (500 MHz; DMSO-

d_6): δ 14.23 (s, 1 H), 9.07 (br s, 1 H), 8.39 (s, 3 H), 8.25 (br s, 1 H), 8.07 (d, J = 8.6 Hz, 1 H), 7.92 (d, J = 2.1 Hz, 1 H), 7.89 (d, J = 1.2 Hz, 1 H), 7.82 (dd, J = 8.5, 1.4 Hz, 1 H), 7.78 (dd, J = 8.6, 2.2 Hz, 1 H), 7.24 (d, J = 8.7 Hz, 1 H), 6.93 (s, 1 H), 4.18 (br q, J = 6.9 Hz, 2 H), 4.07 (d, J = 5.4 Hz, 2 H), 2.65 (s, 3 H), 1.42 (t, J = 6.9 Hz, 3 H); ^{13}C-NMR (126 MHz; DMSO-d_6): δ 157.5, 154.4, 152.6, 143.5, 136.7, 130.6, 129.6, 129.2, 126.7, 123.7, 123.1, 120.5, 114.4, 113.0, 112.7, 64.5, 37.9, 19.4, 15.0; HRMS calcd for $C_{19}H_{22}N_3O^+$: 308.1757; found, 308.1772.

7-(3-(Aminomethyl)-4-propoxyphenyl)-4-methylquinolin-2-amine Dihydrochloride (25).

Compounds **39** (0.075 g, 0.245 mmol) and **104** (0.093 g, 0.269 mmol) were coupled using General Procedure 1. Purification by flash column chromatography, eluting with a gradient of 5% EtOAc in CH_2Cl_2 to 35% EtOAc in CH_2Cl_2, afforded protected phenylquinoline **123** as an off-white solid (0.083 g, 73%). This compound was immediately deprotected using General Procedure 2. After deprotection, the free aminoquinoline was triturated with 5% EtOAc in hexanes (15 mL), and the obtained solid was diluted in ether/MeOH (2:1). After treatment with methanolic HCl, the mixture was concentrated, the residue was azeotroped twice with toluene, and **25** was obtained as a yellow glassy solid (0.044 g, 62% from **123**) after precipitating twice from hot MeOH (2 mL) with ether (10 mL), and drying in vacuo: mp 220 ˚C (softens), 264–266 ˚C (bubbles, melts). ^{1}H-NMR (500 MHz; DMSO-d_6): δ 14.06 (s, 1H), 9.00 (br s, 1 H), 8.32 (s, 4 H), 8.07 (d, J = 8.5 Hz, 1 H), 7.91 (d, J = 2.2 Hz, 1 H), 7.89 (d, J = 1.4 Hz, 1 H), 7.82 (dd, J = 8.6, 1.2 Hz, 1 H), 7.78 (dd, J = 8.6, 2.3 Hz, 1 H), 7.25 (d, J = 8.7 Hz, 1 H), 6.91 (s, 1 H), 4.09 (br t, J = 6.5 Hz, 4 H), 2.63 (t, J = 1.8 Hz, 3 H), 1.83 (sextet, J = 7.0 Hz, 2 H), 1.03 (t, J = 7.4 Hz, 3 H); ^{13}C-NMR (126 MHz; DMSO-d_6): δ 157.6, 154.4, 143.51, 130.7, 129.4, 129.2, 126.7, 123.6, 123.2, 120.6, 114.6, 113.1, 112.7, 70.2, 37.8, 22.4, 19.4, 10.9; two of the quinoline carbons are not visible due to baseline broadening; HRMS calcd for $C_{20}H_{24}N_3O^+$: 322.1914; found, 322.1927.

7-(3-(Aminomethyl)-4-isopropoxyphenyl)-4-methylquinolin-2-amine Dihydrochloride (26).

Compounds **39** (0.075 g, 0.245 mmol) and **105** (0.093 g, 0.269 mmol) were coupled using General Procedure 1. Purification by flash column chromatography, eluting with a gradient of 5% EtOAc in CH_2Cl_2 to 35% EtOAc in CH_2Cl_2, afforded protected phenylquinoline **124** as an off-white solid (0.083 g, 73%). This compound was immediately deprotected using General Procedure 2. After deprotection, the free aminoquinoline was precipitated from EtOAc (1 mL) with hexanes (10 mL) and the obtained solid was diluted in ether/MeOH (4:1). After treatment with methanolic HCl, the mixture was concentrated and azeotroped twice with toluene, and **26** was obtained as an off-white solid (0.0097 g, 14% from **124**) after precipitating twice from hot MeOH (1 mL) with ether (10 mL), washing with ether, and drying in vacuo: mp 237–239 ˚C (softens), 245–246 ˚C (melts). ^{1}H-NMR (500 MHz; DMSO-d_6): δ 13.97 (s, 1 H), 9.00 (br s, 1 H), 8.26 (br s, 4 H), 8.07 (d, J = 8.6 Hz, 1 H), 7.89 (d, J = 9.5 Hz, 2 H), 7.81 (d, J = 8.3 Hz, 1 H), 7.77 (d, J = 8.7 Hz, 1 H), 7.28 (d, J = 8.4 Hz, 1 H), 6.91 (s, 1 H), 4.81–4.75 (m, 1 H), 4.06 (d, J = 4.9 Hz, 2 H), 2.66 (s, 3 H), 1.37 (d, J = 6.0 Hz, 6 H; ^{13}C-NMR (126 MHz; DMSO-d_6): δ 156.5, 154.5, 152.5, 143.5, 136.9, 130.4, 129.5, 129.0, 126.7, 123.80, 123.61, 120.5, 114.5, 114.2, 112.7, 71.0, 37.9, 22.2 (2 C), 19.4; HRMS calcd for $C_{20}H_{24}N_3O^+$: 322.1914; found, 322.1933.

7-(3-(Aminomethyl)-4-isobutoxyphenyl)-4-methylquinolin-2-amine Dihydrochloride (27).

Compounds **39** (0.050 g, 0.163 mmol) and **106** (0.058 g, 0.160 mmol) were coupled using General Procedure 1. Purification by flash column chromatography, eluting with a gradient of 5% EtOAc in CH_2Cl_2 to 35% EtOAc in CH_2Cl_2, afforded protected phenylquinoline **125** as a yellow (0.056 g, 72%). This compound was immediately deprotected using General Procedure 2. After deprotection, the free aminoquinoline was diluted in MeOH (10 mL), filtered, and diluted with 4 mL ether. After treatment with methanolic HCl, the mixture was concentrated and azeotroped with toluene twice to yield **27** as a cream-colored solid (0.043 g, 90% from **125**) after precipitating from MeOH (2 mL) with ether (15 mL), washing with ether, and drying in vacuo: mp: 283–285 ˚C (softens, bubbles), 308 ˚C (chars). ^{1}H-NMR (500 MHz; DMSO-d_6): δ 13.85 (s, 1 H), 8.26 (s, 3 H), 8.08 (d, J = 8.5 Hz, 1 H), 7.89 (dd, J = 8.8, 1.6 Hz, 2 H), 7.82–7.78 (m, 2 H), 7.26 (d, J = 8.7 Hz, 1 H), 6.90 (s, 1 H), 4.11 (q, J = 5.4 Hz, 2 H), 3.91 (d, J = 6.5 Hz, 2 H), 2.66 (s, 3 H), 2.16–2.10 (m, 1 H), 1.04 (d, J = 6.7 Hz, 6 H); the aminoquinoline –NH protons are broadened into the baseline around 8.5 ppm; ^{13}C-NMR (126 MHz; DMSO-d_6): δ 157.5, 154.4, 152.7, 143.5, 130.7, 129.23, 129.12, 126.7, 123.6, 123.2, 120.6, 114.5, 113.1, 112.7, 74.8, 37.7, 28.1, 19.60, 19.43; one of the aminoquinoline carbons is not visible due to baseline broadening; HRMS calcd for $C_{21}H_{26}N_3O^+$: 336.2070; found, 336.2080.

7-(3-(Aminomethyl)-4-(cyclobutylmethoxy)phenyl)-4-methylquinolin-2-amine Dihydrochloride (28).

Compounds **39** (0.082 g, 0.270 mmol) and **107** (0.110 g, 0.300 mmol) were coupled using General Procedure 1. Purification by flash column chromatography, eluting with a gradient of 5% EtOAc in CH_2Cl_2 to 80% EtOAc in CH_2Cl_2, afforded protected phenylquinoline **126** as a tan foam (0.052 g, 40%). A portion of this compound (0.04 g) was immediately deprotected using General Procedure 2. After workup, the free aminoquinoline was taken up in MeOH (1.0 mL) and treated with methanolic HCl for 18h. The mixture was concentrated to minimal solvent and triturated with ether (10 mL) 3 × to afford **28** as an off-white solid (0.031 g, 88% from **126**) after filtering, washing with ether, and drying in vacuo: mp 83–84 ˚C (softens) >209.5 ˚C (darkens) >241.2 ˚C (dec) ^{1}H-NMR (500 MHz, DMSO-d_6) δ 14.38 (s, 1 H), 9.20 (bs, 1 H), 8.58 (s, 3 H), 8.28 (bs, 1 H), 8.05 (d, J = 8.4 Hz, 1 H), 7.97 (d, J = 2.3 Hz, 1H), 7.88 (d, J = 1.7 Hz, 1H), 7.84 (dd, J = 8.6, 1.7 Hz, 1 H), 7.75 (dd, J = 8.6, 2.4 Hz, 1 H), 7.24 (d, J = 8.6 Hz, 1 H), 6.96 (s, 1 H), 4.09 (d, J = 6.4 Hz, 2 H), 4.06 (d, J = 5.3 Hz, 2 H), 2.81 (hept, J = 7.0 Hz, 1 H), 2.64 (s, 3 H), 2.18 – 2.05 (m, 2 H), 1.99 – 1.82 (m, 4 H). ^{13}C-NMR (126 MHz, DMSO-d_6) δ 156.97, 153.88, 151.95, 143.00, 135.99, 130.05, 128.66, 128.37, 126.08, 123.12, 122.73, 119.86, 113.68, 112.59, 112.08, 71.86, 36.84, 33.78, 24.15, 18.85, 18.07; one of the aminoquinoline carbons is not visible due to baseline broadening; HRMS calcd for $C_{22}H_{26}N_3O^+$: 348.2076; found, 348.2073.

7-(3-(Aminomethyl)-4-(cyclopropylmethoxy)phenyl)-4-methylquinolin-2-amine Dihydrochloride (29).

Compound **108** (0.078 g, 0.219 mmol), tetrahydroxydiboron (0.059 g, 0.77 mmol), KOAc (0.064 g, 0.66 mmol), XPhos-Pd-G3 (2.4 mg, 2.8 μmol), and XPhos (2.6 mg, 5.5 μmol) were added to an oven-dried glass vial equipped with a Teflon-lined cap.[47] EtOH (2.2 mL,

degassed) was then added to the reaction vessel and a nitrogen stream was allowed to bubble through the solution at room temperature for 15 min with stirring. The vessel was then sealed, and the reaction mixture was heated to 80 °C for 2 h. The reaction was then allowed to cool to ambient temperatures before 3 equiv (0.364 mL, 0.66 mmol) of 1.8 M degassed aqueous K_2CO_3 was added via syringe followed by compound **38** (0.055 g, 0.20 mmol). The reaction vial was degassed with argon, resealed with a Teflon-lined cap, and left to stir at 80 °C for an additional 15 h. The reaction mixture was cooled to room temperature and partitioned between EtOAc and H_2O (20 mL each). The layers were separated, the aqueous layer was extracted with EtOAc (3 × 20 mL), the organic layer was washed with 5% aq. NaCl (2 × 20 mL) and sat. aq. NaCl (20 mL), dried over anhydrous sodium sulfate, and concentrated. Purification by flash column chromatography, eluting with a gradient of 5% EtOAc in CH_2Cl_2 to 90% EtOAc in CH_2Cl_2, afforded protected phenylquinoline **127** as a colorless solid (0.073 g, 78%). A portion of this compound (0.069 g) was immediately deprotected using General Procedure 2. After workup, the free aminoquinoline was taken up in MeOH (3.0 mL) and treated with methanolic HCl for 18 h, and concentrated to dryness. The title compound (**29**) was obtained as a yellow-colored solid (0.029 g, 49% from **127**) after reverse phase flash column chromatography, eluting through a 15.5 g C18 RediSep RF Gold cartridge column with a gradient of 100% water to 100% acetonitrile, azeotropic removal of water with toluene, and drying in vacuo: mp >193.5 ˚C (foam dec) ^{1}H-NMR (500 MHz, DMSO-d_6) δ 14.30 (s, 1 H), 8.50 (s, 3 H), 8.06 (d, J = 8.5 Hz, 1 H), 7.95 (d, J = 2.4 Hz, 1 H), 7.89 (d, J = 1.7 Hz, 1 H), 7.83 (dd, J = 8.6, 1.8 Hz, 1 H), 7.75 (dd, J = 8.7, 2.4 Hz, 1 H), 7.23 (d, J = 8.7 Hz, 1 H), 6.99 – 6.87 (m, 1 H), 4.09 (d, J = 5.0 Hz, 2 H), 3.99 (d, J = 6.9 Hz, 2 H), 2.65 (s, 3 H), 1.33 (tt, J = 7.3, 5.0 Hz, 1 H), 0.61 (td, J = 7.7, 6.1, 4.5 Hz, 2 H), 0.41 (q, J = 4.9 Hz, 2 H); ^{13}C NMR (126 MHz, DMSO-d_6) δ 156.93, 153.87, 151.99, 142.97, 136.11, 130.08, 128.75, 128.43, 126.09, 123.08, 122.71, 119.91, 113.79, 112.80, 112.10, 72.70, 37.08, 18.84, 9.93, 3.01; HRMS calcd for $C_{21}H_{24}N_3O^+$: 334.1914; found, 334.1910.

7-(3-(Aminomethyl)-4-((3-fluorobenzyl)oxy)phenyl)-4-methylquinolin-2-amine Dihydrochloride (30).

Compounds **39** (0.060 g, 0.196 mmol) and **109** (0.090 g, 0.216 mmol) were coupled using General Procedure 1. Purification by flash column chromatography, eluting with a gradient of 5% EtOAc in CH_2Cl_2 to 35% EtOAc in CH_2Cl_2, afforded protected phenylquinoline **128** as a brown foam (0.078 g, 76%). This compound was immediately deprotected using General Procedure 2. After deprotection, the free aminoquinoline was purified by passing through a short plug of SiO_2, washing with EtOAc and then 10% MeOH in EtOAc. Concentration afforded a residue that was diluted in ether/MeOH (2:1). After treatment with methanolic HCl, the mixture was concentrated, and **30** was obtained as a white solid (0.057 g, 84% from **128**) after precipitating twice from MeOH (2 mL) with ether (10 mL), and drying in vacuo: mp 242–243.5 ˚C. ^{1}H-NMR (500 MHz; DMSO-d_6): δ 14.00 (s, 1 H), 9.00 (br s, 1 H), 8.35 (br s, 4 H), 8.07 (d, J = 8.5 Hz, 1 H), 7.94 (d, J = 2.2 Hz, 1 H), 7.89 (d, J = 1.4 Hz, 1 H), 7.81 (ddd, J = 12.4, 8.8, 1.8 Hz, 2 H), 7.50–7.46 (m, 1 H), 7.43–7.38 (m, 2 H), 7.29 (d, J = 8.7 Hz, 1 H), 7.19 (td, J = 8.7, 2.2 Hz, 1 H), 6.91 (s, 1 H), 4.16 (br q, J = 5.5 Hz, 2 H), 2.65 (s, 3 H); ^{13}C-NMR (126 MHz; DMSO-d_6): δ (163.8 +161.8, 1 C) 157.0, 154.4, 152.8, 143.4, (140.16 + 140.10, 1 C), 131.19, (131.06 + 130.99, 1 C), 129.7, 129.2, 126.7,

123.88, (123.86 + 123.67, 1 C), 123.5, 120.6, (115.31 + 115.15, 1 C), (114.74 + 114.57, 1 C), 113.6, 112.8, 69.4, 37.9, 19.4; three of the quinoline and aryl ring carbons are not visible because of baseline broadening; HRMS calcd for $C_{24}H_{23}FN_3O^+$: 388.1820; found, 388.1828.

4-((4-(2-Amino-4-methylquinolin-7-yl)-2-(aminomethyl)phenoxy)methyl)benzonitrile Dihydrochloride (31).

Compounds **39** (0.075 g, 0.245 mmol) and **110** (0.102 g, 0.245 mmol) were coupled using General Procedure 1. After workup, the crude residue was suspended in EtOAc/ether (1:1) and filtered through a small pad of Celite overlaid with silica. The filtrate was concentrated to yield a residue that was washed with 5% hexanes/EtOAc (30 mL) to afford **129** as a white solid (0.073 g, 56%) after washing with hexanes. This compound was immediately deprotected using General Procedure 2. After deprotection, the free aminoquinoline was purified by flash column chromatography, eluting with a gradient of EtOAc to 2% MeOH in EtOAc to yield a white solid that was diluted in ether/MeOH (2:1). After treatment with methanolic HCl, the mixture was concentrated, the residue was azeotroped with toluene, and **31** was obtained as a white solid (0.054 g, 84% from **129**) after precipitating twice from MeOH (3 mL) with ether (15 mL), and drying in vacuo: mp 280–282 ˚C. ^{1}H-NMR (500 MHz; DMSO-d_6): δ 14.03 (s, 1 H), 8.37 (s, 3 H), 8.06 (d, J = 8.4 Hz, 1 H), 7.94–7.88 (m, 4 H), 7.80–7.75 (m, 4 H), 7.27 (d, J = 8.5 Hz, 1 H), 6.90 (s, 1 H), 5.40 (s, 2 H), 4.17 (s, 2 H), 2.64 (s, 3 H); the aminoquinoline –NH protons are not visible as discrete peaks, but are broadened into the baseline around 8.4 and 7.9 ppm; ^{13}C-NMR (126 MHz; DMSO-d_6): δ 19.38, 37.79, 69.30, 111.09, 112.77, 113.52, 115.19, 119.23, 120.72, 123.49, 126.60, 128.52, 129.11, 129.80, 131.43, 132.93, 143.01, 143.16, 154.74, 156.78; three of the aminoquinoline and aryl carbons are not visible because of baseline broadening; HRMS calcd for $C_{25}H_{23}N_4O^+$: 395.1866; found, 395.1872.

7-(3-(Aminomethyl)-4-(pyridin-2-ylmethoxy)phenyl)-4-methylquinolin-2-amine Trihydrochloride (32).

Compounds **39** (0.075 g, 0.245 mmol) and **111** (0.096 g, 0.245 mmol) were coupled using General Procedure 1. Purification by flash column chromatography, eluting with a gradient of 10% EtOAc in CH_2Cl_2 to 85% EtOAc in CH_2Cl_2, afforded protected phenylquinoline **130** as a white powder (0.091 g, 72%) after precipitating from EtOAc (1 mL) with hexanes (20 mL). This compound was immediately deprotected using General Procedure 2. After deprotection, the free aminoquinoline was purified by flash column chromatography, eluting with a gradient of EtOAc to 15% MeOH in EtOAc. Concentration afforded a residue that was diluted in MeOH. After treatment with methanolic HCl, the mixture was concentrated, the residue was azeotroped three times with toluene, and **32** was obtained as a white powder (0.063 g, 74% from **130**) after precipitating three times from MeOH (5 mL) with ether (10 mL), washing with ether, and drying in vacuo: mp 231–233 ˚C (dec). ^{1}H-NMR (500 MHz; DMSO-d_6): δ 14.08 (s, 1 H), 9.04 (br s, 1 H), 8.66 (d, J = 4.8 Hz, 1 H), 8.46 (s, 3 H), 8.22 (br s, 1 H), 8.08 (d, J = 8.6 Hz, 1 H), 7.99 (t, J = 7.3 Hz, 1 H), 7.94 (d, J = 2.3 Hz, 1 H), 7.89 (d, J = 1.6 Hz, 1 H), 7.82 (dd, J = 8.6, 1.7 Hz, 1 H), 7.79 (dd, J = 8.6, 2.3 Hz, 1 H), 7.72 (d, J = 7.8 Hz, 1 H), 7.49 (t, J = 6.1 Hz, 1 H), 7.33 (d, J = 8.7 Hz, 1 H), 6.92 (s, 1 H), 4.21 (d, J = 5.7 Hz, 2 H); the pyridinium –NH proton is broadened into residual water around 4.3 ppm;

^{13}C-NMR (126 MHz; DMSO-d_6): δ 157.1, 156.0, 154.4, 152.7, 148.7, 143.4, 139.0, 136.6, 131.5, 130.0, 129.3, 126.8, 124.2, 123.73, 123.67, 122.8, 120.6, 114.6, 113.8, 112.8, 70.4, 38.3, 19.4; HRMS calcd for $C_{23}H_{23}N_4O^+$: 371.1866; found, 371.1880.

7-(3-(Aminomethyl)-4-(pyridin-3-ylmethoxy)phenyl)-4-methylquinolin-2-amine Trihydrochloride (33).

Compounds **39** (0.075 g, 0.245 mmol) and **112** (0.096 g, 0.245 mmol) were coupled using General Procedure 1. As the product was poorly soluble in EtOAc, the aqueous layer was extracted with 200 mL of EtOAc during the workup. After concentration, the residue was washed with 50% hexanes/EtOAc (30 mL) to afford **131** as an off-white solid (0.100 g, 80%) after washing with hexanes. This compound was immediately deprotected using General Procedure 2. After deprotection, the free aminoquinoline was purified by flash column chromatography, eluting with a gradient of 3% MeOH in EtOAc to 15% MeOH in EtOAc to yield a colorless foam. This was diluted with ether/MeOH (1:1). After treatment with methanolic HCl, the mixture was concentrated, and **33** was obtained as a pale orange solid (0.062 g, 66% from **131**) after precipitating twice from hot MeOH (1 mL) with ether (10 mL), washing with ether, and drying in vacuo: mp 238–240 ˚C (softens) 248–250 ˚C (melts). ^{1}H-NMR (500 MHz; DMSO-d_6): δ 14.07 (s, 1H), 9.00 (br s, 1 H), 8.94 (s, 1 H), 8.72 (d, J = 4.7 Hz, 1 H), 8.39 (s, 3 H), 8.30 (d, J = 6.9 Hz, 1 H), 8.25 (br s, 1 H), 8.08 (d, J = 8.6 Hz, 1 H), 7.95 (d, J = 2.1 Hz, 1 H), 7.90 (d, J = 1.3 Hz, 1 H), 7.84–7.81 (m, 2 H), 7.74–7.72 (m, 1 H), 7.35 (d, J = 8.7 Hz, 1 H), 6.93 (s, 1 H), 5.40 (s, 2 H), 4.15 (q, J = 5.5 Hz, 3 H), 2.66 (s, 3 H); the pyrdinium –NH proton is broadened into residual water around 4.0 ppm; ^{13}C-NMR (126 MHz; DMSO-d_6): δ 156.9, 154.4, 152.8, 146.9, 143.4, 136.6, 134.4, 131.4, 130.0, 129.3, 126.8, 125.4, 123.74, 123.55, 120.6, 114.5, 113.6, 112.8, 67.5, 37.9, 19.4; one of the quinoline carbons is not visible due to baseline broadening; ^{13}C-NMR (126 MHz; DMSO-d_6): δ 157.1, 156.0, 154.4, 152.7, 148.6, 143.4, 139.0, 136.6, 131.5, 130.0, 129.3, 126.8, 124.2, 123.73, 123.67, 122.8, 120.6, 114.6, 113.8, 112.8, 70.4, 38.3, 19.4; HRMS calcd for $C_{23}H_{23}N_4O^+$: 371.1866; found, 371.1878.

7-(3-(Aminomethyl)-4-((5-methylisoxazol-3-yl)methoxy)phenyl)-4-methylquinolin-2-amine Dihydrochloride (34).

Compounds **39** (0.085 g, 0.276 mmol) and **113** (0.132 g, 0.33 mmol) were coupled using General Procedure 1. Purification by flash column chromatography, eluting with a gradient of 5% EtOAc in CH_2Cl_2 to 70% EtOAc in CH_2Cl_2, afforded protected phenylquinoline **133** as a white solid (0.032 g, 22%). This compound was immediately deprotected using General Procedure 2. After workup, the free aminoquinoline was taken up in MeOH (1.0 mL) and treated with methanolic HCl (1 mL) for 18 h, resulting in the formation of a white precipitate, which was concentrated to dryness. The title compound (**34**) was obtained as a tan solid (0.012 g, 43% from **132**) after recrystallization overnight from methanol that was slowly diffused with ether, followed by removal of mother liquor, washing with 1:20 methanol-ether, and drying in vacuo: mp >267 ˚C (browns slowly) 272–274 ˚C (melts/gels) >277 ˚C (foams and decomp.). ^{1}H NMR (500 MHz, DMSO-d_6) δ 14.29 (s, 1 H), 8.52 (s, 3 H), 8.10 – 8.01 (m, 1 H), 8.01 – 7.93 (m, 1 H), 7.90 (s, 1 H), 7.83 (dd, J = 8.5, 2.0 Hz, 1 H), 7.79 (dt, J = 8.8, 2.4 Hz, 1 H), 7.36 (d, J = 8.6 Hz, 1 H), 6.94 (d, J = 4.6 Hz, 1 H), 6.49 (d, J = 4.4 Hz, 1 H), 5.32 (s, 2 H), 4.10 (d, J = 5.6 Hz, 2 H), 2.65 (s, 3 H), 2.44 (s, 3 H); ^{13}C NMR

(126 MHz, DMSO-d_6) δ 169.98, 164.79, 160.32, 156.15, 153.88, 142.80, 130.94, 129.19, 128.56, 126.44, 126.14, 123.17, 122.96, 120.01, 114.03, 112.93, 112.20, 101.47, 61.85, 37.13, 18.84, 11.76; HRMS calcd for $C_{22}H_{23}N_4O_2^+$: 375.1821; found, 375.1816.

7-(3-(Aminomethyl)-4-(thiazol-4-ylmethoxy)phenyl)-4-methylquinolin-2-amine Trihydrochloride (35).

Compounds **39** (0.087 g, 0.282 mmol) and **114** (0.122 g, 0.304 mmol) were coupled using General Procedure 1. Purification by flash column chromatography, eluting with a gradient of 5% EtOAc in CH_2Cl_2 to 80% EtOAc in CH_2Cl_2, afforded protected phenylquinoline **133** as a cream-colored solid (0.056 g, 38%). A portion of this compound (0.047 g) was immediately deprotected using General Procedure 2. After workup, the free aminoquinoline was treated with methanolic HCl (2 mL), and sonicated for 10 minutes before stirring at room temperature for 18 h. The resulting grey precipitate was collected to afford **35** as a grey solid (0.044 g, 99% from **133**) after filtering, washing with ether, and drying in vacuo. Because of the NMR spectral overlap of differing HCl species of **35**, the precipitate was further purified using reverse phase chromatography, eluting through a 15.5 g C18 RediSep RF Gold cartridge column with a gradient of 100% water to 100% acetonitrile to afford **35** as a yellow solid (0.009 g, 38%) which was used for characterization: mp 210.8–212 ˚C (softens) >315 ˚C (dec); ^{1}H-NMR (500 MHz, DMSO-d_6) δ 14.20 (s, 1 H), 9.18 (d, J = 1.9 Hz, 1 H), 8.43 (s, 4 H), 8.05 (d, J = 8.5 Hz, 1 H), 7.94 (d, J = 2.4 Hz, 1 H), 7.92 (d, J = 2.0 Hz, 1 H), 7.89 (d, J = 1.8 Hz, 1 H), 7.84 – 7.75 (m, 2 H), 7.42 (d, J = 8.6 Hz, 1 H), 6.91 (s, 1 H), 5.42 (s, 2 H), 4.12 (s, 2 H), 2.64 (s, 3 H); ^{13}C-NMR (126 MHz, 500 MHz, DMSO-d_6) δ 156.45, 154.96, 154.03, 152.12, 151.95, 142.98, 136.00, 130.73, 129.20, 128.44, 126.18, 123.27, 123.18, 119.99, 118.35, 113.82, 113.36, 112.24, 65.99, 37.17, 18.97. HRMS calcd for $C_{21}H_{21}N_4OS^+$: 377.1436; found, 377.1429.

7-(3-(Aminomethyl)-4-(oxazol-4-ylmethoxy)phenyl)-4-methylquinolin-2-amine Trihydrochloride (36).

Compounds **39** (0.089 g, 0.289 mmol) and **115** (0.133 g, 0.347 mmol) were coupled using General Procedure 1. Purification by flash column chromatography, eluting with a gradient of 5% EtOAc in CH_2Cl_2 to 80% EtOAc in CH_2Cl_2, afforded protected phenylquinoline **134** as a tan powder (0.027 g, 19%). A portion of this compound (0.024 g) was immediately deprotected using General Procedure 2. After workup, the free aminoquinoline was taken up in MeOH (1.0 mL) and treated with methanolic HCl (1.5 mL) for 18h, and concentrated to dryness. The title compound (**36**) was obtained as a tan solid (0.014 g, 65% from **134**) in 90% purity after recrystallizing once from 1:3 methanol-ethanol followed by an additional overnight recrystallization from methanol that was slowly diffused with ether, followed by removal of mother liquor, washing with 1:20 methanol-ether, and drying in vacuo. Additional purification of the crude product was achieved after reverse phase flash column chromatography, eluting through a 15.5 g C18 RediSep RF Gold cartridge column with a gradient of 100% water to 100% acetonitrile to afford pure **36** as a cream-colored solid (0.011 g, 47% from **135**) after azeotropic removal of water with toluene and drying in vacuo: mp >151 ˚C (slowly browns) 253–254 ˚C). ^{1}H-NMR (500 MHz, DMSO-d_6) δ 8.45 (s, 1 H), 8.30 (s, 1 H), 8.22 – 7.91 (m, 1 H), 7.88 (d, J = 2.5 Hz, 1 H), 7.82 (d, J = 8.4 Hz, 1 H), 7.75

(dd, J = 8.6, 2.5 Hz, 1 H), 7.72 (d, J = 1.9 Hz, 1 H), 7.50 (dd, J = 8.5, 2.1 Hz, 1 H), 7.35 (dd, J = 8.7, 2.8 Hz, 1 H), 6.61 (s, 1 H), 6.33 (s, 2 H), 5.18 (s, 2 H), 4.05 (s, 2 H), the aminoquinoline -NH proton is broadened into baseline and the benzylic CH_3 protons are obscured by the solvent peak around 2.5; ^{13}C NMR (126 MHz, DMSO-d_6) δ 158.23, 155.33, 152.46, 148.39, 143.80, 139.52, 137.92, 135.55, 132.62, 128.25, 127.67, 124.30, 123.67, 122.30, 121.93, 119.46, 113.05, 112.08, 62.21, 37.52, 18.08. HRMS calcd for $C_{21}H_{21}N_4O_2^+$: 361.1659; found, 361.1655.

7-(3-(Aminomethyl)-4-(thiazol-5-ylmethoxy)phenyl)-4-methylquinolin-2-amine Trihydrochloride (37).

Compounds **39** (0.081 g, 0.265 mmol) and **116** (0.127 g, 0.32 mmol) were coupled using General Procedure 1. Purification by flash column chromatography, eluting with a gradient of 5% EtOAc in CH_2Cl_2 to 70% EtOAc in CH_2Cl_2, afforded protected phenylquinoline **135** as a tan solid (0.036 g, 26%). A portion of this compound (0.032 g) was immediately deprotected using General Procedure 2. After workup, the free aminoquinoline was taken up in MeOH (1.0 mL) and treated with methanolic HCl (1 mL) for 18 h, resulting in the formation of a white precipitate, which was concentrated to dryness. The pure title compound (**37**) was obtained as a brown crystalline solid (0.018 g, 60% from **135**) after recrystallizing once from 1:5 methanol-ethanol and then from methanol, washing with 1:20 methanol-ether, and drying in vacuo: mp >238 ˚C (darkens) 252–255 ˚C (slowly softens) >256 ˚C (decomposes into brown foam). ^{1}H NMR (500 MHz, DMSO-d_6) δ 14.33 (s, 1 H), 9.18 (s, 1 H), 8.54 (d, J = 6.1 Hz, 3 H), 8.12 (s, 1 H), 8.06 (d, J = 8.5 Hz, 1 H), 7.98 (d, J = 2.4 Hz, 1 H), 7.90 (d, J = 1.8 Hz, 1 H), 7.84 (dd, J = 8.6, 1.8 Hz, 1 H), 7.79 (dd, J = 8.6, 2.3 Hz, 1 H), 7.42 (d, J = 8.7 Hz, 1 H), 6.96 (s, 1 H), 5.57 (s, 2 H), 4.06 (q, J = 5.8 Hz, 3 H), 2.65 (s, 4 H); ^{13}C NMR (126 MHz, DMSO) δ 155.94, 155.51, 153.86, 152.02, 142.93, 142.82, 135.97, 133.64, 130.85, 129.06, 128.42, 126.13, 123.18, 123.04, 119.97, 115.67, 113.86, 113.19, 112.18, 62.40, 37.04, 18.85; HRMS calcd for $C_{21}H_{21}N_4OS^+$: 377.1436 found, 377.1431.

Potassium 2-Acetamido-4-methylquinoline-7-trifluoroborate (39).

Compound **38** (0.368 g, 1.32 mmol), B_2Pin_2 (0.503 g, 1.98 mmol), anhydrous KOAc (0.388 g, 3.96 mmol), and Pd(dppf)Cl_2 (5 mol%, 0.048 g) were combined in a sealable vial and diluted with anhydrous dioxane (5 mL). The mixture was purged with argon, sealed, and heated at 75 ˚C for 19 h. The mixture was then cooled, diluted with EtOAc (20 mL) and filtered through a pad of Celite overlaid with a thin layer of SiO_2. The pad was washed with EtOAc (200 mL), and the combined filtrate was washed with 5% aq. NaCl and sat. aq. NaCl (100 mL each). The organic layer was dried over anhydrous sodium sulfate and concentrated to yield a brown foam containing the crude 7-BPin quinoline, which was immediately diluted in THF/H_2O (5 mL/1.5 mL). KHF_2 (0.412 g, 5.28 mmol) was added, and the mixture was stirred at r.t. for 3 h. THF (2 mL) and H_2O (1 mL) were then added, and the mixture was sonicated vigorously for 5 min and concentrated. The residue was azeotroped three times with toluene, diluted with acetone, and filtered. The filter cake was extracted with boiling acetone (6 × 60 mL), and the combined acetone filtrates were concentrated. The residue was washed with 10% hexanes in CH_2Cl_2 to yield **39** as a light tan powder (0.371 g, 92%): mp > 260 ˚C (darkens), 290–292 ˚C (dec). ^{1}H-NMR (500 MHz; acetone-d_6): δ 9.33

(s, 1 H), 8.12 (s, 1 H), 7.91 (s, 1 H), 7.71 (d, J = 8.2 Hz, 1 H), 7.66 (d, J = 8.2 Hz, 1 H), 2.63 (d, J = 0.8 Hz, 3 H), 2.23 (s, 3 H); ^{13}C-NMR (126 MHz; DMSO-d_6): δ 169.4, 150.2, 146.0, 145.1, 129.46, 129.45, 129.42, 123.9, 121.0, 112.7, 24.0, 18.7; this compound does not ionize well by ESI-MS or LC-TOF.

Purified NOS Enzyme Assays.

Rat and human nNOS, rat nNOS mutants, murine macrophage iNOS, human iNOS, and human eNOS were recombinant enzymes (expressed in *E. coli* and purified as reported previously).[21,48,49,50] To test for NOS inhibition, the hemoglobin capture assay was used to measure nitric oxide production. The assay was performed at 37 ˚C in HEPES buffer (100 mM with 10% glycerol, pH 7.4) in the presence of 10 μM L-arginine, used because a) it is close to the K_m values all three isoforms, where detection of competitive inhibitors is most sensitive, and b) significant NOS uncoupling does not occur at this concentration. Also included were 100 μM NADPH, 0.83 mM $CaCl_2$, approximately 320 units/mL of calmodulin, 10 μM H_4B, and human oxyhemoglobin (3 μM). For iNOS, the $CaCl_2$ and calmodulin were omitted and replaced with HEPES buffer (as neither are required for activation of iNOS). The assay was performed in 96-well plates using a Synergy 4 BioTek hybrid reader. The dispensing of NOS enzyme and hemoglobin was automated, and after 30 sec (maximum delay), NO production was read by monitoring the absorbance at 401 nm (resulting from the conversion of oxyhemoglobin to methemoglobin). Kinetic readouts were performed for 5 min. Each compound was assayed at least in duplicate, and six to nine concentrations (500 μM-50 nM or 100 μM-10 nM for eNOS and iNOS; 50 μM to 5 nM for rat and human nNOS) were used to construct concentration-response curves. IC_{50} values were calculated by nonlinear regression (variable slope, four parameters) using GraphPad Prism software (standard error is reported for the $LogIC_{50}$), and K_i values were obtained from IC_{50} values using the Cheng-Prusoff[51] equation [$K_i = IC_{50}/(1+[S]/K_m)$] with the following K_m values: 1.3 μM (rat nNOS), 1.6 μM (human nNOS), 8.2 μM (murine macrophage iNOS), 8 μM (human iNOS),[52] 3.9 μM (human eNOS),[53] 1.7 μM (rat nNOS D597N single mutant),[54] and 1.9 μM (rat nNOS D597N/M336V double mutant).[48]

PAMPA-BBB Assay.

The PAMPA-BBB assay was performed following a protocol described previously.[21] Briefly, the assay was done in 10 mM phosphate-buffered saline (PBS) buffer (pH 7.5), and compounds were tested at a concentration of 200 μM. The donor plate was first coated with 4 μL of porcine brain lipid (20 mg/mL in dodecane), followed by addition of 250 μL of a test compound. The acceptor plate was filled with 250 μL of PBS, and the donor plate was carefully placed on top of the acceptor plate to make a “sandwich”. The plate was incubated at 25 °C for 17 h in a saturated humidity atmosphere with orbital agitation at 100 rpm. Verapamil, chlorpromazine, and dopamine were used as a positive, intermediate, and negative control, respectively. After incubation, 150 μL of test solution was taken from each well from both sides (donor and acceptor) and transferred to the UV plate for measurement. The effective permeability (P_e) was calculated using the following equation[55]:

$$P_e = \frac{2.303}{A \cdot (t - \tau_{ss})} \cdot \frac{V_A \cdot V_D}{(V_A + V_D)} \cdot lg\left[1 - \left(\frac{V_A + V_D}{(1 - R) \cdot V_D}\right) \cdot \left(\frac{C_A(t)}{C_D(0)}\right)\right]$$

, where P_e is the effective permeability (cm/s), V_A and V_D are the volume of the acceptor and donor well (0.25 cm^3),

respectively, C_A (t) is the concentration of the acceptor well at time t, C_D (0), C_D (t) is the concentration of the donor well at t_0 and t, respectively, A is the filter well area (0.21 cm^2). t is the incubation time (s). τ_{ss} is the time to reach a steady state (usually very short compared to the incubation time). R is the retention membrane factor and was calculated using the following equation: $R = \left[1 - \frac{C_D(t)}{C_D(0)} - \frac{V_A}{V_D} \cdot \frac{C_A(t)}{C_D(0)}\right]$. P_e was reported as an average of triplicate measurements with a standard deviation.

Human Liver Microsome Stability Assay.

A 1120 μL aliquot of potassium phosphate buffer (50 mM, pH 7.4) containing liver microsomes (0.714 mg/mL) was added to individual 2 mL tubes (final concentration 0.5 mg/mL). Positive control (terfenadine) and **12** (1 mM DMSO stocks) were directly spiked into respective tubes to prepare a concentration of 1.428 μM (final concentration 1 μM). From the above mixture, 70 μL was added to individual wells of 96-well reaction plates and preincubated at 37 ˚C for 5 min. All reactions were initiated by adding 30 μL of 3.33 mM NADPH (1 mM final concentration). Reactions without NADPH and buffer controls (minus NADPH) at 0 min and 60 min were also incubated to rule out non-NADPH metabolism or chemical instability in the incubation buffer. All reactions were terminated using 100 μL of ice-cold acetonitrile containing internal standard (glipizide) at 0, 5, 15, 30, and 60 min. The plates were centrifuged at 4000 rpm for 15 min and 100 μL aliquots were analysis for parent compound disappearance in multiple-reaction monitoring (MRM) mode using LC-MS/MS. The percent remaining of test compounds and positive controls in each sample was determined by considering peak area ratio in the 0-minute sample as 100%. The half-life ($t_{1/2}$ in min), and the *in vitro* intrinsic clearance (CL'_{int} units in mL/min/kg) were calculated according to the following equations, where k is the gradient of line determined from a plot of peak area ratio (compound peak area / internal standard peak area) against time:

$$t_{1/2} = \frac{0.693}{k} \quad ; CL'_{\text{int}} = \frac{0.693}{in\ \ vitro t_{1/2}} \cdot \frac{\text{mL incubation}}{\text{mg microsomes}} \cdot \frac{\text{45 mg microsomes}}{\text{gm liver}} \cdot \frac{\text{20 mg liver weight}}{\text{kg b.w}}$$

For liver microsomes, a scaling factor used was 45 mg microsomal protein per g liver.

Inhibitor Complex Crystal Preparation.

The sitting drop vapor diffusion method was used to grow crystals at 4 °C for the heme domains of rnNOS (8 mg/mL containing 20 mM histidine), the hnNOS K301R/R354A/G357D mutant (10 mg/mL containing 20 mM histidine), and heNOS (6 mg/mL). The crystal growth conditions were as described previously.[8] The only exception is that the pH for the heNOS crystal growth is 7.5 rather than 6.5 as mistakenly reported there. Fresh crystals were first passed stepwise through cryoprotectant solutions. The pH of the final soaking solution for rnNOS was adjusted from 5.8 through 6.5, 7.0 (in MES) to 7.5 (in HEPES) and that for hnNOS from pH 7.2 to 7.5 (in HEPES), for heNOS the BIS-TRIS buffer at pH 7.5 was unchanged. At pH 7.5, crystals were soaked with 5–10 mM inhibitor for 2–4 h at 4 °C before being flash cooled with liquid nitrogen and stored until data collection.

X-ray Diffraction Data Collection, Data Processing, and Structural Refinement.

The cryogenic (100 K) X-ray diffraction data were collected remotely at the Stanford Synchrotron Radiation Lightsource (SSRL) or Advanced Light Source (ALS) through the data collection control software Blu-Ice[56] and a crystal-mounting robot. When a CCD detector was used, 100–125° of data were typically collected with 0.5° per frame. If a Pilatus pixel array detector was used, 140–200° of fine-sliced data were collected with 0.2° per frame. More data frames were collected for heNOS which has a low symmetry ($P2_1$). Raw CCD data frames were indexed, integrated, and scaled using iMOSFLM,[57] but the pixel array data were preferably processed with XDS[58] and scaled with Aimless.[59] The binding of inhibitors was detected by initial difference Fourier maps calculated with REFMAC.[60] The inhibitor molecules were then modeled in Coot[61] and refined using REFMAC or PHENIX.[62] The symmetry of heNOS crystals was changed from the orthorhombic $P2_12_12_1$ reported previously[63] to monoclinic $P2_1$, with a β angle only 0.6–0.7° off compared to the original 90°. Therefore, a molecular replacement calculation with PHASER-MR[64] was needed to solve the structure. In the $P2_1$ space group, there are two heNOS dimers in the asymmetric unit. Disordering in portions of inhibitors bound in the NOS active sites was often observed, sometimes resulting in poor density quality. However, partial structural features were usually still visible if the contour level of the sigmaA weighted 2m|Fo| − D|Fc| map was dropped to 0.5 σ, which afforded the building of reasonable models into the disordered regions. Water molecules were added in PHENIX and visually checked by Coot. The TLS[65] protocol was implemented in the PHENIX refinements with each subunit as one TLS group. The omit Fo − Fc density maps were calculated by the Polder map facility in PHENIX for the bound inhibitors.[66] The refined structures were validated in Coot before deposition in the Protein Data Bank. The X-ray diffraction data collection and structure refinement statistics are summarized in Table S1 in Supporting Information.

Supplementary Material

Refer to Web version on PubMed Central for supplementary material.

Acknowledgments

The authors thank the National Institutes of Health (R01 GM049725 and R35 GM131788 to R.B.S.; GM057353 and GM131920 to T.L.P.) for their support of this work. We thank the beamline staff at SSRL and ALS for their assistance during the remote X-ray diffraction data collections. H. L. would like to thank Carla Plaza for her efforts in protein preparations, which provided samples for both the structure determinations and the inhibitory assays. M. A. C. would like to thank Mr. Saman Shafaie and Dr. S. Habibi Goudarzi for assistance with HRMS experiments. This work made use of IMSERC at Northwestern University, which has received support from the Soft and Hybrid Nanotechnology Experimental (SHyNE) Resource (NSF NNCI-1542205), the State of Illinois, and the International Institute for Nanotechnology (IIN).

Abbreviations Used.

NO	nitric oxide
nNOS	neuronal nitric oxide synthase
iNOS	inducible nitric oxide synthase
eNOS	endothelial nitric oxide synthase

rnNOS	rat neuronal nitric oxide synthase
hnNOS	human neuronal nitric oxide synthase
heNOS	human endothelial nitric oxide synthase
miNOS	murine inducible nitric oxide synthase
hiNOS	human inducible nitric oxide synthase
FMN	flavin mononucleotide
H_4B	(6*R*)-5,6,7,8-tetrahydrobiopterin
tPSA	total polar surface area
Bis-Tris	bis(2-hydroxyethyl)amino-tris(hydroxymethyl)-methane
HEPES	4-(2-hydroxyethyl)-1-piperazineethanesulfonic acid
PAMPA-BBB	parallel artificial membrane permeability for the blood–brain barrier
PDSP	Psychoactive Drug Screening Program
WT	wild-type

References Cited

(1). Torreilles F; Salman-Tabcheh S; Guérin M; Torreilles J Neurodegenerative disorders: the role of peroxynitrite. Brain Res. Rev 1999, 30, 153–163. [PubMed: 10525172]

(2). Uehara T; Nakamura T; Yao D; Shi Z; Gu Z; Ma Y; Masliah E; Nomura Y; Lipton SA *S*-Nitrosylated protein-disulphide isomerase links protein misfolding to neurodegeneration. Nature 2006, 441, 513–517. [PubMed: 16724068]

(3). Trippier PC; Jansen Labby K; Hawker DD; Mataka JJ; Silverman RB Target- and mechanism-based therapeutics for neurodegenerative diseases: strength in numbers. J. Med. Chem 2013, 56, 3121–3147. [PubMed: 23458846]

(4). Campbell MG; Smith BC; Potter CS; Carragher B; Marletta MA Molecular architecture of mammalian nitric oxide synthase. Proc. Natl. Acad. Sci. U. S. A 2014, 111, E3614–E3623. [PubMed: 25125509]

(5). Gamboa A; Shibao C; Diedrich A; Choi L; Pohar B; Jordan J; Paranjape S; Farley G; Biaggioni I Contribution of endothelial nitric oxide to blood pressure in humans. Hypertension 2007, 49, 170–177. [PubMed: 17130304]

(6). Cinelli MA; Li H; Chreifi G; Martasek P; Roman LJ; Poulos TL; Silverman RB Simplified 2-aminoquinoline-based scaffold for potent and selective neuronal nitric oxide synthase inhibition. J. Med. Chem 2014, 57, 1513–1530. [PubMed: 24472039]

(7). Cinelli MA; Li H; Pensa AV; Kang S; Roman LJ; Martasek P; Poulos TL; Silverman RB Phenyl ether- and aniline-containing 2-aminoquinolines as potent and selective inhibitors of neuronal nitric oxide synthase. J. Med. Chem 2015, 58, 8694–8712. [PubMed: 26469213]

(8). Cinelli MA; Li H; Chreifi G; Poulos TL; Silverman RB Nitrile in the hole: discovery of a small auxiliary pocket in neuronal nitric oxide synthase leading to the development of potent and selective 2-aminoquinoline inhibitors. J. Med. Chem 2017, 60, 3958–3978. [PubMed: 28422508]

(9). Pensa AV; Cinelli MA; Li H; Chreifi G; Mukherjee P; Roman LJ; Martasek P; Poulos TL; Silverman RB Hydrophilic, potent, and selective 7-substituted 2-aminoquinolines as improved human neuronal nitric oxide synthase inhibitors. J. Med. Chem 2017, 60, 7146–7165. [PubMed: 28776992]

(10). Ballell L; Bates RH; Young RJ; Alvarez-Gomez D; Alvarez-Ruiz E; Barroso V; Blanco D; Crespo B; Escribano J; González R; Lozano S; Huss S; Santos-Villarejo A; Martín-Plaza JJ; Mendoza A; Rebollo-Lopez MJ; Remuiñan-Blanco M; Lavandera JL; Pérez-Herran E; Gamo-Benito FJ; García-Bustos JF; Barros D; Castro JP and Cammack N Fueling open-source drug discovery: 177 small-molecule leads against tuberculosis. ChemMedChem 2013, 8, 313–321. [PubMed: 23307663]

(11). Mugumbate G; Abrahams KA; Cox JAG; Papadatos G; van Westen G; Lelièvre J; Calus ST; Loman NJ; Ballell L; Barros D; Overington JP; Besra GS Mycobacterial dihydrofolate reductase inhibitors identified using chemogenomic methods and in vitro validation. PLOS ONE 2015, 10, e0121492. [PubMed: 25799414]

(12). Xue F; Li H; Fang J; Roman LJ; Martásek P; Poulos TL; Silverman RB Peripheral but crucial: A hydrophobic pocket (Tyr706, Leu337, and Met336) for potent and selective inhibition of neuronal nitric oxide synthase. Bioorg. Med. Chem. Lett 2010, 20, 6258–6261. [PubMed: 20833542]

(13). Duquenne C; Johnson N; Knight SD; Lafrance L; Miller WH; Newlander K; Romeril S; Rouse MB; Tian X; Verma SK Indazoles. WO2011140325, A1 November 10, 2011.

(14). Borg G; Cogan DA; Ellman JA; One-pot asymmetric synthesis of *tert*-butanesulfinyl-protected amines from ketones by the *in situ* reduction of *tert*-butanesulfinyl ketimines. Tetrahedron Lett. 1999, 40, 6709–6712.

(15). Lind KE; Cao K; Lin EY-S; Nguyen TB; Tangonan BT; Erlanson DA; Guckian K; Simmons RC; Lee W-C; Sun; Hansen S; Pathan N; Zhang. Pyridinonyl pdk1 Inhibitors. WO 2008005457, 1 10, 2008.

(16). Heil M; Heilmann EK; Sudau A; Kapferer T; Muhlthau FA; Jeschke P; Voerste R; Gorgens U; Raming K; Ebbinghaus-Kinstscher U; Drewes M; Adamczewski M; Becker A Halogenalkyl-Substituted Amides Used as Insecticides and Acaricides. WO2011054436, 7 7, 2010.

(17). Brunton SA; Guicherit OM; Kruse LI; Haydar SN; and Springer DM Small Organic Molecule Regulators of Cell Proliferation. WO2008057469, 5 15, 2008.

(18). Labby KJ; Xue F; Kraus JM; Ji H; Mataka J; Li H; Martásek P; Roman LJ; Poulos TL; Silverman RB Intramolecular hydrogen bonding: A potential strategy for more bioavailable inhibitors of neuronal nitric oxide synthase. Bioorg. Med. Chem 2012, 20, 2435–2443. [PubMed: 22370337]

(19). Hevel JM; Marletta MA [25] Nitric-oxide synthase assays. Methods in Enzymology 1994, 233, 250–258. [PubMed: 7516999]

(20). Delker SL; Xue F; Li H; Jamal J; Silverman RB; Poulos TL Role of zinc in isoform-selective inhibitor binding to neuronal nitric oxide synthase. Biochemistry 2010, 49, 10803–10810. [PubMed: 21138269]

(21). Do HT; Li H; Chreifi G; Poulos TL; Silverman RB Optimization of blood-brain barrier permeability with potent and selective human heuronal nitric oxide synthase inhibitors having a 2-aminopyridine scaffold. J. Med. Chem 2019, 62, 2690–2707. [PubMed: 30802056]

(22). Poulos TL; Li H Structural basis for isoform-selective inhibition in nitric oxide synthase. Acc. Chem. Res 2013, 46, 390–398. [PubMed: 23030042]

(23). Huang H; Li H; Martasek P; Roman LJ; Poulos TJ; Silverman RB Structure-guided design of selective inhibitors of neuronal nitric oxide synthase. J. Med. Chem 2013, 56, 3024–3032. [PubMed: 23451760]

(24). Delker SL; Ji H; Li H; Jamal J; Fang J; Xue F; Silverman RB; Poulos TL Unexpected binding modes of nitric oxide synthase inhibitors effective in the prevention of cerebral palsy. J. Am. Chem. Soc 2010, 132, 5437–5442. [PubMed: 20337441]

(25). Mukherjee P; Li H; Sevrioukova I; Chreifi G; Martásek P; Roman LJ; Poulos TL; Silverman RB Novel 2,4-disubstituted pyrimidines as potent, selective, and cell-permeable inhibitors of neuronal nitric oxide Synthase. J. Med. Chem 2015, 58, 1067–1088. [PubMed: 25489882]

(26). Garcin ED; Arvai AS; Rosenfeld RJ; Kroeger MD; Crane BR; Andersson G; Andrews G; Hamley PJ; Mallinder PR; Nicholls DJ; St-Gallay SA; Tinker AC; Gensmantel NP; Mete A; Cheshire DR; Connolly S; Stuehr DJ; Aberg A; Wallace AV; Tainer JA; Getzoff ED Anchored plasticity opens doors for selective inhibitor design in nitric oxide synthase. Nat. Chem. Biol 2008, 4, 700–707. [PubMed: 18849972]

(27). Besnard J; Ruda GF; Setola V; Abecassis K; Rodriguiz RM; Huang X; Norval S; Sassano MF; Shin AI; Webster LA; Simeons FRC; Stojanovski L; Prat A; Seidah NG; Constam DB; Bickerton GR; Read KD; Wetsel WC; Gilbert IH; Roth BL; Hopkins AL Automated design of ligands to polypharmacological profiles. Nature 2012, 492, 215–220. [PubMed: 23235874]

(28). Basith S; Cui M; Macalino SJY; Park J; Clavio NAB; Kang S; Choi S Exploring G-protein-coupled Receptors (GPCRs) ligand space via cheminformatics approaches: impact on rational drug design. Front. Pharmacol 2018, 9, 128, doi: 10/3389/fphar.2018.00128. [PubMed: 29593527]

(29). Yanagisawa I; Hirata Y; Ishii Y Studies on histamine H2 receptor antagonists. 2. Synthesis and pharmacological activities of *N*-sulfamoyl and *N*-sulfonyl amidine derivatives. J. Med. Chem 1987, 30, 1787–1793. [PubMed: 2888895]

(30). Rankovic Z CNS drug design: balancing physicochemical properties for optimal brain exposure J. Med. Chem 2015, 58, 2584–2608. [PubMed: 25494650]

(31). Di L; Kerns EH; Fan K; McConnell OJ; Carter GT High throughput artificial membrane permeability assay for blood– brain barrier. Eur. J. Med. Chem 2003, 38, 223–232. [PubMed: 12667689]

(32). Di L; Kerns EH; Bezar IF; Petusky SL; Huang Y Comparison of blood–brain barrier permeability assays: in situ brain perfusion, MDR1-MDCKII and PAMPA-BBB J. Pharm. Sci 2009, 98, 1980–1991. [PubMed: 18837012]

(33). Könczöl Á; Müller J; Földes E; Béni Z; Végh K; Kéry Á; Balogh GT Applicability of a blood–brain barrier specific artificial membrane permeability assay at the early stage of natural product-based CNS drug discovery J. Nat. Prod 2013, 76, 655–663 [PubMed: 23565574]

(34). Daina A, Michielin O & Zoete V SwissADME: a free web tool to evaluate pharmacokinetics, drug-likeness and medicinal chemistry friendliness of small molecules. Sci. Rep 7, 42717 (2017) doi:10.1038/srep42717 [PubMed: 28256516]

(35). Daina A, Zoete V, A BOILED-Egg to predict gastrointestinal absorption and brain penetration of small molecules. ChemMedChem 2016, 11, 1117–1121. [PubMed: 27218427]

(36). Dialer LO; Selivanova SV; Muller CJ; Muller A; Stellfeld T; Graham K; Dinkelborg LM; Kramer SD; Schibli R; Reiher M, Ametamey SM Studies toward the development of new silicon-containing building blocks for the direct (18)F-labeling of peptides. J. Med. Chem 2013, 56, 7552–7563. [PubMed: 23992105]

(37). Demont EH; Garton NS; Gosmini RLM; Hayhow TGC; Seal J; Wilson DM; Woodrow MD Tetrahydroquinoline Derivatives and their Pharmaceutical Use. WO2011054841, 5 12, 2011.

(38). Gunbas DD and Brouwer AM Degenerate molecular shuttles with flexible and rigid spacers. J. Org. Chem 2012, 77, 5724–5735. [PubMed: 22663771]

(39). Brown AD; Bunnage ME; Glossop PA; James K; Lane CAL; Lewthwaite RA; Moses IA; Price DA; Thomson NM Sulfonamide Derivatives for the Treatment of Diseases. US Patent 20100273758, 10 28, 2010.

(40). Jarboe SG; Terrazas, and Beak, P. The endocyclic restriction test: the geometries of nucleophilic substitutions at sulfur (VI) and sulfur (II). J. Org. Chem 2008, 73, 9627–9632. [PubMed: 19053614]

(41). Ballatore C; Soper JH; Piscitelli F; James M; Huang L; Atasoylu O; Huryn DM; Trojanowski JQ; Lee VM; Brunden KR; Smith AB Cyclopentane-1,3-dione: a novel isostere for the carboxylic acid functional group. Application to the design of potent thromboxane (A2) receptor antagonists. J. Med. Chem 2011, 54, 6969–6983. [PubMed: 21863799]

(42). Fisher TH; Dershem S,M; Prewitt ML *Meta*-substituent effects on benzyl free-radical stability. J. Org. Chem 1990, 55, 1040–1043.

(43). Hoyt SB; Petrilli WL; London C; Xiong Y; Taylor JA; Ali A; Lo M; Henderson TJ; Hu Q; Hartmann R; Yin L; Heim R; Bey E; Saxena R; Samanta SK; Kulkarni BA Aldosterone Synthase Inhibitors. WO2012148808, 11 1, 2012.

(44). Finkelstein BL; Taggi AE; Long JK; Sharpe PL; Tseng C-P; McCann SF; Ding AX; Swann SL Jr Substituted Benzene Fungicides. WO 2008124092, 12 18, 2008.

(45). Nielsen SF; Larsen M; Boesen T; Schonning K; Kromann H Cationic chalcone antibiotics. Design, synthesis, and mechanism of action. J. Med. Chem 2005, 48, 2667–2677. [PubMed: 15801857]

(46). Andreini M; Gabellieri E; Guba W; Marconi G; Narquizian R; Power E; Travagli M; Woltering T; Wostl W 4,5-Dihydro-oxazol-2-yl Amine Derivatives. US Patent 10090209529, 8 20, 2009.

(47). Molander GA; Trice SLJ; Kennedy SM Scope of the two-step, one-pot palladium-catalyzed borylation/suzuki cross-coupling reaction utilizing bis-boronic acid. J. Org. Chem 2012, 77, 8678–8688. [PubMed: 22994557]

(48). Roman LJ; Sheta EA; Martásek P; Gross SS; Liu Q; Masters BSS High-level expression of functional rat neuronal nitric oxide synthase in *Escherichia coli*. Proc. Natl. Acad. Sci. U.S.A 1995, 92, 8428–8432. [PubMed: 7545302]

(49). Hevel JM; White KA; Marletta MA Purification of the inducible murine macrophage nitric oxide synthase: identification as a flavoprotein. J. Biol. Chem 1991, 266, 22789–22791. [PubMed: 1720773]

(50). Gerber NC; Ortiz de Montellano PR Neuronal nitric oxide synthase: expression in *Escherichia coli*, irreversible inhibition by phenyldiazene, and active site topology. J. Biol. Chem 1995, 270, 17791–17796. [PubMed: 7543092]

(51). Cheng Y-C; Prusoff WH Relationship between the inhibition constant (K_i) and the concentration of the inhibitor which causes 50 per cent inhibition (IC_{50}) of an enzymatic reaction. Biochem. Pharmacol 1973, 22, 3099–3108. [PubMed: 4202581]

(52). Fossetta JD; Niu XD; Lunn CA; Zavodny PJ; Narula SK; Lundell D Expression of human inducible nitric oxide synthase in Escherichia coli. FEBS Letters 1996, 379, 135–138. [PubMed: 8635578]

(53). Leber A; Hemmens B; Klosch B; Goessler W; Raber G; Mayer B; Schmidt K Characterization of recombinant human endothelial nitric-oxide synthase purified from the yeast *pichia pastoris*. J. Biol. Chem 1999, 274, 37658–37665. [PubMed: 10608822]

(54). Li H; Wang HY; Kang S; Silverman RB; Poulos TL Electrostatic control of isoform selective inhibitor binding in nitric oxide synthase. Biochemistry 2016, 55, 3702–3707. [PubMed: 27250740]

(55). Müller J; Esső K; Dargó G; Könczoö Á; Balogh GT Tuning the predictive capacity of the PAMPA-BBB model. Eur. J. Pharm. Sci 2015, 79, 53–60. [PubMed: 26344358]

(56). McPhillips TM; McPhillips SE; Chiu H-J; Cohen AE; Deacon AM; Ellis PJ; Garman E; Gonzalez A; Sauter NK; Phizackerley RP; Soltis SM; Kuhn P Blu-Ice and the Distributed Control System: software for data acquisition and instrument control at macromolecular crystallography beamlines. J. Synchrotron Radiat 2002, 9, 401–406. [PubMed: 12409628]

(57). Battye TGG; Kontogiannis L; Johnson O; Powell HR; Leslie AGW iMOSFLM: a new graphical interface for diffraction-image processing with MOSFLM. Acta Crystallogr., Sect. D: Biol. Crystallogr 2011, 67, 271–281. [PubMed: 21460445]

(58). Kabsch W XDS. Acta Crystallogr., Sect. D: Biol. Crystallogr 2010, 66, 125–132. [PubMed: 20124692]

(59). Evans P Scaling and assessment of data quality. Acta Crystallogr., Sect. D: Biol. Crystallogr 2006, 62, 72–82. [PubMed: 16369096]

(60). Murshudov GN; Vagin AA; Dodson EJ Refinement of macromolecular structures by the maximum-likelihood method. Acta Crystallogr., Sect. D: Biol. Crystallogr 1997, 53, 240–255. [PubMed: 15299926]

(61). Emsley P; Cowtan K Coot: model-building tools for molecular graphics. Acta Crystallogr., Sect. D: Biol. Crystallogr 2004, 60, 2126–2132. [PubMed: 15572765]

(62). Adams PD; Afonine PV; Bunkoczi G; Chen VB; Davis IW; Echols N; Headd JJ; Hung L-W; Kapral GJ; Grosse-Kunstleve RW; McCoy AJ; Moriarty NW; Oeffner R; Read RJ; Richardson DC; Richardson JS; Terwilliger TC; Zwart PH PHENIX: a comprehensive Python-based system for macromolecular structure solution. Acta Crystallogr., Sect. D: Biol. Crystallogr 2010, 66, 213–221. [PubMed: 20124702]

(63). Li H; Jamal J; Plaza C; Pineda SH; Chreifi G; Jing Q; Cinelli MA; Silverman RB; Poulos TL Structures of human constitutive nitric oxide synthases. Acta Crystallogr., Sect. D: Biol. Crystallogr 2014, 70, 2667–2674. [PubMed: 25286850]

(64). McCoy AJ; Grosse-Kunstleve RW; Adams PD; Winn MD; Storoni LC; Read RJ Phaser crystallographic software. J. Appl. Crystallogr 2007, 40, 658–674. [PubMed: 19461840]

(65). Winn MD; Isupov MN; Murshudov GN Use of TLS parameters to model anisotropic displacements in macromolecular refinement. Acta Crystallog., Sect. D: Biol. Crystallogr 2001, 57, 122–133.

(66). Liebschner D; Afonine PV; Moriarty NW; Poon BK; Sobolev OV; Terwilliger TC; Adams PD Polder maps: improving OMIT maps by excluding bulk solvent. Acta Crystallog., Sect. D: Biol. Crystallogr 2017, 73, 148–157.

(67). Schrodinger LLC. The PyMOL Molecular Graphics System, Version 1.8, 2015.

(68). Do HT; Wang H-Y; Li H; Chreifi G; Poulos TL; Silverman RB Improvement of Cell Permeability of Human Neuronal Nitric Oxide Synthase Inhibitors Using Potent and Selective 2-Aminopyridine-Based Scaffolds with a Fluorobenzene Linker. J. Med. Chem 2017, 60, 9360–9375. [PubMed: 29091437]

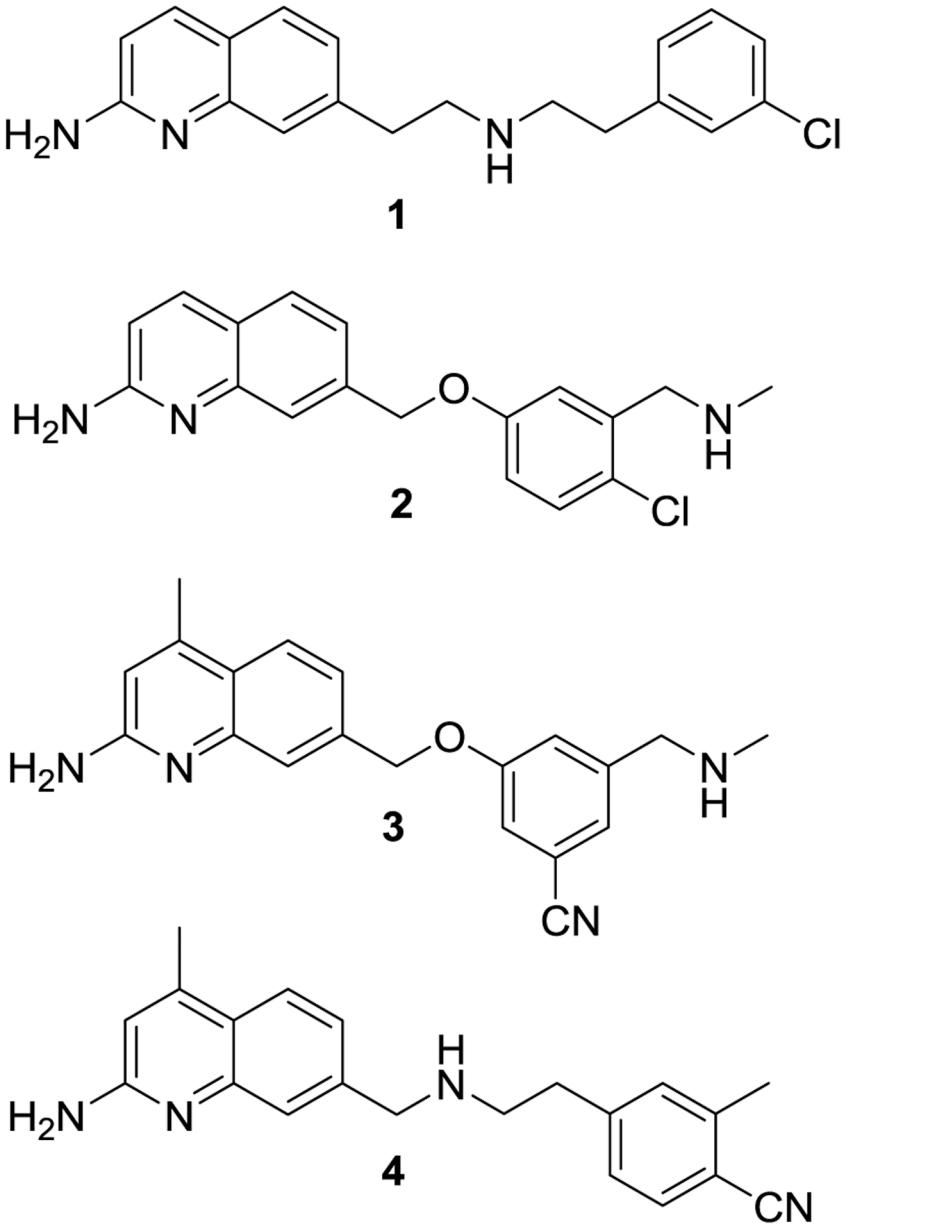

Figure 1.
Representative aminoquinoline nNOS inhibitors

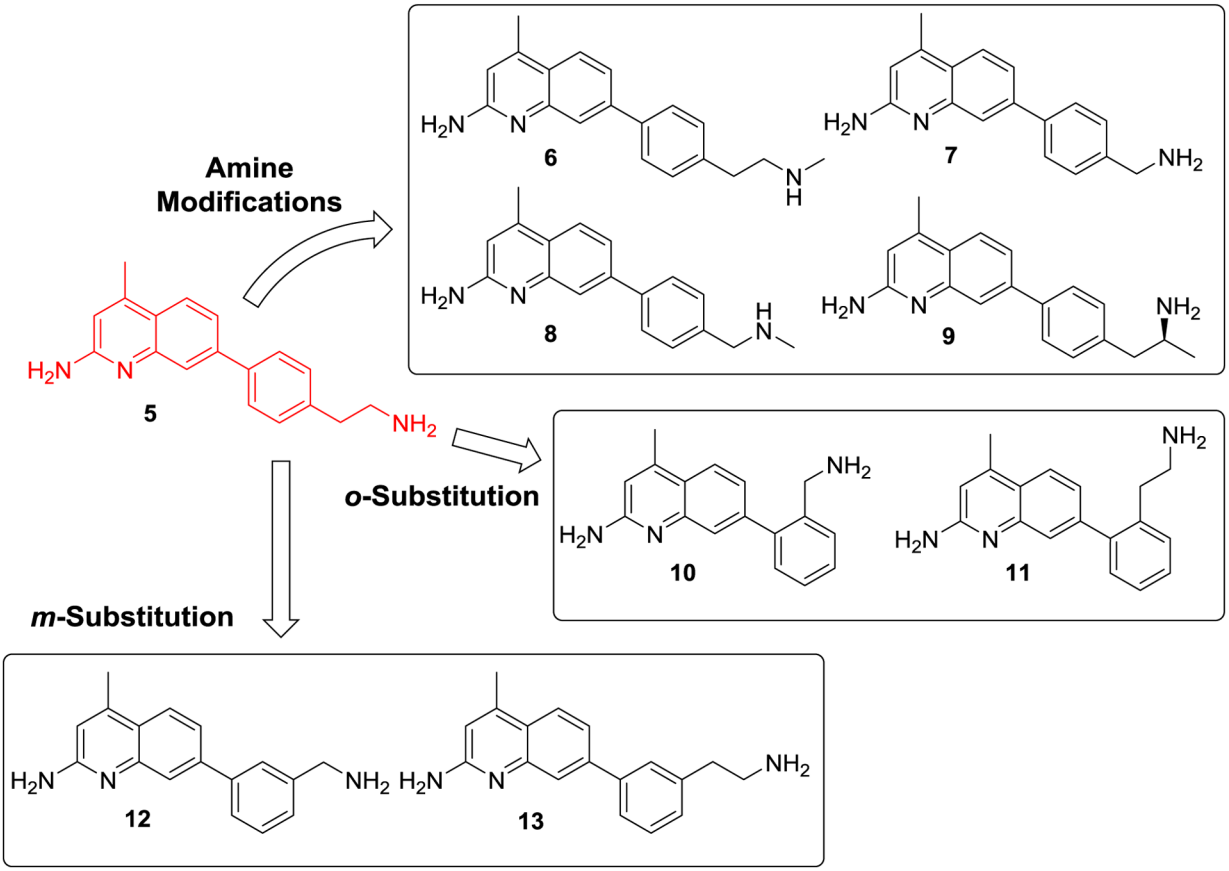

Figure 2.
Initial derivatives of **5** prepared in this study

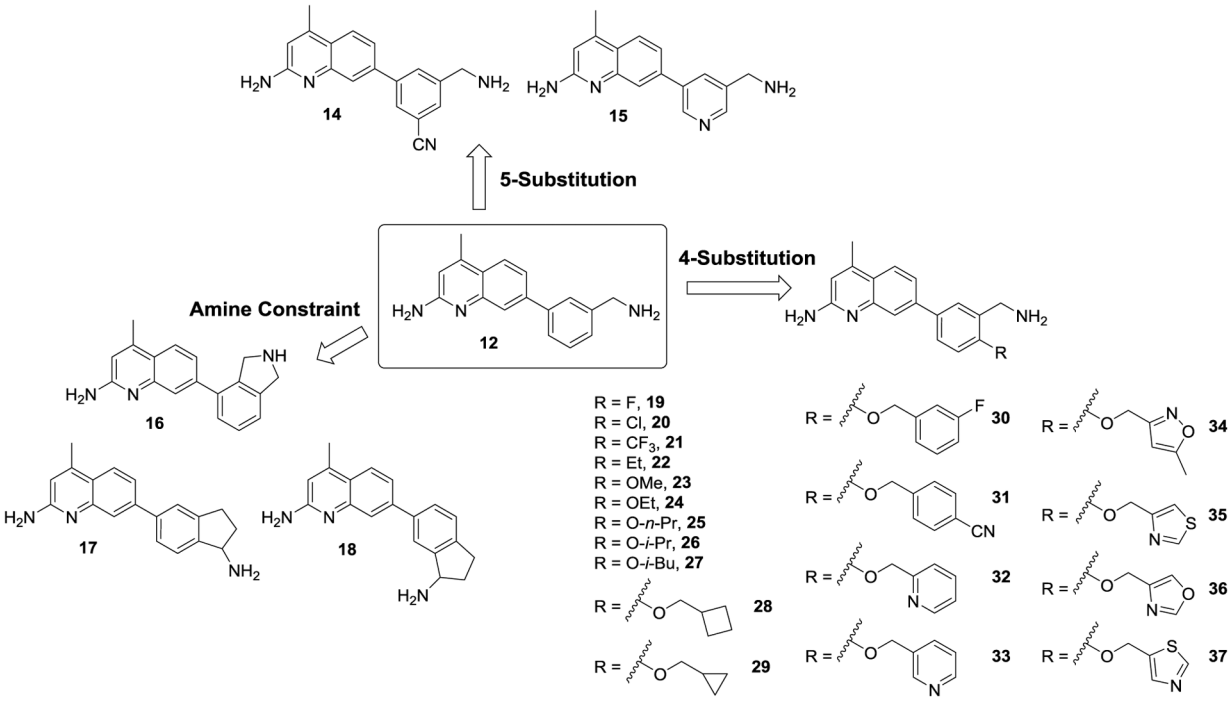

Figure 3.

Optimization of **12** by 5-substitution, amino group constraint, and 4-substitution

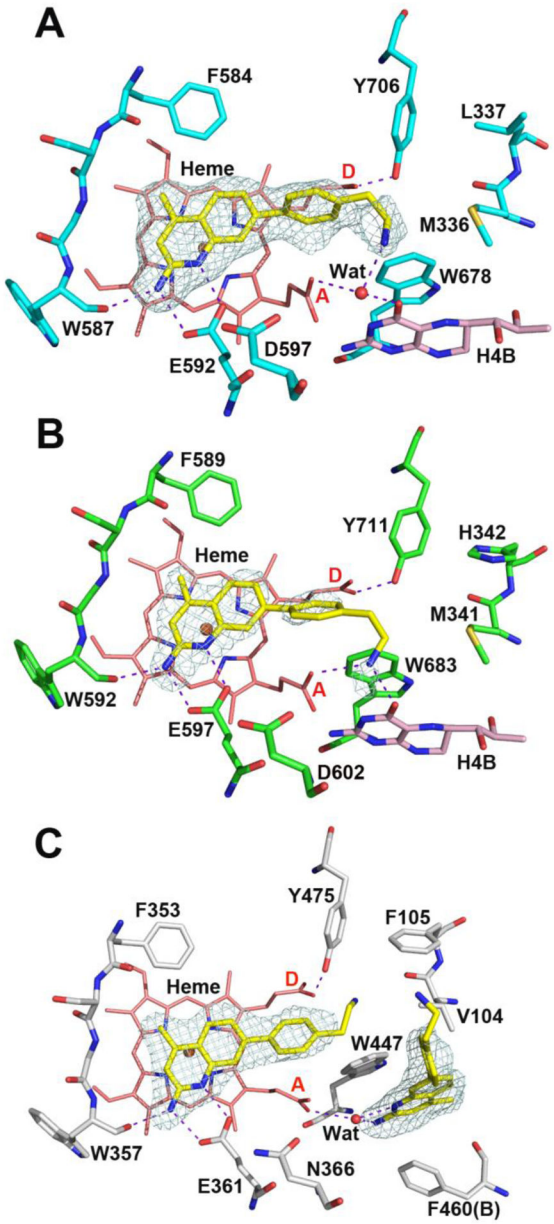

Figure 4.

X-ray crystal structures of **5** bound in the active sites of (A) rnNOS, (B) hnNOS, and (C) heNOS at 1.80 Å, 1.95 Å, and 2.19 Å resolution, respectively. In this and all of the following figures the Polder Fo – Fc omit maps are contoured at 3.5 σ for the bound inhibitors. Major hydrogen bonds are depicted with dashed lines. Two heme propionates are labeled as A and D. Figures were made with PyMol.[67]

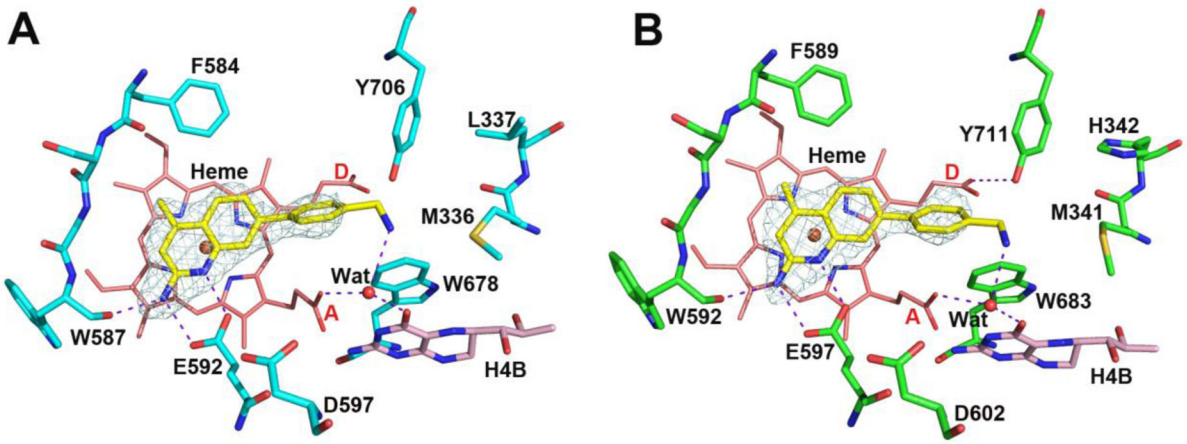

Figure 5.

X-ray crystal structures of **7** bound in the active sites of (A) rnNOS and (B) hnNOS at 1.75 Å, and 2.05 Å resolution, respectively

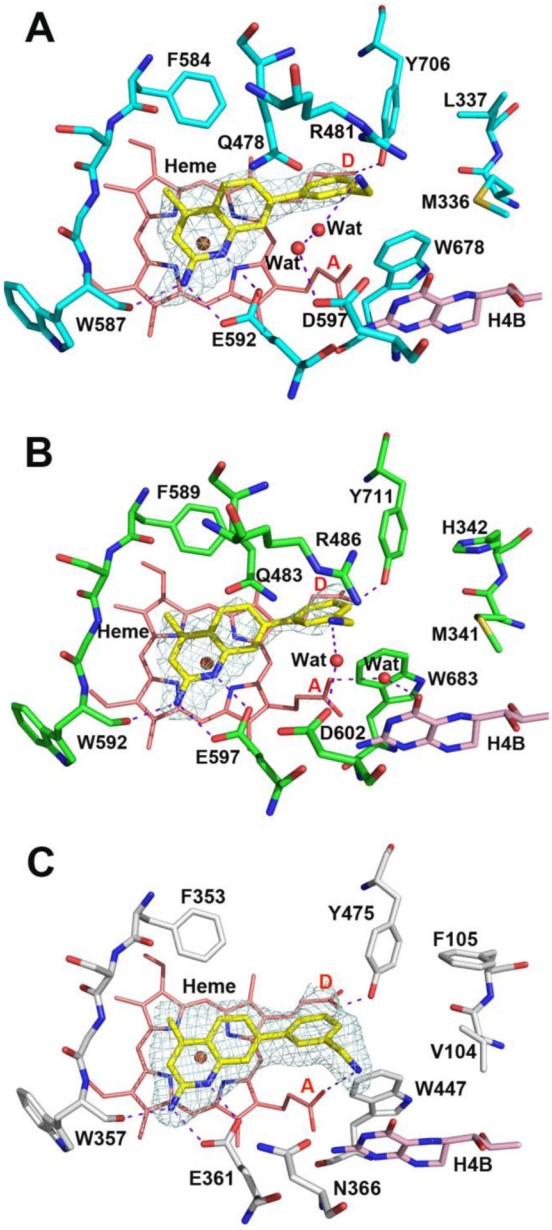

Figure 6.

X-ray crystal structures of **12** bound in the active sites of (A) rnNOS, (B) hnNOS, and (C) heNOS at 2.05 Å, 2.15 Å, and 2.05 Å resolution, respectively

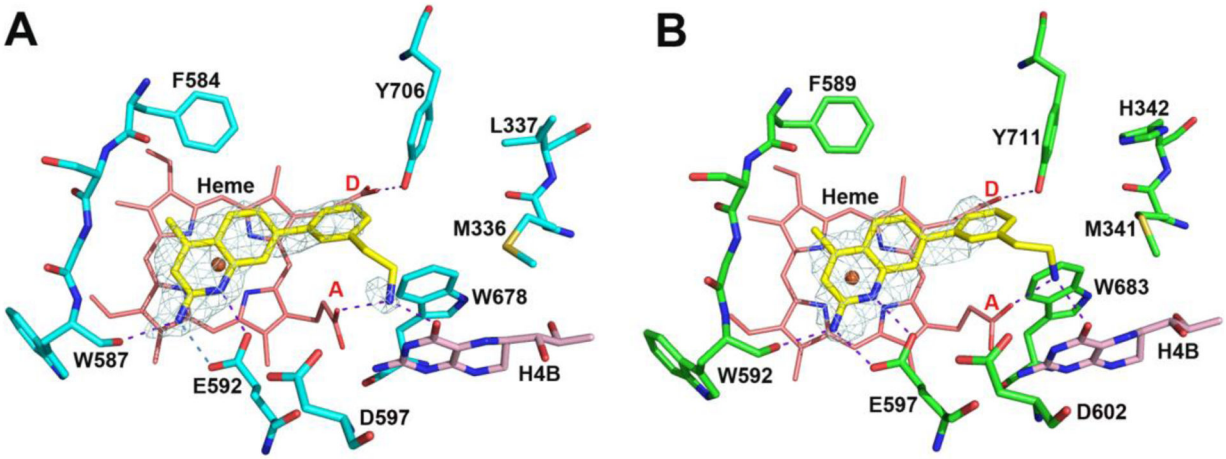

Figure 7.

X-ray crystal structures of **13** bound in the active sites of (A) rnNOS and (B) hnNOS at 1.95 Å and 2.40 Å resolution, respectively

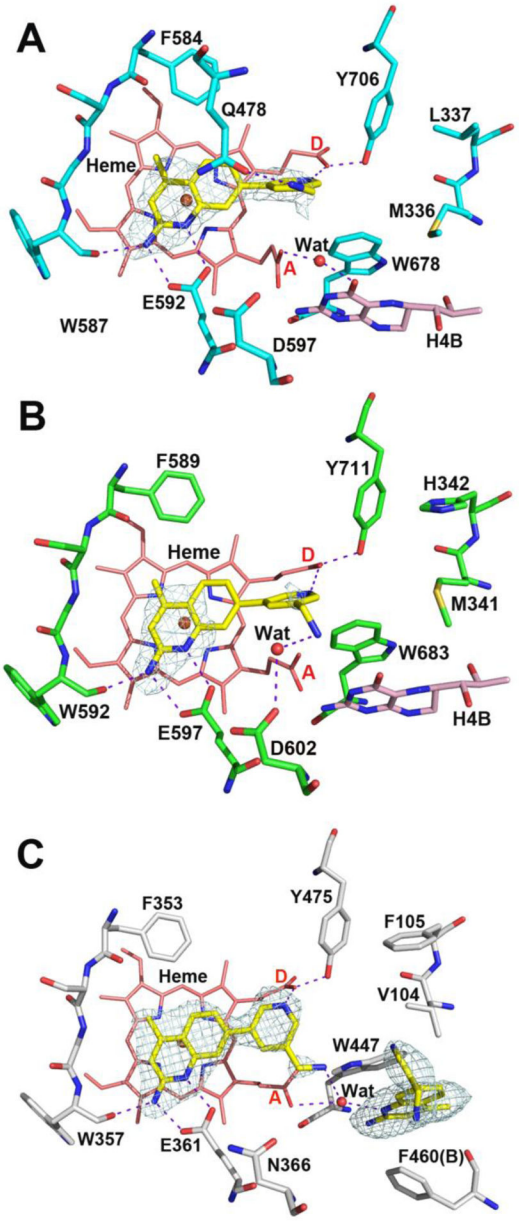

Figure 8.

X-ray crystal structures of **15** bound in the active sites of (A) rnNOS, (B) hnNOS, and (C) heNOS at 2.10 Å, 2.10 Å and 2.15 Å resolution, respectively

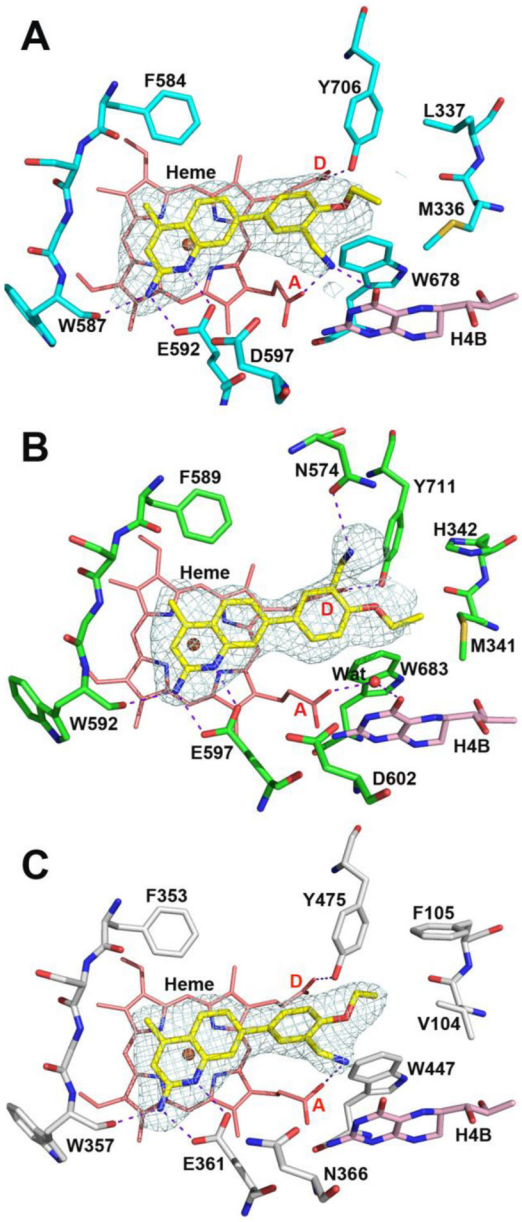

Figure 9.

X-ray crystal structures of **24** bound in the active sites of (A) rnNOS, (B) hnNOS, and (C) heNOS, at 2.23 Å, 2.10 Å, and 2.20 Å resolution, respectively

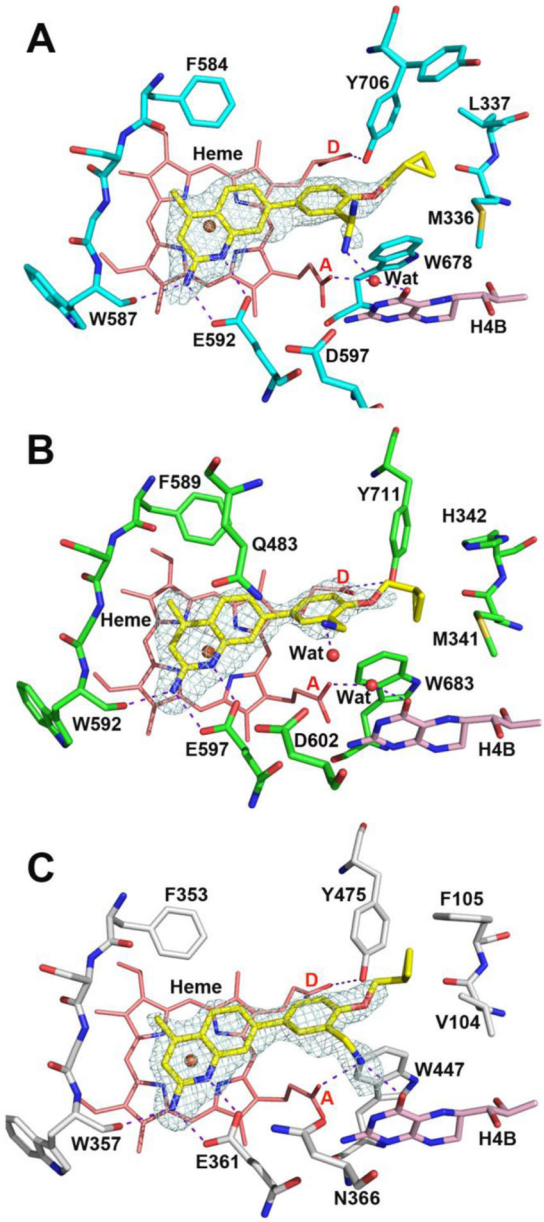

Figure 10.

X-ray crystal structures of **29** bound in the active sites of (A) rnNOS, (B) hnNOS, and (C) heNOS at 1.90 Å, 1.95 Å and 1.76 Å resolution, respectively

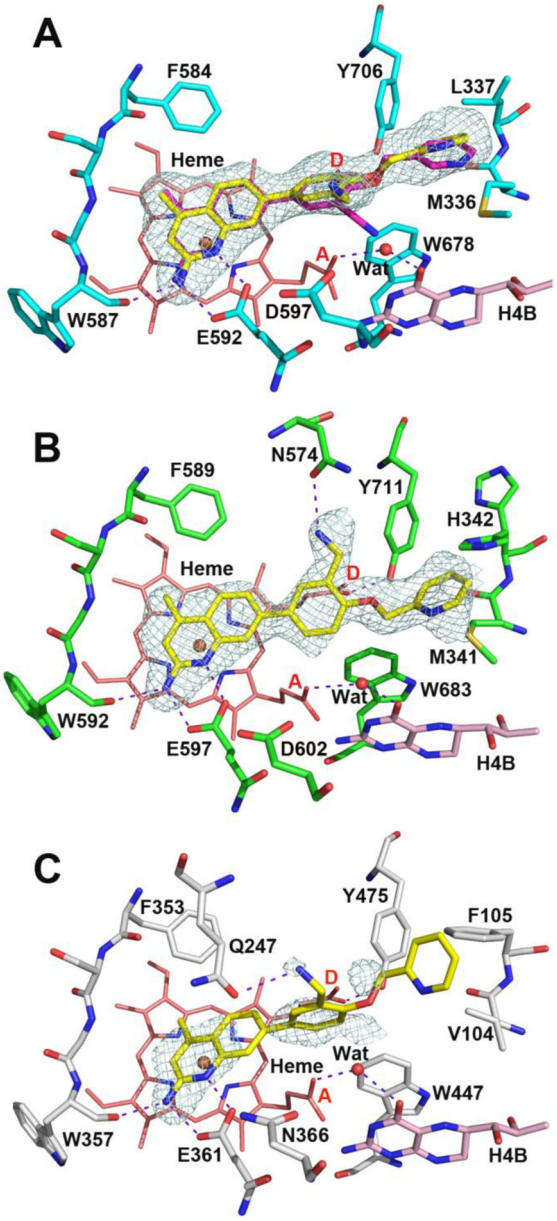

Figure 11.

X-ray crystal structures of **32** (yellow) bound in the active sites of (A) rnNOS with **33** (magenta) overlaid, (B) hnNOS, and (C) heNOS, at 1.70 Å, 1.81 Å, and 1.95 Å resolution, respectively

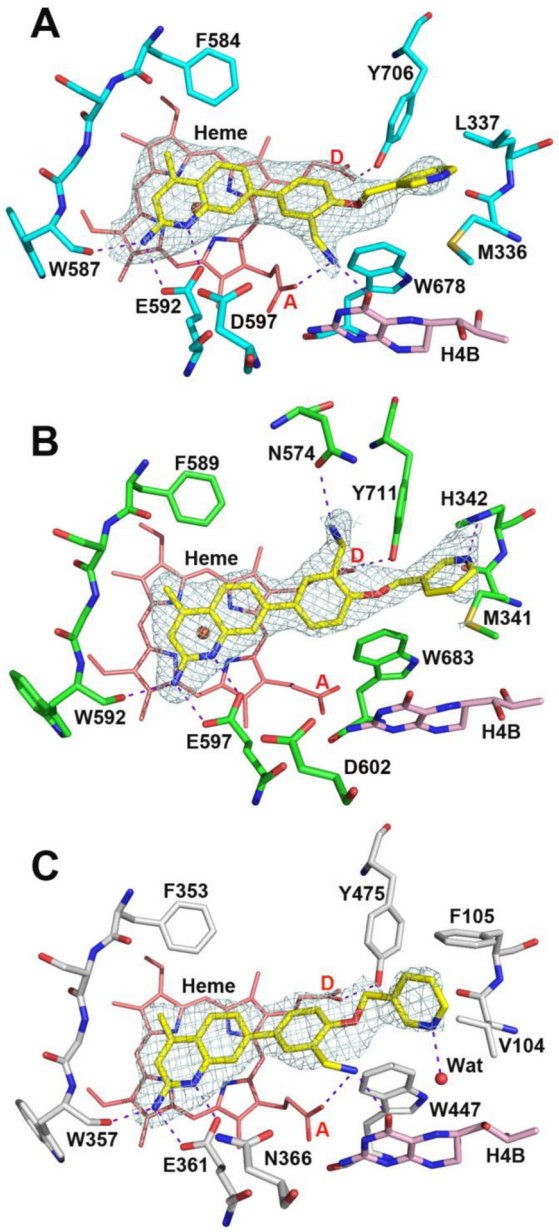

Figure 12.

X-ray crystal structures of **33** bound in the active sites of (A) rnNOS, (B) hnNOS, and (C) heNOS at 1.84 Å, 1.81 Å and 2.20 Å resolution, respectively

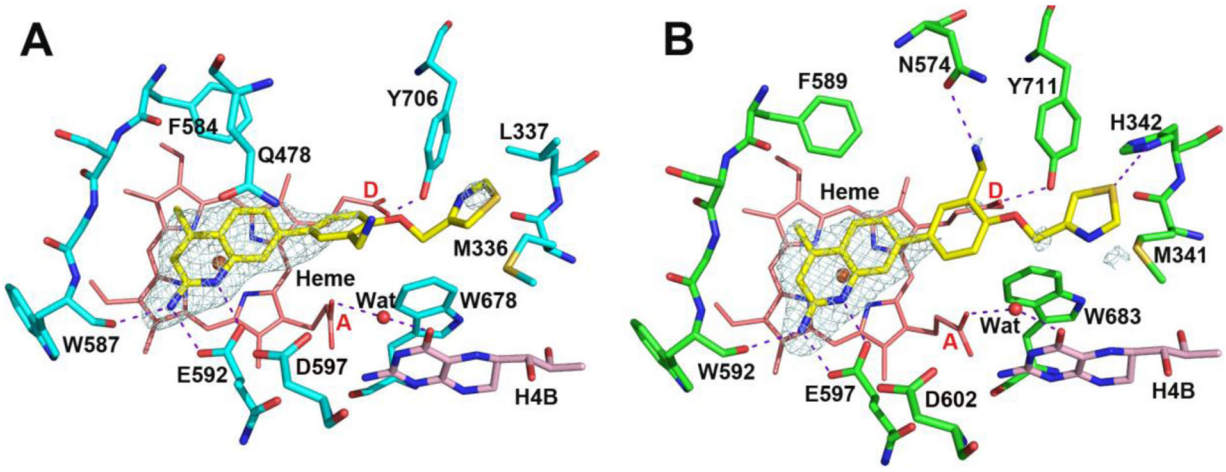

Figure 13.

X-ray crystal structures of **35** bound in the active site of (A) rnNOS and (B) hnNOS at 1.88 Å and 1.95 Å resolution, respectively

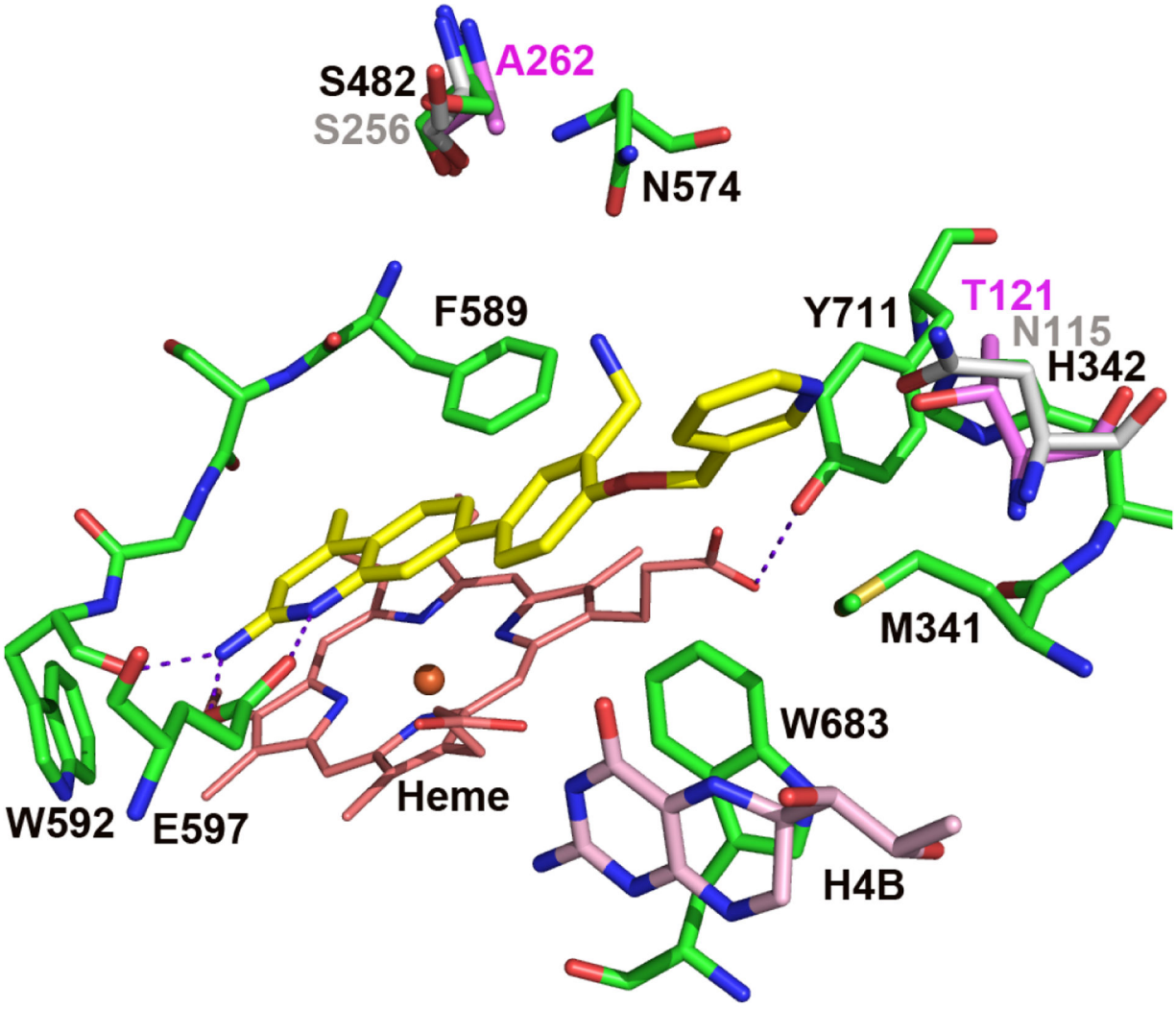

Figure 14.

The structure of hnNOS-**33** (yellow) with the variant residues of miNOS (Asn115 and Ser256, gray, PDB code 1NOD) and hiNOS (Thr121 and Ala262, magenta, PDB code 4NOS) overlaid

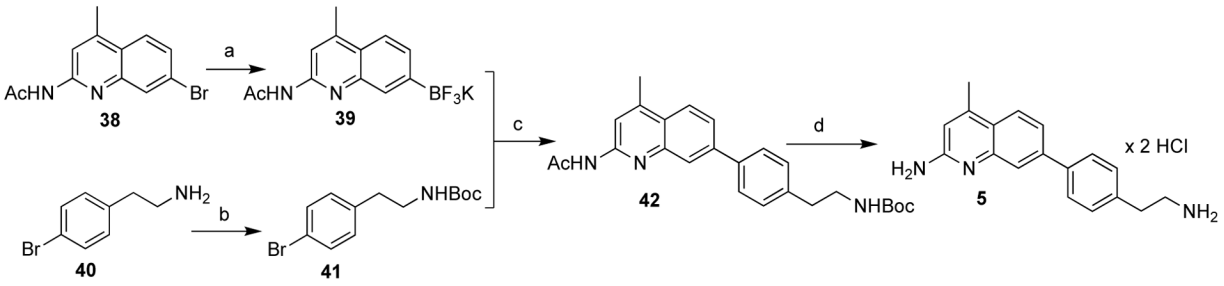

[a]Reagents and conditions: (a) *i.* B_2Pin_2, KOAc, $Pd(dppf)Cl_2$, dioxane, 75 Â°C, *ii.* KHF_2, THF/H_2O, r.t.; (b) Boc_2O, THF, r.t.; (c) $Pd(dppf)Cl_2$, $NaHCO_3$, 1,2-dimethoxyethane (DME)/H_2O, Âµwave, 120 Â°C; (d) *i.* K_2CO_3, MeOH, reflux, *ii.* HCl/MeOH, ether, r.t. (after isolation).

Scheme 1[a].

Synthesis of lead **5**

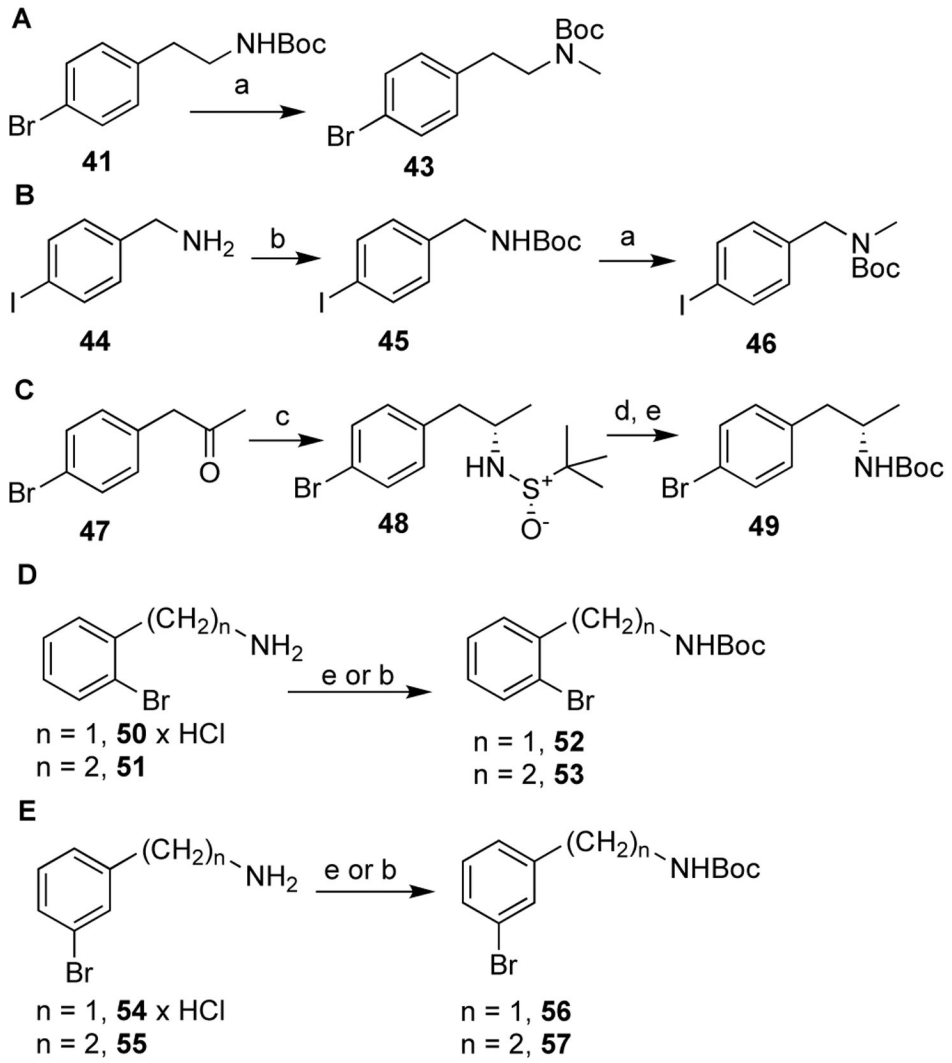

[a]Reagents and conditions: (a) *i.* NaH, THF, 0 ˚C - r.t., *ii.* MeI, r.t. or reflux; (b) Boc_2O, THF, r.t.; (c) *i. (S)-t*-butylsulfinamide, $Ti(OEt)_4$, THF, 70 ˚C, *ii.* $NaBH_4$, THF, -40 ˚C; (d) *i.* HCl/MeOH, ether, r.t.; (e) Boc_2O, Et_3N, THF/MeOH, r.t.

Scheme 2[a].

Preparation of precursor *p*-, *o*-, and *m*-substituted halides

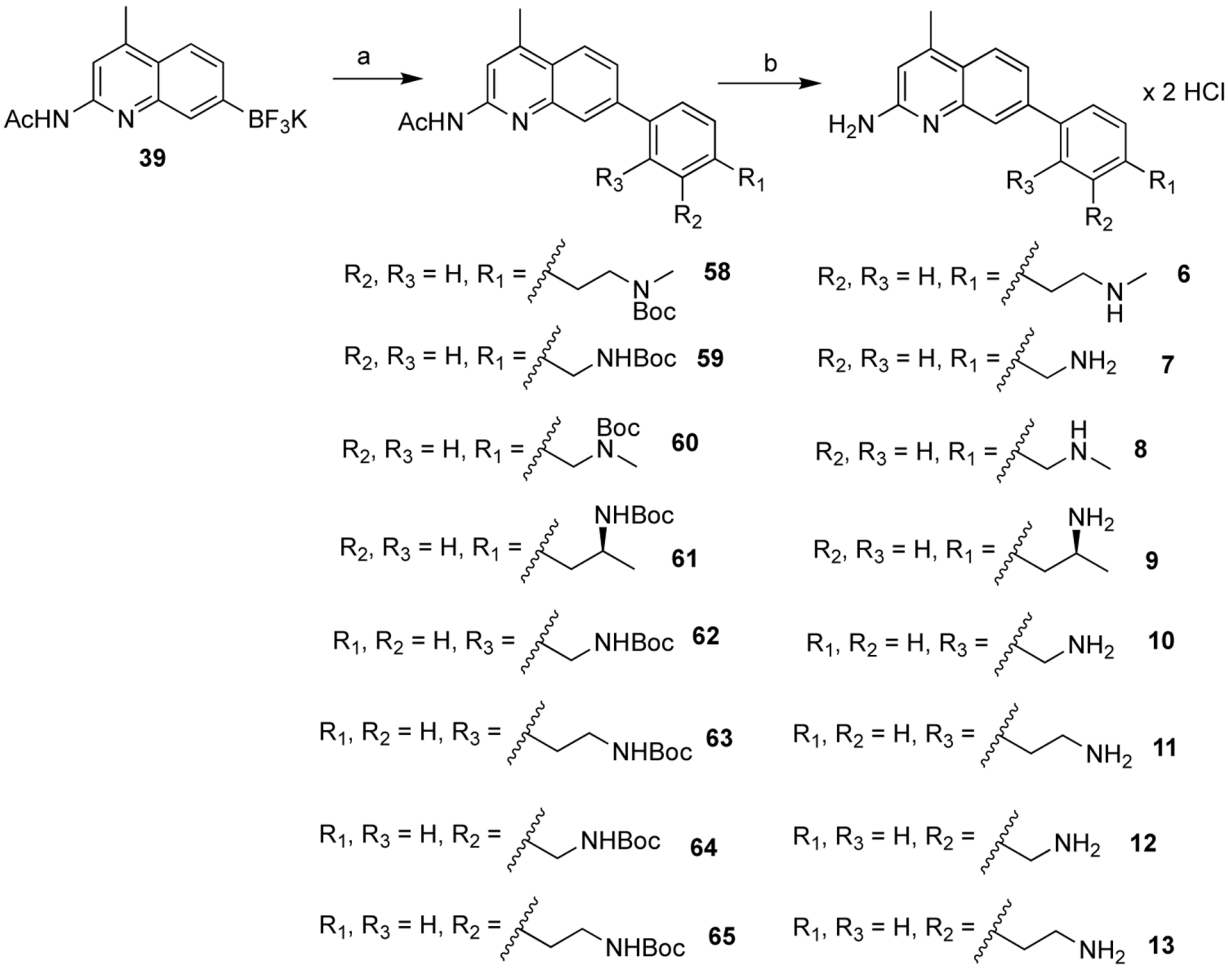

[a]Reagents and conditions: (a) halides **43**, **45-46**, **49**, **52-53**, **56-57,** $Pd(dppf)Cl_2$, $NaHCO_3$, 1,2-dimethoxyethane (DME)/H_2O, μwave, 120 ˚C; (b) *i.* K_2CO_3, MeOH, reflux, *ii.* HCl/MeOH, ether, r.t. (after isolation).

Scheme 3.

Assembly and deprotection of *p*-, *o*-, and *m*-substituted phenylquinolines.

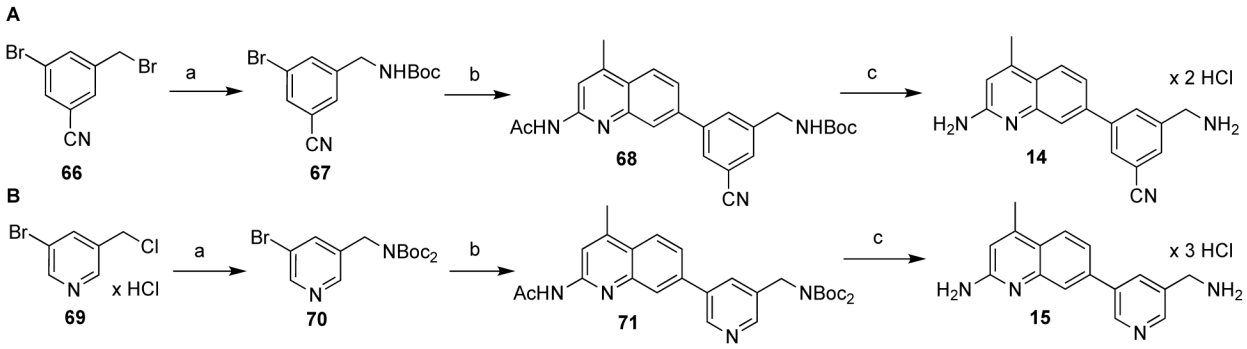

[a]Reagents and conditions: (a) *i.* NaH, Boc_2NH, THF, r.t., *ii.* halide, r.t. or r.t.-50 ˚C (for **69**); (b) **39**, $Pd(dppf)Cl_2$, $NaHCO_3$, 1,2-dimethoxyethane (DME)/H_2O, μwave, 120 ˚C; (c) *i.* K_2CO_3, MeOH, reflux, *ii.* HCl/MeOH, ether, r.t. (after isolation).

Scheme 4.
Synthesis of **14** and **15**.

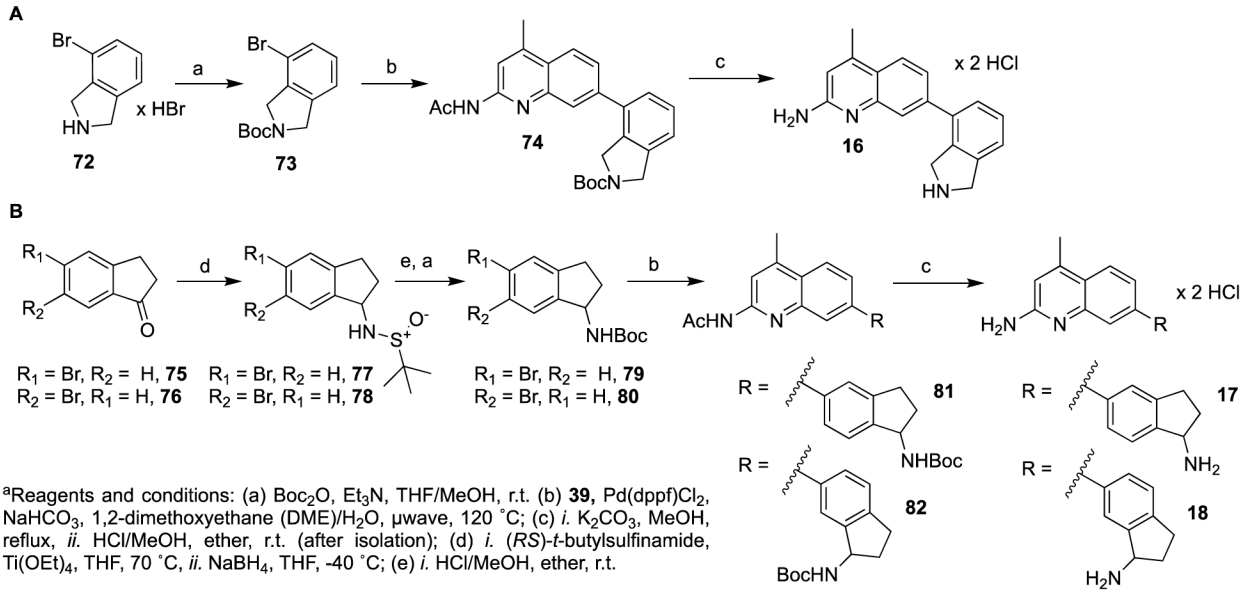

[a]Reagents and conditions: (a) Boc_2O, Et_3N, THF/MeOH, r.t. (b) **39,** $Pd(dppf)Cl_2$, $NaHCO_3$, 1,2-dimethoxyethane (DME)/H_2O, μwave, 120 ˚C; (c) *i.* K_2CO_3, MeOH, reflux, *ii.* HCl/MeOH, ether, r.t. (after isolation); (d) *i.* (*RS*)-*t*-butylsulfinamide, $Ti(OEt)_4$, THF, 70 ˚C, *ii.* $NaBH_4$, THF, -40 ˚C; (e) *i.* HCl/MeOH, ether, r.t.

Scheme 5[a].

Synthesis of conformationally constrained derivatives **16**-**18**

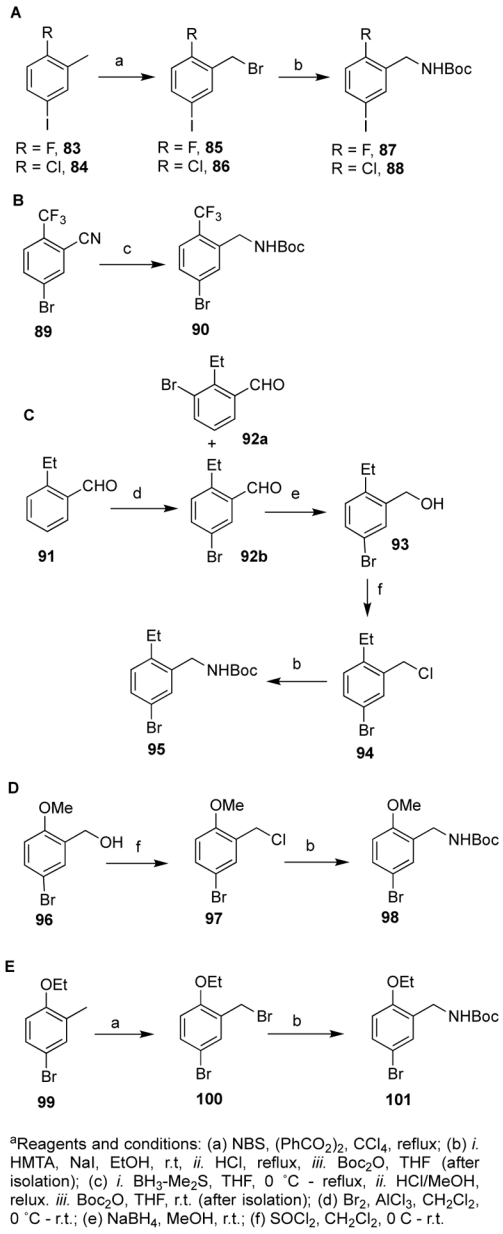

[a]Reagents and conditions: (a) NBS, $(PhCO_2)_2$, CCl_4, reflux; (b) *i.* HMTA, NaI, EtOH, r.t, *ii.* HCl, reflux, *iii.* Boc_2O, THF (after isolation); (c) *i.* BH_3-Me_2S, THF, 0 ˚C - reflux, *ii.* HCl/MeOH, relux. *iii.* Boc_2O, THF, r.t. (after isolation); (d) Br_2, $AlCl_3$, CH_2Cl_2, 0 ˚C - r.t.; (e) $NaBH_4$, MeOH, r.t.; (f) $SOCl_2$, CH_2Cl_2, 0 C - r.t.

Scheme 6[a].

Preparation of intermediate carbamates for the preparation of 4-substituted derivatives

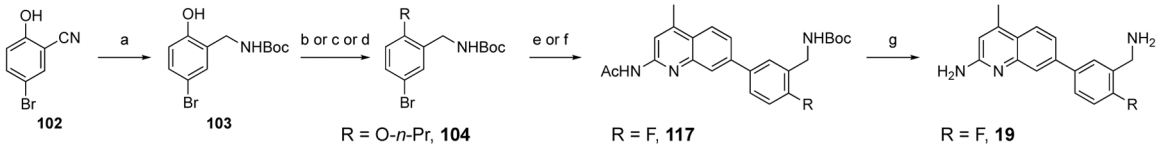

R = O-*n*-Pr, **104**
R = O-*i*-Pr, **105**
R = O-*i*-Bu, **106**
R = O-methylcyclobutyl **107**
R = O-methylcyclopropyl, **108**[b]
R = O-(3-fluorobenzyl), **109**
R = O-(4-cyanobenzyl), **110**
R = O-(2-pyridinylmethyl), **111**
R = O-(3-pyridinylmethyl), **112**
R = O-(5-methylisoxazol-3-yl)methyl, **113**
R = O-(thiazol-4-methyl), **114**
R = O-(oxazol-4-methyl), **115**
R = O-(thiazol-5-methyl), **116**

(or halides **87-88**, **90**, **95**, **98**, or **101**)

R = F, **117**
R = Cl, **118**
R = CF_3, **119**
R = Et, **120**
R = OMe, **121**
R = OEt, **122**
R = O-*n*-Pr, **123**
R = O-*i*-Pr, **124**
R = O-*i*-Bu, **125**
R = O-methylcyclobutyl **126**
R = O-methylcyclopropyl, **127**
R = O-(3-fluorobenzyl), **128**
R = O-(4-cyanobenzyl), **129**
R = O-(2-pyridinylmethyl), **130**
R = O-(3-pyridinylmethyl), **131**
R = O-(5-methylisoxazol-3-yl)methyl, **132**
R = O-(thiazol-4-methyl), **133**
R = O-(oxazol-4-methyl), **134**
R = O-(thiazol-5-methyl), **135**

R = F, **19**
R = Cl, **20**
R = CF_3, **21**
R = Et, **22**
R = OMe, **23**
R = OEt, **24**
R = O-*n*-Pr, **25**
R = O-*i*-Pr, **26**
R = O-*i*-Bu, **27**
R = O-methylcyclobutyl **28**
R = O-methylcyclopropyl, **29**
R = O-(3-fluorobenzyl), **30**
R = O-(4-cyanobenzyl), **31**
R = O-(2-pyridinylmethyl), **32**
R = O-(3-pyridinylmethyl), **33**
R = O-(5-methylisoxazol-3-yl)methyl, **34**
R = O-(thiazol-4-methyl), **35**
R = O-(oxazol-4-methyl), **36**
R = O-(thiazol-5-methyl), **37**

[a]Reagents and conditions: (a) *i.* BH_3-Me_2S, THF, 0 °C - reflux; *ii.* HCl-MeOH, reflux; *iii.* Boc_2O, MeOH/THF, r.t. (after isolation); (b) *i.* NaH, DMF, 0 °C; *ii.* alkyl or benzyl iodide or bromide, 0 °C - r.t.; (c) alkyl bromide, K_2CO_3, Acetone, reflux. (d) heterocyclic halides, Cs_2CO_3, DMF, rt (e) **39**, $Pd(dppf)Cl_2$, $NaHCO_3$, 1,2-dimethoxyethane (DME)/H_2O, μwave, 120 °C; (f)[b] *i.* $B_2(OH)_2$, KOAc, XPhos-Pd-G_3, XPhos, EtOH, 80 °C, 2h; *ii.* **38**, K_2CO_3, H_2O, 80 °C, 15h; (g) *i.* K_2CO_3, MeOH, reflux; *ii.* HCl/MeOH, ether, r.t. (after isolation).

Scheme 7[a].

Preparation of ether-substituted carbamates and final assembly of 4-substituted analogues **19–37**

Table 1.

Inhibition of NOS enzymes by synthesized compounds **5–37.**[a]

	K_i (μM)[a]				Selectivity	
compd	**rnNOS**	**hnNOS**	**miNOS**	**heNOS**	**$^{rn}/_{mi}$**	**$^{hn}/_{he}$**
1	0.066	0.440	28.4	11.8	431	27
2	0.058	0.295	27.7	7.41	478	25
3	0.033	0.031	6.7	5.63	203	181
4	0.025	0.030	4.83	5.76	193	192
5	0.105	0.122	21.7	23.3	207	191
6	0.246	-	-	-	-	-
7	0.045	0.088	16.3	18.7	362	212
8	0.090	0.149	-	-	-	-
9	0.140	-	27.5	-	197	-
10	0.119	0.151	2.86	41.9	24	277
11	0.935	-	-	-	-	-
12	0.055	0.060	24.2	52.6	440	877
13	0.107	-	-	-	-	-
14	1.03	-	-	-	-	-
15	0.285	-	-	-	-	-
16	0.254	-	-	-	-	-
17	0.159	-	-	-	-	-
18	0.180	-	-	-	-	-
19	0.108	-	-	-	-	-
20	0.235	-	-	-	-	-
21	1.42	-	-	-	-	-
22	0.390	-	-	-	-	-
23	0.106	-	-	-	-	-
24	0.058	0.111	24.2	18.2	418	164
25	0.072	0.058	23.9	12.9	333	223
26	0.071	0.066	25.5	20.2	360	307
27	0.062	0.072	9.66	5.65	156	78
28	0.049	0.096	10.4	22.8	212	238
29	0.039	0.046	32.8	21.0	841	457
30	0.083	-	-	-	-	-
31	0.055	0.114	13.5	8.31	246	73
32	0.052	0.076	45.7	23.7	879	312
33	0.044	0.045	8.18	7.73	186	172
34	0.056	0.106	-	-	-	-
35	0.043	0.031	4.32	6.20	100	200
36	0.043	0.063	16.4	27.3	382	433
37	0.053	0.046	21.0	20.0	397	435

[a]The compounds were assayed for in vitro inhibition against four purified NOS isoforms: rat nNOS (rnNOS), human nNOS (hnNOS), murine iNOS (miNOS), and human eNOS (heNOS) using known literature methods (see Experimental Section for details), and K_i values are calculated directly from IC_{50} values. IC_{50} values are the average of at least two replicates from 6–9 data points; all experimental standard error values (for the $LogIC_{50}$) are less than 10%, and all correlation coefficients are good ($r^2 > 0.87$). Selectivity values are ratios of respective K_i values.

Table 2.

Inhibition of rat and human nNOS compared to murine and human iNOS by selected compounds[a]

	K_i (μM)				Selectivity	
compd	**rnNOS**	**hnNOS**	**miNOS**	**hiNOS**	**$^{rn}/_{mi}$**	**$^{hn}/_{hi}$**
7	0.045	0.088	16.3	6.94	362	79
10	0.119	0.151	2.86	3.55	24	24
12	0.055	0.060	24.2	29.9	441	498
29	0.039	0.046	32.8	21.1	841	459
32	0.052	0.076	45.7	43.9	879	578
33	0.044	0.045	8.18	29.4	186	653
36	0.043	0.063	16.4	24.6	382	390
37	0.053	0.046	21.0	34.8	397	757

[a]Compounds **7, 10, 12, 29, 32, 33, 36, and 37** were assayed for in vitro inhibition against purified human iNOS (hiNOS) using known literature methods, and K_i values were calculated directly from IC_{50} values using the Cheng–Prusoff equation. IC_{50} values are the average of at least two replicates from 6–9 data points; all experimental standard error values (for the LogIC_{50}) are less than ± 0.10. K_i values for isoforms: rat nNOS (rnNOS), human nNOS (hnNOS), and murine iNOS (miNOS) were included for comparison. Selectivity values are ratios of respective K_I values.

Table 3.

Inhibition data for wild-type and mutant NOS enzymes by selected compounds (**7**, **10**, **12**, **29**, **32**, and **36**)[a]

	K_i (μM)				Selectivity	
Compd	**WT-rnNOS**	**heNOS**	**D597N rnNOS**	**M336V/D597N rnNOS**	$^{WT}/_{SM}$	$^{WT}/_{DM}$
7	0.045	18.7	0.273	0.215	6	5
10	0.119	41.9	2.11	1.57	18	13
12	0.055	52.6	0.416	1.60	8	29
29	0.039	21.0	0.246	0.189	6	5
32	0.052	23.7	0.384	0.159	7	3
36	0.043	27.3	0.575	0.114	13	3

[a]The compounds were assayed for in vitro inhibition against purified NOS isoforms: rat nNOS (rnNOS, and human eNOS (heNOS), as well as single mutant (SM) (D597N) and double mutant (DM) (M336V/D597N) of rat nNOS using known literature methods, and K_i values were calculated directly from IC_{50} values using the Cheng–Prusoff equation. IC_{50} values are the average of at least two replicates from 6–9 data points; all experimental standard error values (for the LogIC_{50}) are less than ± 0.10. Selectivity values are ratios of respective K_i values.

Table 4.

PDSP Binding Summary for Selected Compounds[a]

Compd	Concerning	moderate	weak	insignificant	Total
1	8	7	22	8	45
4	3	6	17	22	45
12	1	0	21	23	45
29	1	4	27	13	45
32	4	7	22	12	45
33	3	5	17	20	45

[a]Off-target binding is classified into four categories: concerning (K_i < 100 nM, or < ~2× nNOS K_i value), moderate (100–300 nM, or ~2– 5× nNOS K_i value), weak (>300 nM, or > ~5× nNOS K_i value, typically ~1 μM), and insignificant (<50% bound at 10 μM), for a total of 45 receptors as assayed by the PDSP's "comprehensive screen" (see ref 28).

Table 5.

Effective Permeability (P_e) of Five Commercial Drugs and nNOS Inhibitors in the PAMPA–BBB Assay[a]

Compd	log D[b]	log P[b]	TPSA (Å^2)[c]	reported P_e (10^{-6} cm s^{-1})[d]	determined P_e (10^{-6} cm s^{-1})[e]	BBB permeant prediction[c]	prediction
verapamil	2.29	4.55	63.95	16	21.3 ± 1.5[f] 18.5 ± 1.9	BBB (+)	CNS (+)
chlorpromazine	2.76	4.56	31.78	6.5	8.04 ± 0.41[f] 8.90 ± 0.68	BBB (+)	CNS (+)
dopamine	−1.50	0.03	66.48	0.2	0.12 ± 0.41[f] 0.125 ± 0.14	BBB (−)	CNS (−)
7	1.36	3.32	64.93		11.3 ± 1.64	BBB (+)	CNS (+)
12	1.27	3.18	64.93		15.5 ± 2.32	BBB (+)	CNS (+)
29	2.37	3.78	74.16		14.6 ± 0.97	BBB (+)	CNS (+)
33	2.13	3.53	87.05		8.09 ± 0.67	BBB (−)	CNS (+)
37	1.94	3.35	115.29		7.04 ± 2.43	BBB (−)	CNS (+)

[a] All assays were performed over 17 h at a concentration of 200 μM; see Experimental Section for details.

[b] Log D (pH = 7.4) and log P values of the free-base species were predicted using ChemAxon software.

[c] TPSA calculations and BBB permeation was predicted using the free web tool SwissADME.

[d] Effective permeability values from literature.[32]

[e] Effective permeability values obtained in-house.

[f] Experimental P_e values reported previously by Do et al.[68]

Table 6.

Metabolic stability of **12** and positive control in human liver microsome.[a]

Compd	% remaining at 60 min (- NADPH)	% remaining at 60 min (Buffer)	$t_{1/2}$ (min)[b]	CL_{int} (mL/min/kg)[c]
12	87	67	>60	8
terfenadine[d]	101	100	23	108

[a] All assays were performed in 50 mM Kphos buffer (pH 7.4) containing HLM (0.714 mg/mL) over 60 min at 1.428 μM drug concentration. Parent compound peak disappearance were monitored by LC-MS/MS.

[b] $t_{1/2}$: half-life.

[c] CL'_{int}: *in vitro* intrinsic clearance.

[d] Positive control.